August 2020

Evaluating Photovoltaics in a Peak-Shaving Supply Management Role in Rural Communities

Patrick Anderson
Clemson University, ptander01@gmail.com

EVALUATING PHOTOVOLTAICS IN A PEAK-SHAVING SUPPLY MANAGEMENT ROLE IN RURAL COMMUNITIES

A Thesis
Presented to
the Graduate School of
Clemson University

In Partial Fulfillment
of the Requirements for the Degree
Master of Science
Plant and Environmental Science

---

by
Patrick Taylor Anderson
August 2020

Accepted by:
Dr. Bülent Koç, Committee Chair
Dr. John P. Chastain
Dr. Christopher Post
Dr. Michael Vassalos

ORGANIZATION OF THESIS

This thesis is organized in manuscript style as two papers to be submitted for publication. Chapter one provides a general overview of the thesis. Chapter two is comparing the accuracy of agricultural building measurements using satellite and Unmanned Aerial Vehicles (UAV) images. Chapter three is about the potential of broiler rooftop photovoltaics as distributed peak-shaving plants for supply side load management. Chapter four contains the overall conclusions.

ABSTRACT I

Little literature exists on measuring agricultural buildings with data collected from an Unmanned Aerial Vehicle (UAV) mounted aerial cameras. Survey grade tools produce highly accurate results, but with high financial and temporal costs. Satellite imagery is readily available and relatively low-cost but has low spatial and temporal resolution. Unmanned Aerial Vehicles are emerging as a balance between these traditional methods for measuring and monitoring natural and constructed environments. The objective of this study was to compare the accuracy of building measurements in the orthophotos generated from satellite and UAV imagery based on control measurements without Ground Control Points (GCP's) or on-board survey-grade georeferencing. The rooftops of 31 broiler houses located in Oconee and Anderson Counties (South Carolina, USA) were evaluated for solar energy applications. Building plan dimensions were acquired and building heights were independently hand-measured. A DJI Mavic Pro UAV flew following a traditional double grid flight path at 69-meter altitude with a 4K-resolution camera angle of -80° from the horizon with a 70% to 80% overlap. The captured images were processed using Agisoft Photoscan Professional digital photogrammetry software. Orthophotos of the study areas were generated from the acquired 3D image sequences using Structure from Motion (SfM) techniques. Building rooftop overhang obscured building footprint in aerial imagery. To accurately measure building dimensions, 0.91 m was subtracted from building roof width and 0.61 m was subtracted from roof length based on observations of roof overhangs from poultry buildings.

The actual building widths and lengths ranged from 10.8 to 184.0 m and the mean measurement error using the UAV-derived orthophotos was 0.69% for all planar dimensions. The average error for building length was 1.66 ± 0.48 m and the average error for widths was 0.047 ± 0.13 m. Building sidewall, side entrance and peak heights ranged from 1.9 to 5.6 m and the mean error was 0.06 ± 0.04 m, or 1.2% mean error. The results proved that using consumer-grade UAV's and photogrammetric SfM could create accurate DSM and orthomosaics of a study area at efficient use of economic and temporal resources without the use of survey grade equipment or GCPs.

When compared to the horizontal accuracy of the same building measurements taken from readily available satellite imagery, the results were mixed. The mean error in satellite images was -0.36%. The average length error was -0.46 ± 0.49 m and -0.44 ± 0.14 m for building widths. It was not possible to measure building heights using satellite image analysis. The satellite orthomosaics were more accurate for length predictions and the UAV orthomosaics were more accurate for width predictions. This disparity was likely due to flight altitude, camera field of view, and building shape. The satellite imagery had low cost and ease of access that allowed a convenient determination of structural orientation and planimetric dimensions. However, the UAV provided dependably current data, vertical dimensions, and had higher absolute accuracy useful for combining with GIS data layers from other sources. With an average flight time of 5.4 min/ha and an average GSD of 4.84 cm/pi, the results obtained from a relatively inexpensive UAV mounted camera and image analysis demonstrated sufficient accuracy for planning and monitoring purposes in agricultural applications.

ABSTRACT II

The primary challenge faced by energy suppliers is forecasting and supplying hourly peak demand. Generating supply at peak demand and efficiently distributing to remote customers are vital supply-side load management practices for controlling supplier cost. This research sought to determine if poultry farms could function as rurally distributed, peak-demand photovoltaic (PV) power plants to sparsely populated areas. Unmanned Aerial Vehicles (UAV) and satellite imagery were used to examine 88 poultry farms. The typical farm consisted of four poultry houses, each 15.2 meters by 152.4 meters, oriented East/West, with a rooftop slope of 22.6º and a suitable rooftop area of 1,254 m^2. The average rooftop supply of all farms was calculated and grouped into key supply categories of seasonal peak, shoulder, base, and energy. The average supply from a farm of typical size was 496 kW/hr during peak periods, 279 kW/hr during summer shoulder periods, and a contribution to base load of 425 kW/hr during summer months. The average rooftop supply estimated for all 88 farms was 59.2 MW/h during summer peak, a contribution to summer base load of 47.0 mW/hr, and total annual energy supply of 127.3 GWh/yr. Calculations of facility demand and energy use were in the range of 10-20% of gross hourly rooftop supply across time categories. This resulted in a net peak demand reduction potential of 51.6 MW/h (83%), and an annual net supply of 109.4 GWh (86%) to the grid. In light of distribution costs, the twenty-seven farms located further than 3.28 km from existing transmission lines proved the most valuable in peak demand reduction and distributing energy to rural areas. Results suggest a promising potential for distributed PV adoption for peak-shaving.

ACKNOWLEDGMENTS

This document was not the result of individual effort, but derived from a multitude of researchers and resources. Primarily, I would like to thank my research committee for their oversight, tireless patience, and commitment to the quality of my education. A special thanks is extended to Dr. Chastain for the initial project proposal, as well as generously funding the project. I would like to thank Dr. Post for assistance in acquiring the FAA sUAS remote pilot license and operational instruction. I also wish to acknowledge the valuable expertise of Dr. Brian Ritter, who was instrumental in establishing the photogrammetric and geospatial workflows used for data processing. Lastly, I would like to thank the Clemson Center for Geospatial Technology for providing the software licenses for Agisoft Photoscan Professional and ArcGIS Pro.

TABLE OF CONTENTS

Page

Table of Contents (Continued)

Page

LIST OF TABLES

List of Tables (Continued)

Table Page

List of Tables (Continued)

Table Page

List of Tables (Continued)

Table Page

LIST OF FIGURES

List of Figures (Continued)

Figure Page

List of Figures (Continued)

Figure Page

CHAPTER ONE

INTRODUCTION

The primary challenge faced by energy suppliers is forecasting and supplying hourly peak demand (DEC, 2017). This challenge has even greater significance in rural communities, where population densities are lower and the total distance electricity must travel between generation and consumption is greater. Effort to supply electrical power during times of peak demand is referred to as peak-shaving. This additional peaking infrastructure creates additional cost for suppliers. Generating supply at peak demand and efficiently distributing to remote customers are vital supply-side load management practices for controlling supplier cost.

Renewable energy has been viewed as an attractive alternative to fossil fuels due to significantly lower fuel costs (Klaić et al, 2015). However, levelized cost of energy calculations demonstrated that inclusion of capital cost required to harvest renewable resources outweighed operating savings. This generally rendered renewable energy more expensive than fossil fuels per kWh produced (Warwick et al, 2016).

The primary commodity of South Carolina's economy according to the Department of Agriculture is its poultry industry (SC DA, 2020). Rooftops of poultry houses are potentially highly suitable for photovoltaic (PV) panel installations. Typical fixed costs in PV installations such as land, distribution infrastructure, permitting, and electricians could be reduced through a mutually beneficial partnership between the utility and their agricultural customers. Solar's low fuel costs and coincidental timing with peak demand support its use as peak-shaving, as well as function as automated fuel

management for a PV peaking-plant. Furthermore, This highly flexible proposal could decrease stress on the utility network and even assist in accelerating economic development for the surrounding territory. An energy supplier using rural poultry house PV could change the tipping point of solar energy as fuel for micro, distributed peak shaving plants to rural communities.

This study explores the utilization of the poultry industry as distributed solar electric energy plants to reduce peak and shoulder demand to the surrounding rural community. This central question was approached from the perspective of the burgeoning Geographic Information Systems (GIS) data analysis. These data, such as orthophotos and Digital Surface Models (DSM's), are essential to the design, execution, and monitoring of projects across disciplines. There are multiple techniques currently employed to obtain GIS data. High-resolution photogrammetric point clouds obtained from UAVs represent an appealing technique currently employed to obtain GIS data (Sammartano et al, 2016; Ajayi et al, 2017; Cook, 2017). The combination of efficient Structure from Motion (SfM) photogrammetry and flexible UAV photogrammetry has the potential to produce a unique surface reconstruction tool, delivering orthophotos and DSMs with exceptional resolution (Colomina et al, 2014). Data collection with UAVs are increasingly adopted directly by researchers of many disciplines (Le Mauff et al, 2018).

This research was conducted as two consecutive studies (papers). The goal of the preliminary study was to explore the limits of UAV adoption for 3D mapping applications in the context of large-scale rural environments (2.5 ha), using a consumer grade UAV with onboard GPS without expensive onboard GNSS or RTK hardware or

Ground Control Points (GCPs) in the field. This was done by a statistical analysis of digital orthophotos produced from UAV-based photogrammetric point clouds. Specifically, the objectives of the first study were to (1) utilize a consumer grade UAV with Inertial Measurement Unit (IMU) to capture aerial images, (2) employ traditional photogrammetry SfM to convert the 2D images into 3D GIS data, (3) determine horizontal and vertical accuracy of UAV imagery, and (4) compare to horizontal accuracy of satellite imagery.

The goal of the second study was to examine the potential of broiler rooftop photovoltaics as distributed peak-shaving plants for supply side load management. The specific objectives were to (1) determine the electrical energy use for individual poultry houses in a broiler producing area in South Carolina, and (2) examine the potential of using buildings on groups of poultry farms as peak shaving power plants in a rural area. This was done through an analysis of solar irradiance and PV technology, farm location, and net supply to grid in light of farm demand and energy use.

CHAPTER TWO

COMPARING THE ACCURACY OF AGRICULTURAL BUILDING MEASUREMENTS USING SATELLITE AND UAV IMAGES

ABSTRACT

Little literature exists on measuring agricultural buildings with data collected from an Unmanned Aerial Vehicle (UAV) mounted aerial cameras. Survey grade tools produce highly accurate results, but with high financial and temporal costs. Satellite imagery is readily available and relatively low-cost but has low spatial and temporal resolution. Unmanned Aerial Vehicles are emerging as a balance between these traditional methods for measuring and monitoring natural and constructed environments. The objective of this study was to compare the accuracy of building measurements in the orthophotos generated from satellite and UAV imagery based on control measurements without Ground Control Points (GCP's) or on-board survey-grade georeferencing. The rooftops of 31 broiler houses located in Oconee and Anderson Counties (South Carolina, USA) were evaluated for solar energy applications. Building plan dimensions were acquired and building heights were independently hand-measured. A DJI Mavic Pro UAV flew following a traditional double grid flight path at 69-meter altitude with a 4K-resolution camera angle of -80° from the horizon with a 70% to 80% overlap. The captured images were processed using Agisoft Photoscan Professional digital photogrammetry software. Orthophotos of the study areas were generated from the acquired 3D image sequences using Structure from Motion (SfM) techniques. Building rooftop overhang obscured building footprint in aerial imagery. To accurately measure

building dimensions, 0.91 m was subtracted from building roof width and 0.61 m was subtracted from roof length based on observations from poultry buildings.

The actual building widths and lengths ranged from 10.8 to 184.0 m and the mean measurement error using the UAV-derived orthophotos was 0.69% for all planar dimensions. The average error for building length was 1.66 ± 0.48 m and the average error for widths was 0.047 ± 0.13 m. Building sidewall, side entrance and peak heights ranged from 1.9 to 5.6 m and the mean error was 0.06 ± 0.04 m, or 1.2% mean error. The results proved that using consumer-grade UAV's and photogrammetric SfM could create accurate DSM and orthomosaics of a study area at efficient use of economic and temporal resources without the use of survey grade equipment or GCPs.

When compared to the horizontal accuracy of the same building measurements taken from readily available satellite imagery, the results were mixed. The mean error in satellite images was -0.36%. The average length error was -0.46 ± 0.49 m and -0.44 ± 0.14 m for building widths. It was not possible to measure building heights using satellite image analysis. The satellite orthomosaics were more accurate for length predictions and the UAV orthomosaics were more accurate for width predictions. This disparity was likely due to flight altitude, camera field of view, and building shape. The satellite imagery had low cost and ease of access that allowed a convenient determination of structural orientation and planimetric dimensions. However, the UAV provided dependably current data, vertical dimensions, and had higher absolute accuracy useful for combining with GIS data layers from other sources. With an average flight time of 5.4 min/ha and an average GSD of 4.84 cm/pi, the results obtained from a relatively

inexpensive UAV mounted camera and image analysis demonstrated sufficient accuracy for planning and monitoring purposes in agricultural applications.

INTRODUCTION

Geographic Information Systems (GIS) data such as orthophotos and Digital Surface Models (DSM) are essential to the design, execution, and monitoring of projects across disciplines such as agriculture, architecture, engineering, energy, mapping, transportation, and surveillance. There are multiple techniques currently employed to obtain GIS data. Traditional methods include manned airborne sensors such as Light Detection and Ranging (LiDAR) or photogrammetric cameras, manned ground methods such as terrestrial laser scanning, or autonomous satellite imagery using Global Navigation Satellite Systems (GNSS). With each technique for data collection, it is important to know the cost, accuracy, and its conformance to applicable standards. Satellite and manned airborne platforms offer spatial coverage at a landscape scale. However, manned aerial vehicles are quite expensive (Remondino et al., 2011) and satellites often provide poor spatial resolution at large cartographic scales, both of which may limit their usefulness. Terrestrial survey equipment is expensive and time-consuming (Hugenholtz, 2016). High-resolution photogrammetric point clouds obtained from small UAVs represent an appealing alternative (Sammartano, 2016; Ajayi, 2017; Cook, 2017).

An alternative approach to survey-grade methods gives georeferencing at levels of spatial precision that are consistent in results without the cost or time necessitated by

surveying equipment. This can be done with the onboard inertial measurement unit (IMU) and GPS used without Ground Control Points (GCPs) to locate and orient the data (Uysal et al., 2015). Currently, the combination of efficient Structure from Motion (SfM) photogrammetry and flexible UAV photogrammetry have the potential to produce a unique surface reconstruction tool, delivering orthophotos and DSMs with exceptional resolution (1.5 cm GSD) and unbeatable price (Colomina and Molina, 2014).

A study conducted in 2012 compared a UAV's consumer-grade digital camera with survey-grade terrestrial laser scanner to demonstrate the 0.10 m vertical accuracy achieved using SfM with complex topography and complex land covers for geoscience applications (Westoby, et al, 2012). Another recent study done in highly variable and vegetated terrain with low-cost UAV's demonstrated that the standard deviation of DEM data with and without GCP's only differed by 0.06 meters (Akturk and Altunel, 2018). Data collection with UAVs are now increasingly adopted directly by researchers of many disciplines (Le Mauff et al., 2018).

This study aimed to explore the limits of UAV adoption for 3D mapping applications in the context of large-scale rural environments (2.5 ha), consumer grade UAV with onboard GPS for precision photo geotagging applications to produce accurate spatial data without expensive onboard GNSS or RTK hardware, terrestrial survey equipment, and without the use of GCP's in the field. This was done by a statistical error analysis of digital orthophotos produced from UAV-based photogrammetric point clouds. Specifically, the objectives of this study were to (1) utilize a consumer grade UAV with IMU to capture aerial images, (2) employ traditional photogrammetry SfM to convert the

2D images into 3D GIS data, (3) determine horizontal and vertical accuracy of UAV imagery, and (4) compare to horizontal accuracy of satellite imagery.

METHODS

The project methodology included identifying the study area and variables of interest, data collection, photogrammetric data processing, and statistical analysis. Each step is explained in further detail.

Study Area

All research methods were tested on poultry farms in Anderson and Oconee Counties in upstate South Carolina. A total of 31 farms (139 poultry houses) were visited within the study area and their locations are provided in Figure 2.1.

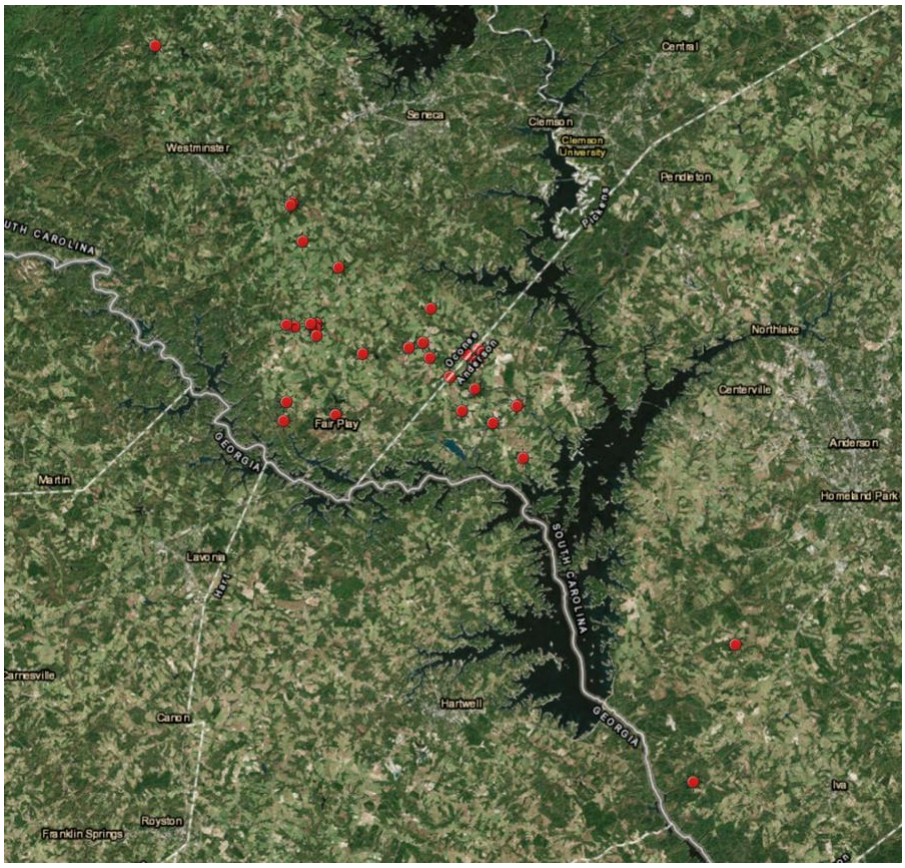

Figure 0.1 Location of the thirty-one poultry farms in Oconne and Anderson Counties (SC) in the study area.

Dimensional accuracy of specific building characteristics was compared in the orthophotos generated from satellite and UAV imagery. Data collection for these variables entailed a combination of remote sensing techniques validated by physical measurements as benchmarks. A description of each variable as well as measurement methodology was described in the subsequent sections for each of these variables.

Poultry Building Characteristics of Interest

Dimensional accuracy was compared for horizontal measurements of the UAV landing pad and poultry house building length (L), width (W) dimensions, and then vertical measurements of building sidewall height (H_s), peak height (H_p), and side entrance ridge height (H_r). The horizontal building measurements were compared to measurements from satellite image. The height measurements were used to calculate roof slope (S) for the solar analysis in the subsequent study.

Physical Measurements

Building Length and Width Dimensions

The grower provided building length and width measurements for the farms visited from building blueprints. Building width and length measurements were taken on a single building at each of the 31 visited farms. These dimensions are illustrated in Figure 2.2.

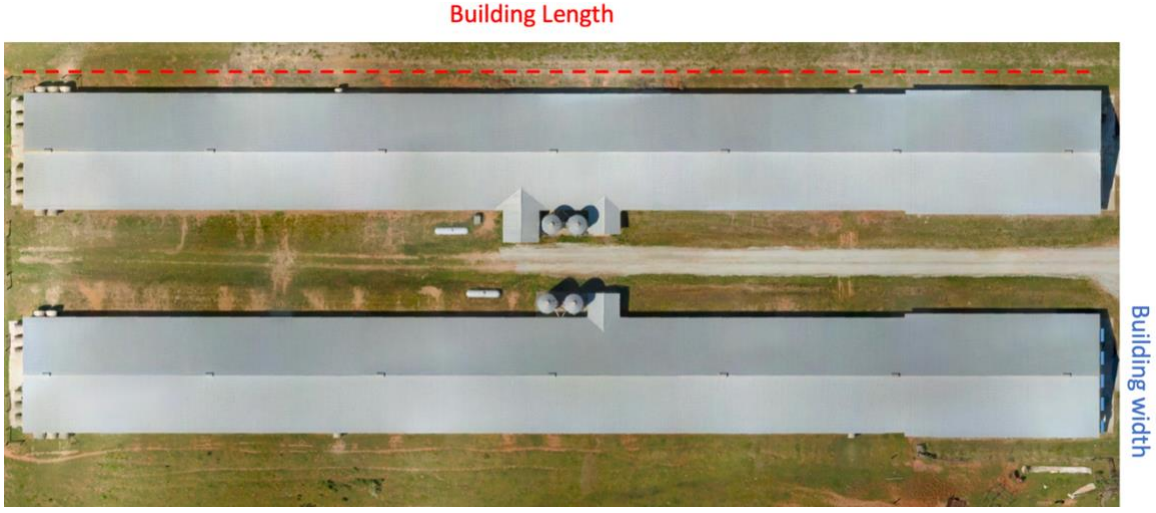

Figure 2.2 Poultry house viewed from above, illustrating length and width measurements observed from UAV images.

Building blueprint dimensions were provided in imperial units (ft) and converted to metric (m) with a conversion factor of 0.3048 meters per foot. These converted units were used as the measured building dimension for comparison to UAV and satellite predictions.

The building footprint cannot be seen from above in UAV generated images due to roof overhang (see Figure 2.2). To account for overhang, an estimated value based on observations made on a large number of poultry barns was subtracted from the overall building roof lengths and widths that were seen in the images. Based on observations from many poultry barns it was determined that the typical overhang added 0.9144 m to the width of the building floorplan and 0.6096 m to the plan length. The building width and lengths observed in the overhead images were adjusted to the floor plan width and length as follows:

$$W = W_i - 0.9144 \text{ m, and} \quad (2.1)$$

$$L = L_i - 0.6096 \text{ m.} \quad (2.2)$$

Where,
W_i = building roof width from aerial imagery, overhang included, and
L_i = building roof length from aerial imagery, overhang included.

Building Heights

Poultry building height measurements were taken to compare vertical dimensions using a simple UAV flight path, and to ensure precise and accurate model reconstruction in the vertical plane. These also were used determine building roof slope. A range of sidewall height (H_s), peak height (H_p), side entrance ridge height (H_r) heights were measured to provide a greater range of vertical heights to compare with measurements from UAV images. The building side entrance can be seen in the center of of the

buildings shown in Figure 2.2. All building heights were measured with a measuring tape (± 0.16 cm) from the concrete base to under the building eave. The location of the sidewall and peak heght measurments, along with the location of building overhangs are illustrated in Figure 2.3.

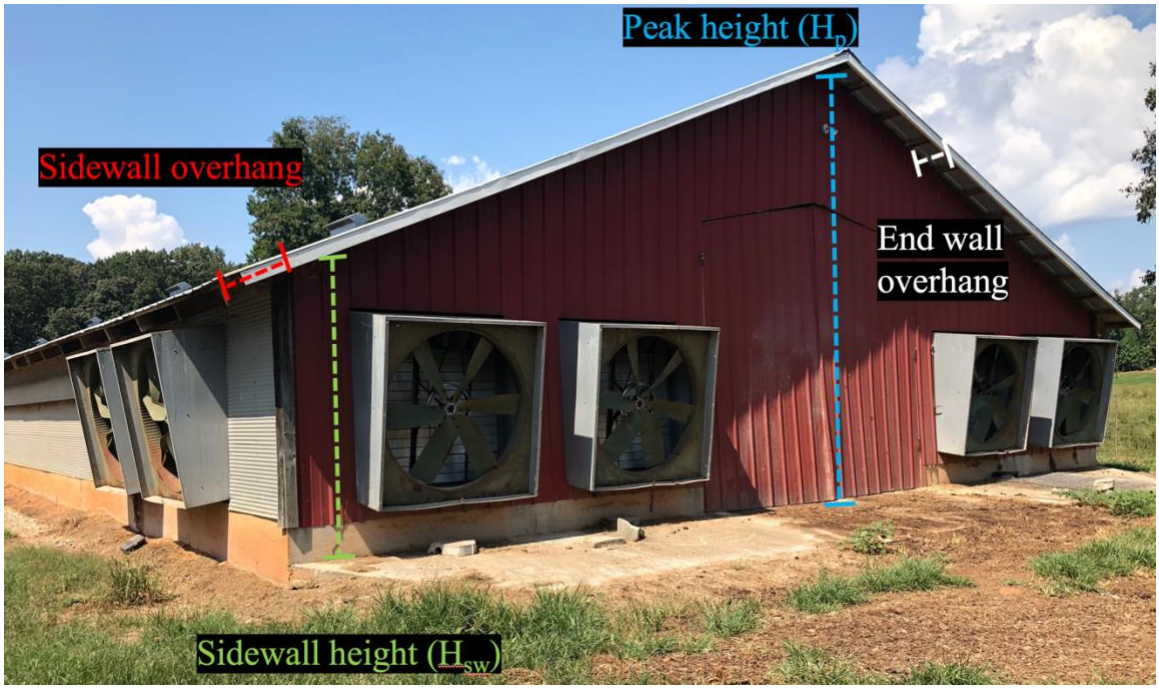

Figure 2.3 Poultry endwall illustrating location of sidewall and peak height measurements and building overhangs.

Building Rooftop Slope

The amount of solar radiation that falls on roof-mounted solar voltaic panels depends on the rooftop azimuth and the slope of the southward facing roof. Consequently, rooftop slope was needed for the current application of UAV and Satellite remote sensing to evaluate poultry buildings for suitability of solar electric production.

Slope was calculated using hand measurements or UAV image derived measurements using the definition of roof slope (S) as:

$$S = (H_p - H_s) / (W \div 2). \quad (2.3)$$

UAV Remote Sensing

A UAV was used to collect aerial images of the farm buildings at each site. The building footprint cannot be seen from above due to roof overhang (see Figure 2.2). The building rooftop lengths (L_i) and widths (W_i) were measured from the aerial images using the Ruler tool (Agisoft, 2019) on each farm's orthomosaic image and they were adjusted to blueprint dimensions by correcting for roof overhangs as shown previously in Equations 2.1 and 2.2 . Poultry building vertical measurements consisted of sidewall heights, peak heights, and side entrance ridge heights. These measurements were obtained using the Ruler tool (Agisoft, 2019) on each farm's DSM.

UAV Licensing and Operation Procedures

Clemson University policy required that all individuals in operation of a UAV for research purposes have a small Unmanned Aerial Systems (sUAS) remote pilot license in compliance with Federal Aviation Administration (FAA, 2016) protocol and carry appropriate insurance. Only a licensed and insured pilot flew UAV missions for this project in compliance with all FAA requirements (Summary of Small Unmanned Aircraft Rule, Part 107, FAA, 2016).

UAV Flights for Data Collection

The remote data collecting equipment was a DJI Mavic Pro UAV with an onboard digital camera. This camera collected aerial images at each site. A flight planner application, Pix4D Capture, was utilized for each flight (Pix4D, 2017). This mobile application automated each flight to improve the results, safety, and efficiency of the data collection process. A double grid flight pattern at an altitude of 69m was used for the aerial surveys. The angle of the UAV camera during flight was set to capture images at an angle of -80 degrees from the horizon. The camera was programmed to capture 80% frontal overlap of image content between consecutive pictures along the flight path and 70% side overlap between images from adjacent flight paths at ground level (Barry and Coakley, 2013). Overlap ensured sufficient subject redundancy captured between photos which improved the quality of 3D digital surface model reconstruction using photogrammetry. An illustration of the flight path is given in Figure 2.4.

Figure 0.4 Sample image of the UAV flight path in Pix4D Capture (Pix4D, 2017).

All equipment, calibrations, and parameters were held constant throughout the data collection process to minimize inflation in the variance of the response and bias in the estimation of the treatment mean.

UAV Image Data Processing

The computing equipment used for data processing was an iMac Desktop with custom configured technical specifications for improved processing performance: 4.2 gigahertz quad core i7 processor (turbo charged to 4.5), 32 GB 2400 megahertz DDR RAM (four 8GB cards), storage capacity of 2 TB fusion drive with 128 GB of flash storage, and an AMD Radeon Pro 580 graphics card with 8GB VRAM.

The aerial photos were processed using Agisoft Photoscan Professional software (Agisoft, 2017) version 1.4.1 to construct 3D models. This processing involved examining relative, absolute, internal, and external orientation and the construction of 3D models from the 2D captured images using SfM photogrammetric range imaging technique (Ulman, 1979; Westoby et al., 2012). The workflow consisted of 6 steps: (1) import and (2) align photos, (3) optimize alignment, (4) build dense point cloud, (5) build digital surface model (6) build orthomosaic image. The general process was to align images by matching common points, which resulted in a sparse point cloud and established camera positions. Then a dense point cloud of improved accuracy was constructed based on the estimated camera positions and pictures. A maximum allowable number of points on every image available for consideration was 40,000 points, and an upper limit of points allowed to match between any two images was set to 10,000,000 points. These constraints allowed for optimization of the alignment process without allowing features to be overlooked. Adaptive camera model fitting was enabled, which automated the selection of camera parameters to be adjusted based on their reliability estimates. The dense point cloud was constructed using 4x downscaled images, which maintained a relatively high accuracy (compared to 16x or 64x downscaling). A mild depth filter was also applied during this step to remove outliers and noise.

Satellite Remote Sensing

The poultry building lengths and widths on 31 farms were also measured using readily available satellite imagery provided by Google, Maxar Technologies, and US Geological Survey (Google, 2019). The collective 139 building rooftop lengths (L_i) and

widths (W_i) were measured using the Measure Distance tool (Google, 2019) on satellite imagery of the 31 farms. Adjusted building width (W) and length (L) measurements from satellite imagery were obtained in the same way as for UAV generated images (Equations 2.2 and 2.3). It was impossible to measure building heights with satellite imagery.

Comparison of Actual Dimensions to Measurements Using UAV and Satellite Remote Sensing Techniques

The predictive accuracy of building measurements within the satellite and UAV derived orthoimages were determined using equation 2.4:

$$\Delta d = A - M. \quad (2.4)$$

Where,
Δd = Difference between the actual dimension and the measured dimension (m),
A = Actual dimension (m), and
M = Measured dimension (m).

Accuracy was measured by quantifying error as the difference between actual building dimensions observed and the dimensions measured from remote sensing derived digital Orthomosaic images. This was done for building length (L), width (W), building sidewall height (H_s), peak height (H_p), and side entrance height (H_r). The actual dimensions were the blueprint dimensions for building length and width, and hand measurements of building heights. The measured dimensions were the predicted building measurements in the UAV and satellite derived orthomosaic images.

The smallest horizontal dimension that was measured for the poultry buildings was the building width and was on the order of 10 m. The diameter of the plastic UAV landing pad was under 1 meter and was used to provide a smaller horizontal dimension to

test the accuracy of using UAV generated images for making horizontal landscape measurements. The UAV landing pad was visible in each flight and was used as a reference point to ensure precise and accurate large-scale horizontal model reconstruction. The pad consisted of a waterproof, high quality nylon stretched between a circular steel ring frame. The ring was manufactured to be flexible for contorted compaction to facilitate storage and transportation. This lack of rigidity also allowed for potential variation in pad diameter measurements. The manufacturer's quoted product size was 75 cm in diameter. The round pad was hand-measured 9 times to the nearest 0.16 cm with a tape measure. The average of these measurements was the actual landing pad diameter. The landing pad diameter was also measured using the computer software's orthomosaic images once per flight to provide 31 obervations. The mean landing pad diameter obtained by hand measurements was compared to the mean pad diameter measured using UAV images by calculating the 95% confidence interval (C.I.) about each mean as (Steel and Torrie, 1991):

$$\text{C.I.} = t_{\alpha,\,(n-1)} \times (s/n_{0.5}). \tag{2.5}$$

Where,
C.I. = 95% confidence interval about the mean (m),
t = t-value $_{0.025,\,(n-1)}$,
s = Standard deviation (m), and
n = Number of replications.

The mean differences (Δd) was calculated for the building lengths (L), and widths (W) measured using both the UAV and satellite images as well as the sidewall (H_s), peak (H_p), and side entrance heights (H_r) measured using only the UAV images. The mean

differences were compared using the 95% confidence interval about the means as shown previously in Equation 2.5.

Relative error was also calculated for differences for all building length, width, and height dimensions obtained using both UAV and satellite images. This was done to place the error in perspective of the size of the measurements and was calculated as:

$$\mu E\ (\%) = [\ \mu \Delta d\ (m) / \mu A\ (m)] \times 100. \quad (2.6)$$

Where,
μ E= Mean error (%),
μ Δd = Mean difference (m), and
μ A = Mean actual dimension (m).

The percent error was calculated as the mean of all calculated differences for a specific building dimension divided by the grand mean of all actual measurements of a specific dimension. This metric established measured error relative to the size of the measurement, which was useful due to the variation in measurements ranging from a UAV landing pad with a diameter less than one meter to a building with a length greater than 150 meters.

It was hypothesized that the variances of ΔW and ΔL obtained based on UAV and satellite remote sensing would not be the same. To test this hypothesis an F-test for common variance was used to determined if results could be pooled. The calculated F determined by dividing the largest variance of one horizontal dimension (ΔW or ΔL) by the smaller variance of the other horizontal dimension (ΔW or ΔL), each from the same remote sensing tool (Steel and Torrie, 1997). The calculated F was compared with the tabulated F using the degrees of freedom for the numerator and denomenator at the 95%

level of probalility. If the F-test indicated that the variances were not significantly different, then the variances would be pooled to provide a better estimate of the variance used for calculation of the 95% C.I.

Finally, the raw data for all heights, widths, and lengths for the UAV image derived measurements were correlated with the actual measurements using a simple line that passed through the origin (A = b M). This was done to allow visualization of the raw data, a check of correlation of the data, and to provide an overall estimate of the average difference between the actual dimensions and the UAV derived measurements. A similar correlation was done for the widths and lengths obtained from the satellite image measurements.

RESULTS

The products of all methods described for remotely sensed data collection, photogrammetric data processing, and statistical analysis are given below. Dimensional accuracy was compared for horizontal measurements of the UAV landing pad and poultry house building dimensions, and then vertical measurements of the building sidewall and peak heights. These numbers were compared to the accuracy of horizontal measurements from satellite image.

The image quality of the digital sensor used in remote sensing was critical to successful adaptation of that tool. Furthermore, the sensor's ability to capture detail of environemnts that contained complex topography and complex land cover would improve its usefulness. The UAV used for this study was the DJI Mavic Pro, mounted with an on-

board 4K digital camera. A sample result of the camera's image quality captuing built and natural environments of highly variable terrain and vegetation can all be seen in Figure 2.5.

Figure 2.5 Sample photo of poultry house rooftop captured with the UAV at 69 m altitude.

This image depicted a portion of a poultry barn and surrounding rural landscape. Technical specifications associated with the onboard UAV camera described in the general image information associated with this image was also noted. The general information recorded with this specific UAV image sample validates the specific equipment and flight parameters utilized. Information including the altitude, GPS coordinates and version, UAV make and model, image size and type, as well as digital sensor type are all given in Table 2.1

Table 0.1. Sample UAV image general information.

Document Type:	JPEG image
File Size:	4,798,896 Bytes
Color Mode:	RGB
Profile Name:	sRGB IEC61966-2.1
DPI Width:	72
DPI Height:	72
Depth:	8
GPS Version:	3.2.0.0
Make:	DJI
Model:	FC220
Latitude:	34° 18’ 32.01” N
Longitude:	82° 45’ 28.88” W
Altitude:	161.75 m
Alt. Reference:	above sea level

Exchangeable Image File Format (EXIF) is a standard that defines specific information related to an image or other media captured by a digital camera (Monsurav, 2020). It was capable of storing such important data as camera exposure, date/time the image was captured, and even GPS location. This information was critical to understanding the operational parameters (such as aperture, shutter speed, exposure) and equipment limitations (image size or focal length) of the tools utilized during data collection. Sample image EXIF data associated with Figure 2.5 is given in Table 2.2.

Table 0.2 Sample UAV image EXIF information.

Aperture Value:	2.27
Color Space:	sRGB
Components Configuration:	0,3,2,1
Compressed Bits per Pixel:	2.897
Contrast:	Normal
Custom Rendered:	Normal Process
Digital Zoom Ratio:	0
EXIF Version:	2.3
Exposure Bias Value:	0
Exposure Index:	0
Exposure Mode:	Auto Exposure
Exposure Program:	Normal Program
Exposure Time:	1/60
File Source:	DSC
Flash:	No Flash Function
FlashPix Version:	0.1
FNumber:	2.2
Focal Length:	4.7
Focal Length in 35mm Film:	26
Gain Control:	None
Photographic Sensitivity (ISA):	147
Light Source:	Unknown
Max Aperture Value:	2.27
Metering Mode:	Center Weighted Average
Pixel X Dimension:	4,000
Pixel Y Dimension:	3,000
Saturation:	Normal
Scene Capture Type:	Standard
Sharpness:	Normal
Shutter Speed:	1/60
White Balance:	Auto white balance

The focal length was 4.7 mm. Digital zoom was 0. The image size was four thousand pixels in length by three thousand pixels in height. These details, amongst others in cluded in the table such as exposure and zoom, are useful for validating remote sensing equipment. This information is also vital to calculating Ground Sampling Distance (GSD, cm/pixel) for relative accuracy of images.

UAV Remote Sensing and Photogrammetry

The results for UAV flight logistics included flight time at each farm and the total number of images captured by the UAV. The software processing of these images resulted in filtering images, identifying tie points between images, and construction of a dense point cloud. A summary of these results for the entire project as well as an estimated average per farm are given in Table 2.3.

Table 0.3 Summary table of the data collection and processing results.

	Average/farm	Project Total
Flight Time (minutes):	13.5	320
Images Captured:	268	8,043
Images Used:	224	6,836
Tie Points Identified:	666,691	20,000,715
Dense Cloud Points:	54,209,477	1,626,284,298

The average UAV flight time per farm was 13 minutes and 26 seconds, and a total flight time of approximately 320 minutes to successfully collect data at all 31 farms. The average flight path aerial grid size was 175 m by 163 m, or 28,523 m^2. The average number of images captured at each farm was 268. Eighty-five percent of the images were utilized by the software. This means that 15% of captured images were deemed of unsuitable quality to benefit the analysis, and automatically excluded by the software in step 1 of the photogrammetry workflow. The project totaled 6,836 images used, from which a collective 20 million tie points were identified with the aforementioned reconstruction parameters. The project study area had a total of 1.63 billion 3D dense cloud points. The results for a reconstructed key point cloud can be seen in Figure 2.6(a) and and dense point cloud the output in Figure 2.6(b).

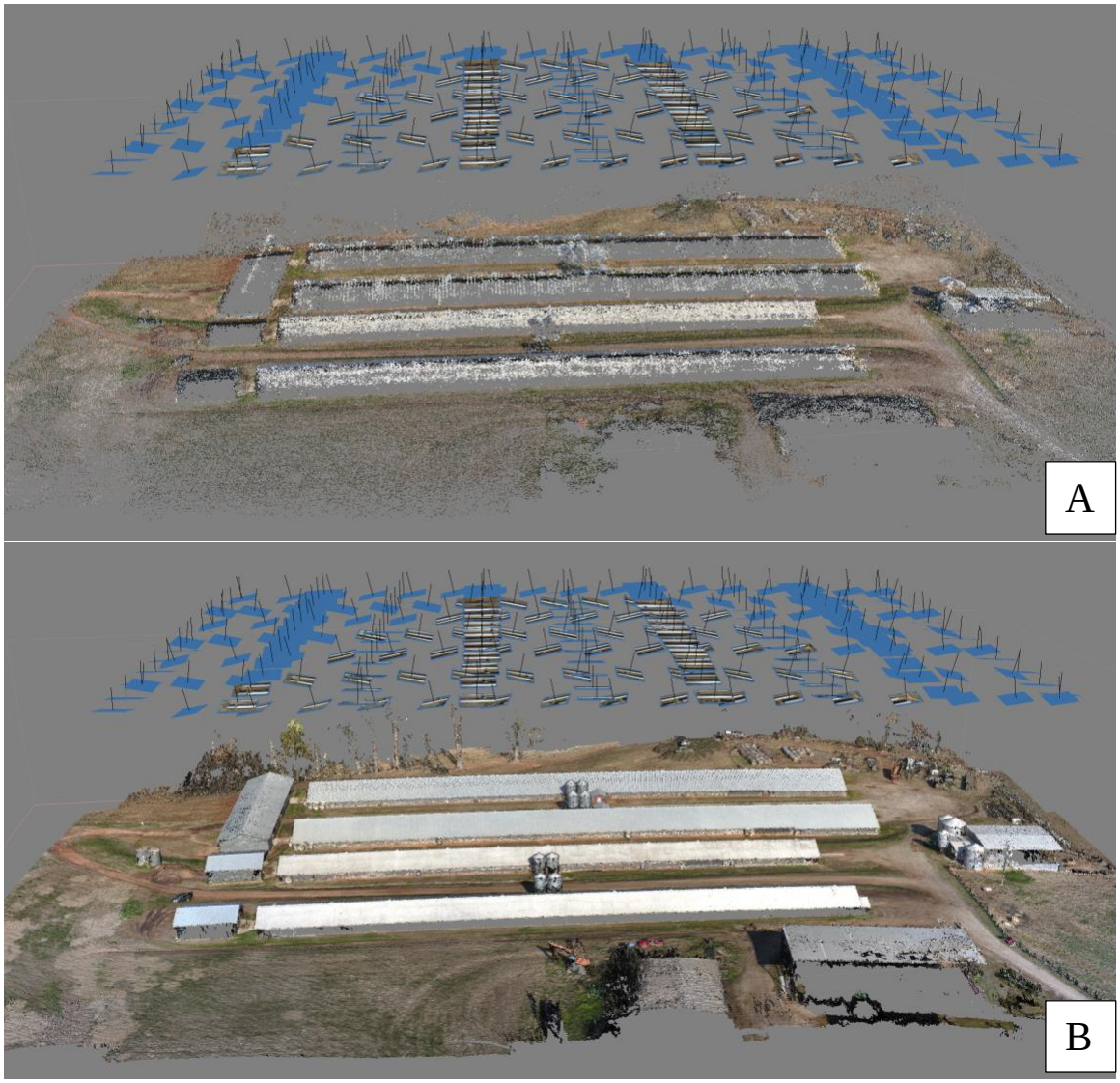

Figure 2.6 Farm buildings reconstructed in Photoscan Pro as (a) Sparse 3D Point Cloud of 650,956 points, and (b) Dense 3D Point Cloud of 46,764,137 points with camera locations and thumbnails above.

The general process was to align images by matching common points, which resulted in a sparse point cloud and established camera positions. Then a dense point cloud of improved accuracy was constructed based on the estimated camera positions and pictures.

The goal of the data collection and analysis was the creation of a digital orthomosaic image as well as a DSM for future solar analysis. The orthomosaic (similar to the digital product provided in satellite imagery) was used to predict building dimensions. The image clarity and resolution of each image, as well as maximizing the tie points between images, were critical to accurate renderings of the subject area. For this study, this affected the confidence of agricultural building dimension measurements. The digital orthomosaic provided aerial perspective, while the DSM provided surface texture and depth for the subject area. An example digital orthoimage is shown in Figure 2.7(a) and DSM of a surveyed farm are shown in Figure 2.7(b).

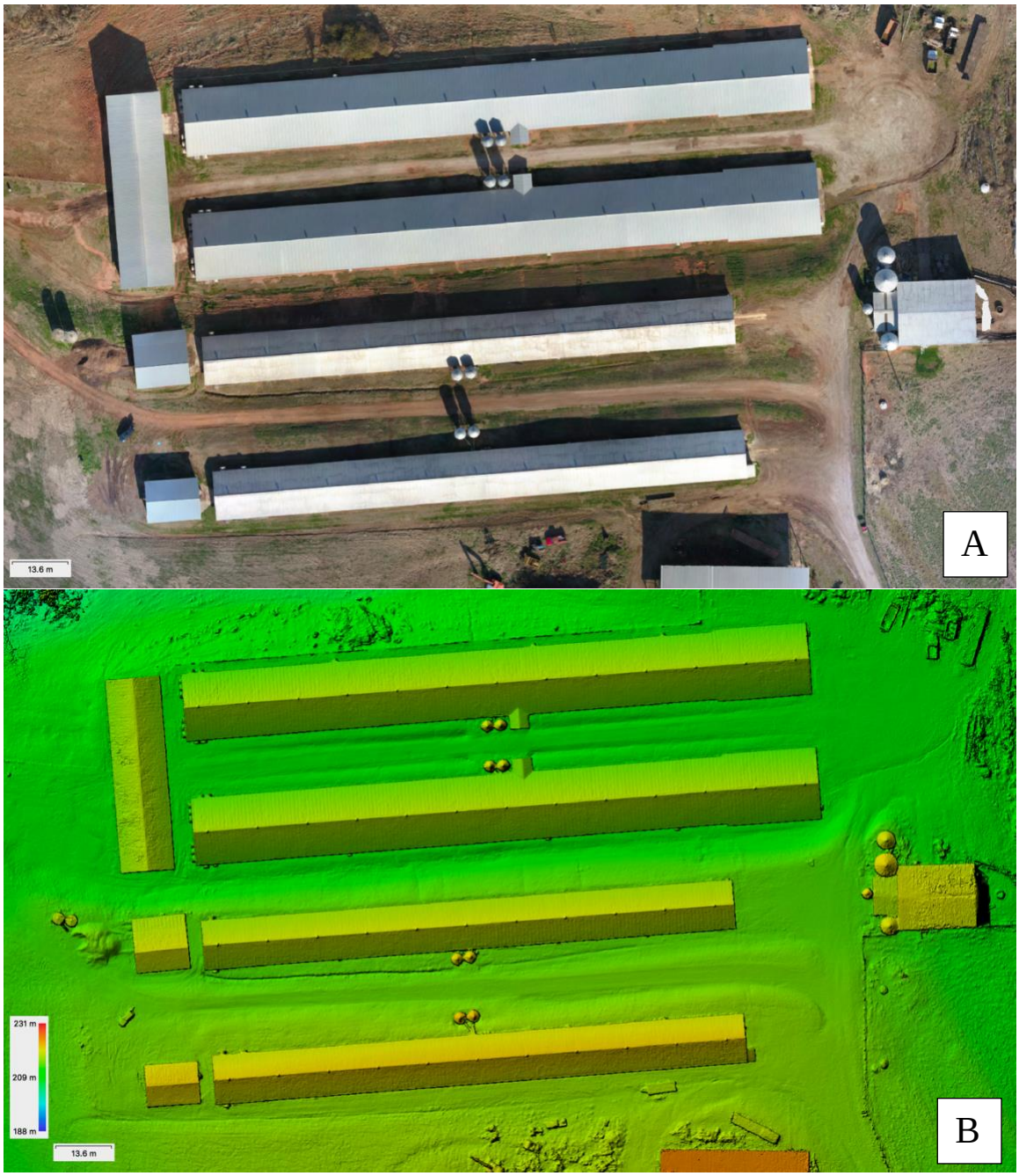

Figure 2.7 (a) Orthomosaic image (14,335x11,647, 1.93 cm/px) and (b) DSM (9,548 x 7,884, 3.86 cm/px) built from Dense Point Cloud (DPC).

Statistical Analysis and Comparison of Actual and Measured Dimesions Obtained from Remotely Sensed Imagery

Measured Error from UAV

The following section contains the results of the analysis of measurement error from the UAV in the horizontal and vertical planes. The horizontal difference analysis was broken into two relative groups: cartographic small scale and large scale. The UAV landing pad functioned as the large-scale horizontal difference analysis, and the poultry house building length and width dimensions functioned as the small-scale horizontal difference analysis. The poultry house building side wall, side entrance, and peak height measurements were used as the vertical difference analysis.

Landing Pad Diameter Measurements

The round pad was hand-measured 9 times in the field. The relatively small number of control trials was due to a low uncertainty associated with the simple hand measurements. The landing pad diameter was measured within the computer software orthomosaic image 31 times. These data are given in Appendix A, Table A1.

The results of the calculated differences between actual (hand) and predicted (UAV) measurements of the landing pad diameter are summarized in Table 2.4. This included the mean error (Equation 2.4), standard deviation, 95% CI (Equation 2.5), and percent error (Equation 2.6).

Table 0.4 Comparison of UAV landing pad diameter measurements.

	Hand	Software
n =	9	31
Mean Pad Diameter (cm)	74.5	74.6
Standard Deviation, s (cm)	0.111	1.120
$t_{0.025, (n-1)}$	2.306	2.042
Standard error (cm)	0.037	0.201
95% Confidence Interval (cm)	± 0.085	± 0.412

The round pad was hand-measured 9 times in the field. The relatively small number of control trials was due to a low uncertainty associated with the simple hand measurements. The average hand measurement in the field was 74.5 cm with a standard deviation of 0.111 cm. The field measurements had a 95% confidence interval of ± 0.085 cm (74.42 cm, 74.59 cm). The landing pad diameter was measured within the computer software orthomosaic image 31 times, which was reflective of the number of flight trials. The average software pad diameter measurement was 74.62 cm with a standard deviation of 1.120 cm. The software model had a 95% confidence interval of ± 0.412 cm (74.21 cm, 75.03 cm). The computed difference between the means was 0.16 cm, or 0.15%. The results show that there was no significant difference between mean pad diameter of physical pad and software pad at the 95% level (Steele and Torrie, 1997).

Poultry House Building Length and Width Measurements

Poultry house building length (L) and width (W) were each measured with plan dimensions obtained from the grower for 31 buildings, once at each farm. This was reflective of the number of flight trials. length (L_i) and width (W_i) were also measured within the UAV-derived orthomosaic image 31 times, and adjusted to account for rooftop overhand. These data are recorded in Appendix A. The building width measurements are

recorded in Table A2, and the length measurements are given in Table A3. A regression analysis of the horizontal building dimensions between blueprint dimensions and adjusted software measurements was done. The results of these measurement data plotted relative to each other are given in Figure 2.8.

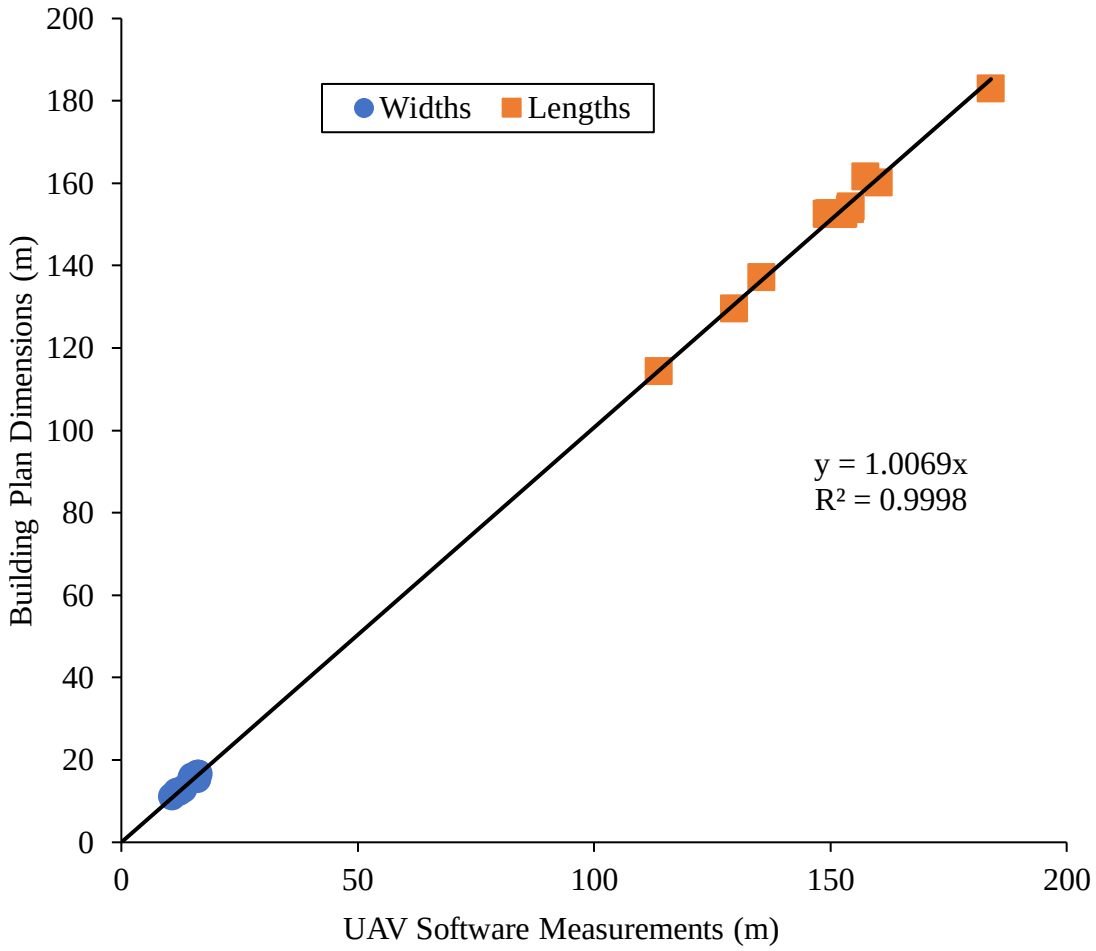

Figure 2.8 Regression of building length and width measurements between building plan dimensions and UAV software measurements (n=62).

The relationship between the 62 UAV measurements and blueprint dimensions had a linear trend line with a slope of 1.0069. This meant the UAV imagery overpredicts the building dimensions by 0.69%, on average.

The results of the calculated differences between the actual measurements (blueprint) and predicted measurements (UAV) for building length and width dimensions were summarized in Table 2.5. This included the mean error (Equation 2.4), standard deviation, 95% CI (Equation 2.5) , and percent error (Equation 2.6). Additionally, an F-test was performed on the length and width error variances, and it was determined that they were significantly different at the 95% level (the F statistic was 1.61, and the calculated F value was 12.523). Thus, the error measurements were kept separate and not pooled in the summary table. The deviation in poultry house building length was denoted as ΔL and deviation in poultry house building width was denoted as ΔW.

Table 0.5 Measured error of building length and width between UAV and plan dimensions.

	ΔW	**ΔL**
n=	31	31
mean error (m)	0.0468	1.6621
standard deviation (m)	0.3679	1.3021
variance (m)	0.1354	1.6954
std error of the mean (m)	0.0661	0.2339
$t_{.025, 30}$	2.042	2.042
95% CI (m)	± 0.135	± 0.478
Blueprint grand mean (m)	14.7681	151.5643
UAV grand mean (m)	14.7213	149.9022
mean percent error (%)	0.32	1.09

The mean error for building width measurements was 0.0468 ± 0.135 m. Building widths could accurately be measured in the digital orthomosaic to within 0.32%. The

mean error for building length measurements was 1.6621 ± 0.478 m. Building lengths could accurately be measured in the digital orthomosaic to within 1.09%. Both of the measurement error's confidence intervals encompassed zero, meaning UAV measurement error was not significantly different from zero at the 95% level.

Poultry House Building Height Measurements

Poultry house building height measurements were taken in the field at 38 instances. These same building dimensions were taken in the UAV derived DSM at 38 instances for paired comparisons. Poultry building sidewall, side entrance, and peak height measurements ranged from 1.86 meters to 5.61 meters. These data were recorded in Appendix A, Table A4. The results of a regression analysis of the building height hand and software measurements are given in Figure 2.9.

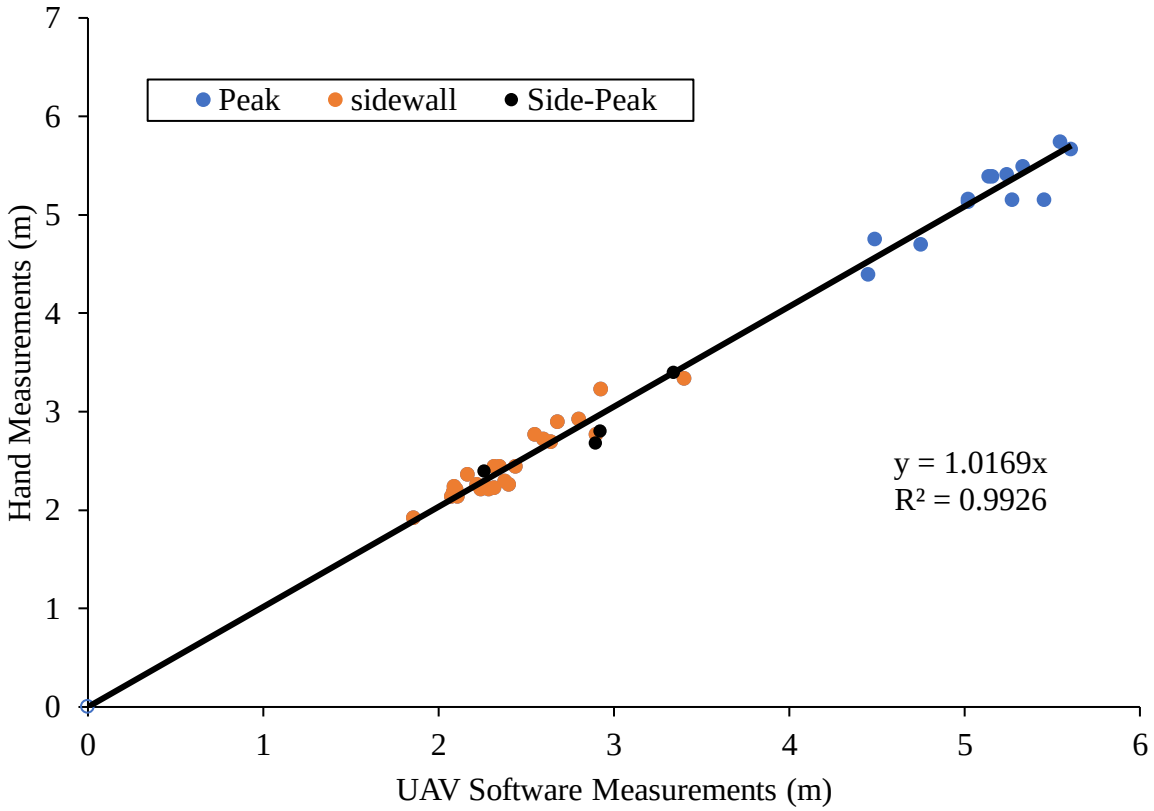

Figure 2.9 Regression analysis results between hand and software measurements of poultry house building side wall, peak, and side entrance heights (R^2 = 0.99; n=38).

The relationship between the 38 UAV measurements and hand measurements had a linear trend line with a slope of 1.0169. This meant that the UAV imagery overpredicted building heights by 1.69%, on average.

The results of the differences between actual (hand) and predicted (UAV) measurements for building height dimensions were summarized in Table 2.6. This included the mean error (Equation 2.4), standard deviation, 95% CI (Equation 2.5) , and percent error (Equation 2.6). The deviation in poultry house wall height was denoted as ΔH.

Table 0.6 Measured error of building heights between UAV and hand measurements.

	ΔH
n	38
mean error (m)	0.0617
standard deviation (m)	0.1338
variance (m)	0.0179
Standard error of the mean (m)	0.0217
$t_{.025, 37}$	2.026
95% CI (m):	0.0440
Hand measured grand mean (m)	3.395
UAV grand mean (m)	3.334
mean percent error:	1.82

The mean error between the hand and software measured values was 0.062 meters. The standard deviation of the software building height measurements was 0.1338 meters. The software model measurements had a 95% confidence interval of ± 0.0440 meters. A sensitivity analysis was done on the number of trials. A higher number of trials did not return a significantly lower t value.

Poultry House Rooftop Slope

Rooftop slope was examined for visited farms using the measured building width and height information as a ratio of height to width using equation 2.3. Of the 139 poultry houses visited in the study area only three houses had a 4:12 slope or 18.4º. All other houses had a 5:12 slope or 22.6º. In light of this 98% majority, it was determined that the assumed slope for all houses in the study area would be 5:12.

Measured Error from Satellite Imagery

The analysis of measurement differences from satellite imagery and blueprint dimensions in the horizontal plane are given in the following section. The difference

analysis was done on the discrepancy between actual building blue print dimensions and software measurement predictions of poultry house building length and width dimensions.

Building Length and Width Measurements

The 31 farms visited had a total 139 buildings. Building length and width measurements were each taken for each in Google Maps (Google, 2019). Width measurements ranged from approximately 12 m to 20 m, and length measurements ranged from approximately 115 meters to 188 m. These same measurements were compared with building blueprint dimensions provided by the grower for paired comparisons. These data were recorded in Appendix A. The building width measurements were recorded in Table A5, and the length measurements were given in Table A6. The results of a regression analysis of the building lengths and widths between satellite imagery and blueprints are given in Figure 2.10.

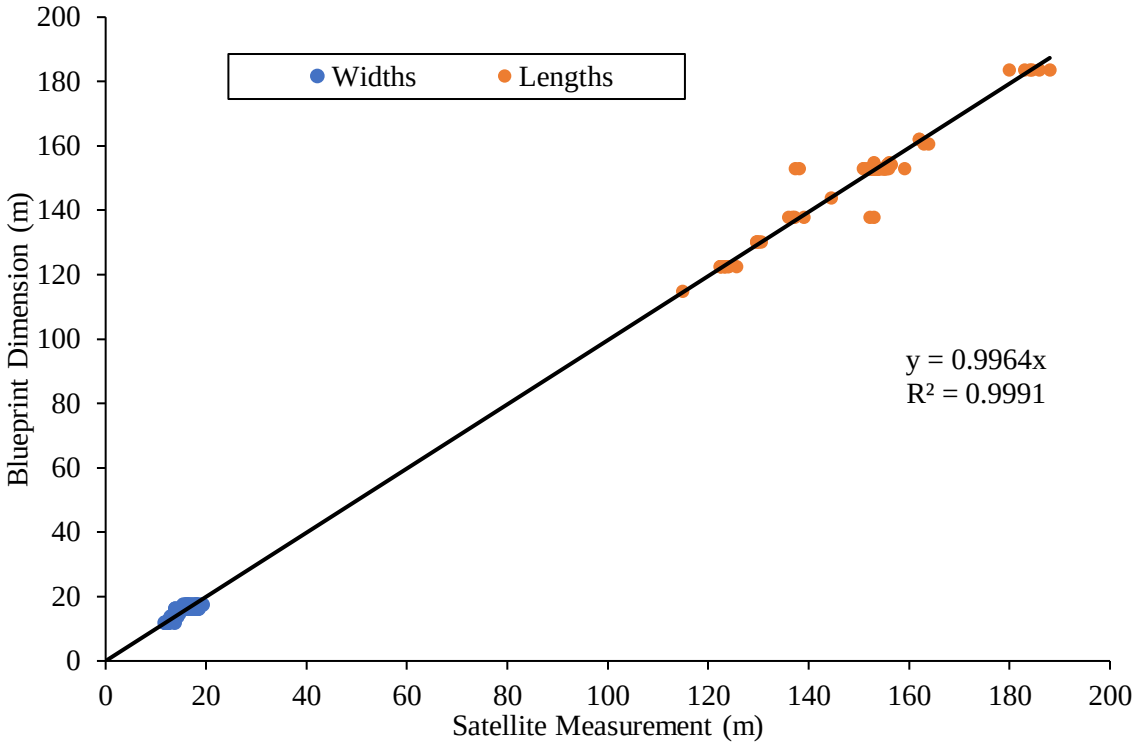

Figure 2.10 Regression analysis results between blueprint and software poultry house building length measurements from satellite imagery (n=278).

The relationship between the 278 satellite measurements and blueprint measurements had a linear trend line with a slope of 0.9964. This meant that the satellite imagery underpredicted the building footprints by -0.36%, on average.

The results of the differences between the actual (blueprint) and measured (satellite) measurements for building length and width dimensions were summarized in Table 2.7. This included the mean error (Equation 2.4), standard deviation, 95% CI (Equation 2.5), and percent error (Equation 2.6). An F test was performed on the length and width error variances, and it was determined that they were significantly different at the 95% level (the F statistic was 1.35, and the calculated F value was 12.0434). Thus,

error measurements were kept separate and not pooled in the summary table. The deviation in poultry house building length was denoted as ΔL. The deviation in poultry house building width was denoted as ΔW.

Table 0.7 Building length and width measured error between satellite and blueprints.

	ΔW	ΔL
n=	139	139
mean error (m)	-0.44	-0.46
standard deviation (m)	0.8151	2.8286
variance (m)	0.6643	8.2114
std error (m)	0.0691	0.2399
$t_{.025, 120}$	1.984	2.042
95% CI (m)	± 0.1372	± 0.4899
Blueprint grand mean (m)	15.62	150.18
Satellite grand mean (m)	16.06	150.63
average percent error (%)	-2.83	-0.30

The mean error between the blueprint width measurements and the satellite width measurements was -0.44 ± 0.1372 m. The satellite imagery could accurately predict building blueprint widths to within 2.83%. The mean error between the blueprint length measurements and the satellite length measurements was -0.46 ± 0.4899 m. The satellite imagery could accurately predict building blueprint lengths to within 0.30%.

Summary of Measured Error Results

The results of the statistical analysis of measured error, given in methods, are provided in Table 2.8. The deviation in poultry house width, length, and wall height were denoted with symbols ΔL, ΔW, and ΔH respectively.

Table 2.8 Summary of Method Results.

	UAV			Satellite	
	ΔW	ΔL	ΔH	ΔW	ΔL
n =	31	31	38	139	139
Mean error (m)	0.047	1.662	0.062	-0.443	-0.457
95% CI (m)	± 0.135	± 0.478	± 0.044	± 0.1372	± 0.4899

The mean error in building width measurements between the blueprint measurements and UAV measurements was 0.0468 ± 0.135 m (-0.09, 0.18). The mean error between the blueprint width measurements and the satellite width measurements was -0.443 ± 0.137 m (-0.58, -0.31). The UAV was more accurate on average for width predictions with a smaller average error. Additionally, the average satellite measurement error is below the confidence interval of the UAV measurements. The confidence intervals for the estimation of the mean do not overlap, meaning the measurement predictions were not in agreement. Lastly, the UAV confidence interval encompassed zero, meaning that there was no significant difference at the 95% level.

The mean error between the blueprint length measurements and the satellite length measurements was -0.457 ± 0.4899 m (-0.95, 0.03). The mean error for building length measurements between the building blueprints and UAV measurements was 1.6621 ± 0.478 m (1.18, 2.14). The satellite was more accurate on average for length predictions with a smaller average error. Additionally, the average satellite measurement error is below the confidence interval of the UAV measurements. The confidence intervals for the estimation of the mean do not overlap, meaning the measurement

predictions were not in agreement. Additionally, the satellite imagery confidence interval encompassed zero, meaning that there was no significant difference at the 95% level.

The rectangular dimensions of the buildings had an average length 10x larger than building width. The UAV operated at a significantly lower altitude than the satellite. This resulted in reduced field of view for the digital camera, and therefore an increased picture frequency. While building widths were typically captured in 1 to 3 photos by the UAV, building lengths required 10 to 15 pictures. If this were expressed as a ratio of image count required to capture building length-to-width, the UAV altitude would dictate a result of 10:1. In contrast, the satellite likely captured an entire building, if not an entire farm, in a single image frame. This would be a length-to-width ratio of 1:1. The increased quantity of photos needed by the UAV remote sensing would explain its larger average error in building length predictions. This lower ratio of images per building dimension may also explain the higher uniformity of error between building length and width measurements from satellite images.

DISCUSSION

This research sought to determine if using consumer-grade UAV's and photogrammetric SfM could create accurate DSM and orthomosaics of a study area, at efficient use of economic and temporal resources and without the use of survey grade equipment or GCPs. The software outputs were exceptionally high quality and can be used for further mapping and analysis. The results proved that consumer grade UAV technology can be used for the accurate collection of current geospatial data with typical

flight path parameters. This methodology established a balance between more economically expensive LiDAR collection methods, lower resolution satellite imagery, as well more time extensive field measurements by hand. Data could be collected and prepared quickly by a single individual. Most data collection, photogrammetric and geospatial processes also had the potential to be automated to increase efficacy and resource allocation further. Even the use of a flight path employing vertical image capture (verse oblique) did not compromise the quality of the model's vertical accuracy. These results could further be used for spatial mapping and analysis.

Two limitations within the experiment were found while remotely collecting data. The weather conditions were not always optimal for UAV operation. Occasionally winds in excess of 9 m/s made data collection impossible. Additionally, the Pix4D flight mapper application required mobile cell service to load background maps, or that the operator prepare digitally cached maps of the flight area over a WiFi network in advance. In several instances, maps could not successfully be loaded in the field due to poor cellular reception in the rural areas.

The accuracy of the GIS data results were highly sensitive to specific parameters employed during both the remote sensing data collection and the photogrammetry processes. Variation in UAV flight path or photogrammetric tie point limit could significantly impact the final reconstructed output.

CONCLUSIONS

(1) A UAV captured 8,043 images at 139 poultry houses in Anderson and Oconee Counties to produce GIS data for solar energy applications, and (2) photogrammetric processing produced dense point clouds of each flight location for a total of 1,626,284,298 points. Orthophotos of the study areas were generated from the acquired 3D image sequences using Structure from Motion (SfM) techniques. (3) The actual building widths and lengths ranged from 10.8 to 184.0 m and the measurement error within the UAV-derived orthophotos was 0.69% on average. Building width measured error was 0.047 ± 0.13 m, or 0.32% mean error. Building lengths had a mean error of 1.66 ± 0.48 m and 1.1% mean error. The actual building sidewall, side entrance, and peak heights ranged from 1.9 to 5.6 m and the measured error within the orthophotos was 1.69% on average. Building heights had a mean error of 0.06 ±.04 m or 1.2% mean error. The higher vertical error was expected with the given flight parameters (non-oblique imagery), which was more suited for horizontal accuracy. (4) In contrast, satellite-derived orthomosaic images of the same building widths and lengths had a measurement error of -0.36%. Building lengths had a mean error of -0.46 ± 0.49 m or -0.30% mean error. Building widths had a mean error of -0.44 ± 0.14 m and -2.83% mean error.

The results proved that using consumer-grade UAV's and photogrammetric SfM could create accurate DSM and orthomosaics of a study area at efficient use of economic and temporal resources without the use of survey grade equipment or GCPs. When compared to the horizontal accuracy of readily available satellite imagery, the results were mixed. The satellite-derived orthomosaic was more accurate on average for length

predictions with a smaller average error. However, the UAV-derived orthomosaic images were more accurate for average width predictions.

The the disparity in horizontal measurement accuracy between the compared remote sensing techniques was likely due to flight altitude and building shape. The rectangular building dimensions had an average length-to-width ratio of 10:1. The lower flight altitude of the UAV required 10 to 15 pictures to capture building lengths, and only 1 to 3 photos for building widths. In contrast, the satellite field of view likely captured an entire building, if not an entire farm, in a single image frame. This would result in less stitching error in remodeling building length and may also explain the higher uniformity of error between building length and width measurements from satellite images.

The satellite imagery had low cost and ease of access that allowed a convenient determination of structural orientation and planimetric dimensions. However, the UAV provided dependably current data, whereas the temporal accuracy of satellite imagery data was highly variable (sometimes ±12 months). The UAV-derived data was also useful for determining vertical dimensions, and therefore variables such as surface slope and aspect. Lastly, the UAV-derived data was more useful for absolute accuracy to establish true object positions in a geodetic coordinate system. This would be critical for analysis of spatial distribution or combining data with GIS data layers from other sources. With an average flight time of 13.5 minutes per farm area (2.5 ha), and an average GSD of 4.84 cm/pi, the results obtained from a relatively inexpensive UAV mounted camera and image analysis demonstrated sufficient accuracy for planning and monitoring purposes in agricultural applications.

CHAPTER THREE

POTENTIAL OF BROILER ROOFTOP PHOTOVOLTAICS AS DISTRIBUTED PEAK-SHAVING PLANTS FOR SUPPLY SIDE LOAD MANAGEMENT

Abstract

The primary challenge faced by energy suppliers is forecasting and supplying hourly peak demand. Generating supply at peak demand and efficiently distributing to remote customers are vital supply-side load management practices for controlling supplier cost. This research sought to determine if poultry farms could function as rurally distributed, peak-demand photovoltaic (PV) power plants to sparsely populated areas. Unmanned Aerial Vehicles (UAV) and satellite imagery were used to examine 88 poultry farms. The typical farm consisted of four poultry houses, each 15.2 meters by 152.4 meters, oriented East/West, with a rooftop slope of 22.6º and a suitable rooftop area of 1,254 m_2. The average rooftop supply of all farms was calculated and grouped into key supply categories of seasonal peak, shoulder, base, and energy. The average supply from a farm of typical size was 496 kW/hr during peak periods, 279 kW/hr during summer shoulder periods, and a contribution to base load of 425 kW/hr during summer months. The average rooftop supply estimated for all 88 farms was 59.2 MW/h during summer peak, a contribution to summer base load of 47.0 mW/hr, and total annual energy supply of 127.3 GWh/yr. Calculations of facility demand and energy use were in the range of 10-20% of gross hourly rooftop supply across time categories. This resulted in a net peak demand reduction potential of 51.6 MW/h (83%), and an annual net supply of 109.4 GWh (86%) to the grid. In light of distribution costs, the twenty-seven farms located

further than 3.28 km from existing transmission lines proved the most valuable in peak demand reduction and distributing energy to rural areas. Results suggest a promising potential for distributed PV adoption for peak-shaving.

INTRODUCTION

Energy suppliers face many challenges in current energy markets. A primary challenge for energy suppliers is the uneven demand for electricity throughout the day. This variation is categorized into a higher 'peak load', transitional 'shoulder' period, and lower 'base load' for a given region of customers (Kostková et al, 2012). Base load is the average expected demand, while shoulder and peak load generally refers to the daily fluctuation between baseload and peak electric demand. Weather heavily influences consumer demand depending on cooling loads in summer and heating needs of a region in winter. Summer peak loads are predominantly controlled by cooling provided by air conditioning in residential and commercial buildings and ventilation of agricultural production facilities. Winter peak loads are predominantly heating equipment such as heat pumps, furnace fans, strip heat in commercial and residential buildings whereas furnace fans, minimum ventilation fans, lighting and heat lamps in swine nurseries are used in agricultural buildings. Peak demands are higher in summer than winter for all utilities in the Southeastern US. The variation in electrical demand (MW) data when graphed over time is known as a demand curve. Electrical demand curves for the longest and shortest day of the year in 2018 and 2019 for a major investor owned utility, SC Duke Energy Progress (DEP), were selected to illustrate common variation between

summer and winter. This data was obtained from the Energy Information Administration (EIA). The system demand curves for these two days, along with the hours of the day that are defined as base, shoulder, and peak are provided in Figure 3.1.

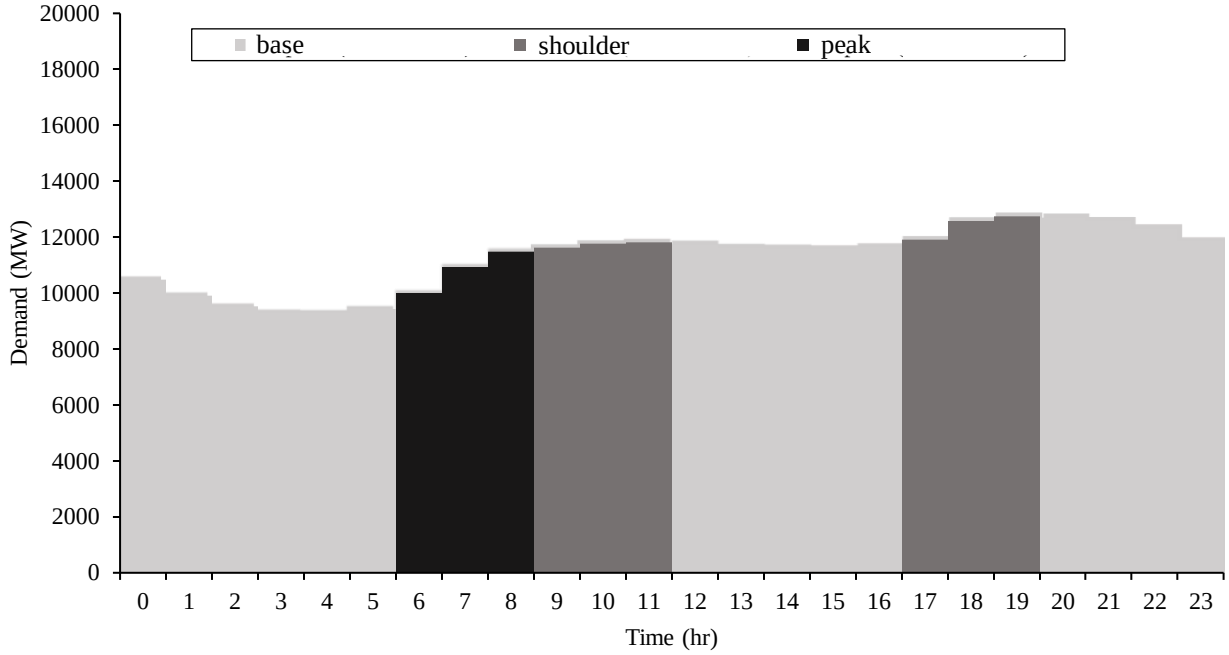

(a) Winter Demand Curve (December 21st 2018)

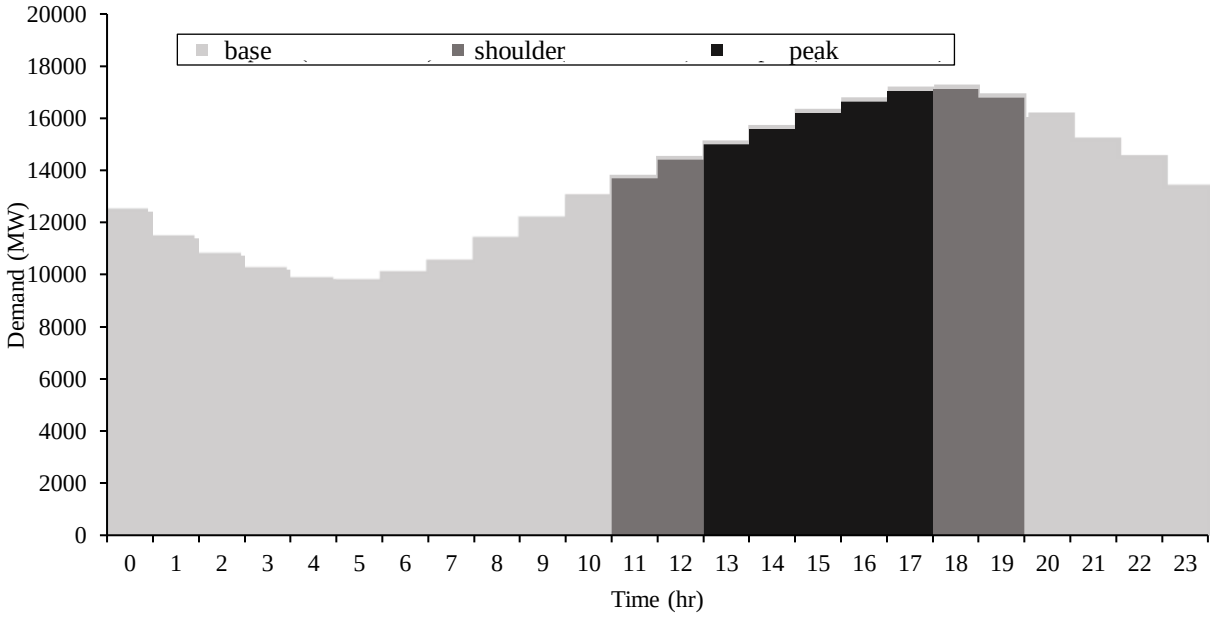

(b) Summer Demand Curve (June 21st 2019)

Figure 0.1 (a) Winter solstice and (b) summer solstice demand curves (US EIA, 2019) and time-of-use categories (DEP, 2019).

Electric utilities must meet fluctuating customer demand each day. Most utilities divide the year into winter and summer demand seasons to match the seasonal shifts in demand periods. The six-month winter season for DEP began in October and lasted until the end of March. The summer demand season began April 1st and continued until September 30th. Figure 3.1 (a) illustrates the recorded hourly demand for DEP on December 21st, 2018. Base time of use category was between the hours of 0:00 and 5:00, 12:00 to 17:00, and 20:00 through 0:00. The average hourly base load for those hours was 9,656 MW with a minimum of 9,287 MW at 3:00 and a maximum of 12,698 MW at hour 20:00. Peak load times occurred between 6:00 and 9:00. The average hourly maximum load was 10,802 MW with a minimum of 10,000 at 6:00 and a maximum of 11,481 at 8:00. Shoulder period was between 9:00 and 12:00, and 17:00 through 18:00. The average hourly shoulder load was 12,072 MW with a minimum of 11,615 MW at hour 9:00 and 12,755 MW at hour 19:00. The data reflected a discrepancy between when demand was expected to peak (6:00 to 9:00) and when demand actually peaked (18:00 to 20:00). This discrepancy was likely due to atypical lower temperatures and demonstrates the challenge suppliers face in accurately forecasting hourly demand.

Figure 3.1 (b) shows the recorded hourly demand on June 21st, 2019 for the same utility (DEP). The time of use categories for each hour varied between the summer and winter seasons. The summer base category was between 0:00 and 11:00, and 20:00 through 23:00. The average hourly base load was 11,015 MW ranging from 9,736 at 5:00 to 14,438 MW at 20:00. The average base load for the summer data was 1,359 MW higher than the average recorded base load for the winter data. The summer shoulder

period was from 11:00 to 13:00, and 18:00 to 20:00. The average hourly shoulder load was 15,497 MW. Peak hours were between 13:00 and 18:00. The average hourly peak load was 16,097 MW ranging from 15,008 MW at 13:00 to 17,043 MW at 17:00. The average peak load for the summer data was 5,295 MW higher than the average recorded peak load for the winter data.

Accurately forecasting hourly peak demand has critical economic impact for an electric supplier (DEC, 2017). Small capacity power plants known as peaking plants are typically used to meet variable demand during peak and shoulder periods. Effort to supply electrical power during times of peak demand is referred to as peak-shaving. This additional peaking infrastructure creates additional cost for suppliers.

Various fuel sources have been used for electric power generation depending on economic and temporal characteristics (Raymond, 2009). The levelized cost of energy (LCOE) has been used to compare electric generation technologies. The levelized costs include the cost to build, finance, operate, and maintain the infrastructure. A summary of levelized costs by fuel type for the US in 2018 are given in Table 3.1.

Table 0.1 Average levelized cost of electricity (LCOE) in the USA by generation resource.

Plant Type	Average for existing electric plants ($/kWh)[1]	Average projected for plants not built ($/kWh)	Average levelized transmission cost ($/kWh)[2]	Range of distribution cost ($/kWh)[3]
Coal[4]	0.040	0.070[1]	0.0011	0.0026 - 0.0043
Gas, combined cycle	0.035	0.040 - 0.045[2]	0.0011	0.0026 - 0.0043
Gas, combustion turbine	0.087	0.075 - 0.086[2]	0.0032	0.0026 - 0.0043
Nuclear	0.032	0.077[2]	0.0010	0.0026 - 0.0043
Geothermal	-	0.040[2]	0.0014	0.0026 - 0.0043
Biomass	-	0.091[2]	0.0012	0.0026 - 0.0043
Hydroelectric	0.037	0.038[2]	0.0016	0.0026 - 0.0043
Wind, onshore	-	0.053[2]	0.0025	0.0026 - 0.0043
Solar Photovoltaic	-	0.06[2] - 0.09[1]	0.0034	0.0026 - 0.0043
Wind, offshore	-	0.09[1] - 0.13[2]	0.0023	0.0026 - 0.0043

[1]Derived from the Institute of Energy Research (Stacy et al, 2018).
[2]Derived from *Annual Energy Outlook, 2019* by U.S. Energy Information Administration (US EIA, 2019).
[3]Derived from Electricity Distribution System baseline Report for US Department of Energy (Warwick, et al, 2016).
[4]Assumes plant technologies that satisfy current CO_2 emission standards under NSPS, Section 111(b) of Clean Air Act (EPA, 2015).

Resources used for generating electricity were ranked by traditional use and expressed in USD/kWh. The most common resources were coal, natural gas, and nuclear due to lower generation costs. Renewable energy has been viewed as an attractive alternative to fossil fuels due to significantly lower fuel costs (Klaić et al, 2015). However, LCOE calculations demonstrate that inclusion of capital cost required to harvest renewable resources outweighed operating savings, thus rendering renewable energy generally more expensive per kWh (Warwick et al, 2016). Existing LCOE values for geothermal, biomass, wind, and solar fuels were not available from DOE, EIA, FERC, or IER databases. The generation costs distinguished existing and unbuilt plants to account for the additional expense to permit, build and operate new plants.

Another challenge for energy suppliers was transporting the energy between power plants and consumers.

Distribution infrastructure had investment and maintenance expenses, and reportedly increased from thirty-two billion dollars in 1997 to fifty billion dollars in 2017 (US EIA, 2018). Despite this significant expenditure, the American Society of Civil Engineers stated in a 2017 infrastructure report card that the existing U.S. infrastructure consisted of complex, inflexible networks that are overdue for maintenance and upgrades (ASCE, 2019). Electricity was also lost over distance traveled via resistance voltage losses and amperage conversions with transformers. The U.S. EIA estimated that average annual line losses nationwide due to transmission and distribution (T&D) between 2013 and 2017 were 5% of total generation in urban areas and 6% in rural areas (US EIA, 2019). Rural environments had lower population density and were farther removed from centralized electric generation plants, resulting in greater line losses than urban suppliers. Generating supply at peak demand and efficiently distributing to customers that are far from main transmission lines are vital supply-side load management practices for controlling supplier cost.

Each energy customer had a unique cost to supply as a function of their location, time of use, rate of use (demand, kW), and total amount used (energy, kWh). Ranges of typical energy rates from three investor owned utilities and three rural electric cooperatives within SC were obtained. The energy rates for the investor owned utilities are compared in Table 3.2.

Table 0.2 Range of electricity rates for investor owned utility companies in South Carolina.

	Residential and small agricultural[1,2]	Irrigation[2]	Industrial and large agricultural[2,3]
I. Service Charge ($/month)			
Non-seasonal:	9 – 13	9 – 23	25 - 1875
II. Energy Charge ($/kWh)			
Non-seasonal:	0.09	N/A	0.04
Time of Day Use			
Summer peak:	0.08 - 0.27	0.22	0.08
Summer off peak:	0.07 - 0.09	0.07	0.04
Winter peak:	0.08 - 0.25	0.13	0.05
Winter off peak:	0.07 - 0.09	0.07	0.04
Quantity of Use			
0 to 1,000 (kWh):	0.11	0.12	0.12
1,000 to 3,000 (kWh):	0.12	0.13	0.12
> 3,000 (kWh):	0.12	0.13	0.05
III. Demand Charge ($/kW)			
Non-seasonal:	N/A	N/A	4.74 - 14.6
Summer:	10.5	N/A	17.7 - 21.2
Winter:	7.5	N/A	4.68 - 5.28

1 Duke Energy (DEP, 2019)
2 South Carolina Electric and Gas (SCEG, 2019)
3 Lockehearte Power (Lockeheart Power, 2019)

Major customer categories included residential, agricultural, and industrial. Energy price was a combination of supply infrastructure, peak demand, and energy charges. Meeting peak demand was often the majority component of determining electric prices. For example, peak energy prices were three times higher than base energy prices for residential and agriculture customers. Industrial customers had a high facility charge due to T&D infrastructure needed to supply high demand and high energy use, and in three-phase. Energy rates from rural cooperatives within SC are given in Table 3.3.

Table 0.3 Range of electricity rates for rural electric cooperatives in South Carolina.

	Residential and small agricultural[1,2]	Irrigation[2]	Industrial and large agricultural[2,3]
I. Facility Charge ($/mo)	18 - 30	9 - 13	45 - 13,900
II. Energy Charge ($/kWh)			
Non-seasonal:	N/A	N/A	0.06
Time of Day Use			
Summer peak:	0.14 - 0.24	0.20	0.27
Summer off peak:	0.06	0.07	0.06
Winter peak:	0.12 - 0.20	N/A	0.27
Winter off peak:	0.06	N/A	0.06
Quantity of Use			
0 to 500 (kWh):	0.14	0.14	0.05 - 0.07
500 to 1,000 (kWh):	0.13	0.13	0.06
> 1,000 (kWh):	0.12	N/A	0.04 – 0.05
III. Demand Charge ($/kW)			
Non-seasonal:	N/A	N/A	N/A
Summer:	10.5	N/A	6.5
Winter:	7.5	N/A	N/A

1 Lynches River Electric Cooperative (US EIA, 2019)
2 Berkeley Electric Cooperative (BEC, 2019)
3 Aiken Electric Cooperative (AEC, 2019)

These electric rates were selected from cooperatives that represented the range of rate schedules across the state. Rural cooperatives charged residential customers a facility charge that was twice as large as investor owned. Industrial customers had a peak demand charge three times larger than industrial customers in a municipal setting. High use rural industrial customers had an exceptional monthly facility charge of $13,900, which was over 1000 times greater than other customer categories. This was due to the infrastructure needed to supply high use customers. Rural customer classes all have more specific quantity categories for energy price compared to investor owned.

As of 2019, the largest agricultural commodity in South Carolina was the poultry industry (USDA, 2019). Poultry production is dependent on climate-controlled buildings that required large ventilation loads. Energy use data taken from seven SC broiler farms

between 2003 and 2007 demonstrated an average annual electrical use of 2,504 kWh per 100m2/yr, with a range of 1,714 to 3,598 kWh per 100m2/yr (Chastain, 2016). The typical broiler house with a floor area of 2,322 m2 required approximately 45,072 kWh/yr (Chastain, 2016). Furthermore, electricity, on average, was over 50% of the annual energy cost (Chastain, 2016) which included the use of LPG or natural gas in the winter season.

The goal of this project was to examine the potential for using roof-mounted photovoltaic (PV) panels on poultry farms to serve as distributed peak-shaving power plants in a costly to serve rural area. The typical broiler house roof tilt, size, orientation, quantity and available sun all support the harvest of solar insolation. An aerial image of three farms in the study area is given in Figure 3.2.

Figure 0.2 Three poultry farms in study area, one with a partial PV installation.

Poultry farms are usually located in rural areas with a low population density far from centralized electric power production, and in some cases are remote from main transmission lines. Poultry farms are also typically spatially confined to approximately an 80 km radius from their contracted integrator company. As can be plainly seen in Figure 3.2, broiler farms are cleared of vegetation, making them ideal for PV relative to most residential and urban buildings. Additionally, the National Poultry Technology Center concluded that the size and weight of rooftop PV posed no threat to the structural integrity of a poultry house (Dennis et al, 2016).

For energy suppliers the challenge of peak demand was caused by solar energy. As solar energy increased for a given region, so did ambient temperature, and so did air conditioning demands in response. Solar irradiance was also the fuel for electricity generation by a PV installation. The additional solar gain produced additional PV electric output almost directly coincided with increased electric loads for climate control. With PV technology the potential exists for solar irradiance may contribute to the problem and solution. Furthermore, an important facet of power supply was managing fuel input to the generating equipment. In the case of PV plants, the increase of solar energy throughout a given day is independent of human oversight. This would function as automated fuel management for a PV peaking-plant. Other potential benefits of an energy supplier using rural poultry house PV include utilization of pre-existing land and distribution costs, as well as in house resources for electricians and permitting. A mutually beneficial partnership between the utility and their agricultural customers would even allow greater

flexibility in initial project scope and assist in accelerating economic development for the surrounding territory.

The objectives of this study were to (1) determine the electrical energy use for individual poultry houses in a broiler producing area in South Carolina, and (2) examine the potential of using buildings on groups of poultry farms as peak shaving power plants in a rural area.

METHODS

The study area was Oconee and Anderson counties in the northwestern Appalachian region of South Carolina. There were 88 poultry farms. An address list of permitted poultry growers in the study area was obtained from the South Carolina's Confined Animal Manure Managers program (Smith, 2017). This address list was validated by satellite imagery using Google Earth. A map of the study area and locations of these poultry farms are provided in Figure 3.3.

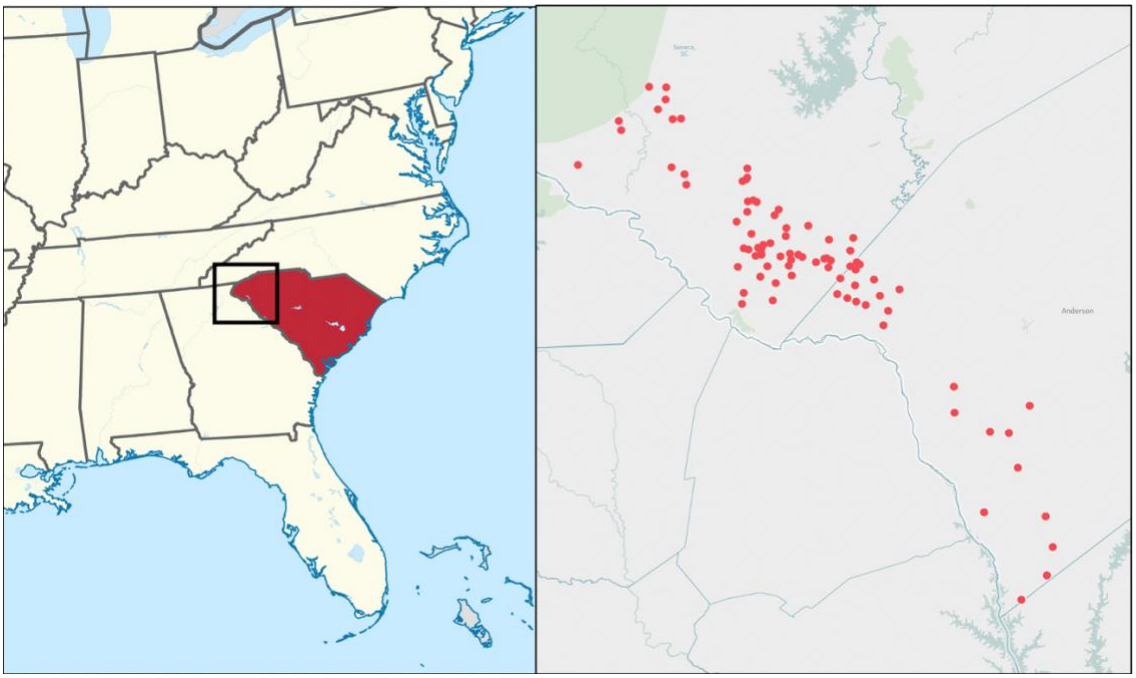

(a) **(b)**

Figure 0.1 (a) The geographical location of South Carolina in the southeastern United States. (b) The georeferenced 88 poultry farms within Anderson and Oconee Counties (ESRI, 2019).

The building characteristics of interest were building length (L), width (W), sidewall height (H_s), peak height (H_p), roof slope, and roof azimuth. Data collection for these variables entailed a combination of remote sensing techniques validated by physical measurements as benchmarks. Measurement methodology is described in the subsequent sections for each of these variables.

Poultry Building Data Collection from Farm Visits

Information used from the methods and results section in Chapter II was used for this study. Thirty-one farms were visited in the study area, which constituted 139 houses and 35% of the population.

Building Length and Width Dimensions

The grower provided building length and width measurements for the 31 farms visited from building blueprints, accurate to 0.312 cm. A UAV was also used to collect aerial images of the farm buildings at each site. A DJI Mavic Pro UAV with an onboard 4K digital camera flew a double-grid flight pattern at 69 m altitude using 80% and 70% image overlap. The UAV landing pad was used in each flight to ensure horizontal accuracy and precision of the digital data. Structure-from-motion (SfM) processing was done on aerial images to reconstruct orthomosaic images of the farms.

Building width and length measurements were done on a single building at each of the 31 visited farms. The building footprint cannot be seen from above due to roof overhang. The building rooftop lengths (L_i) and widths (W_i) were measured using the Ruler tool (Agisoft, 2019) on each farm's orthomosaic image. To account for overhang, an estimated known value was subtracted from the overall building roof lengths (L_i) and widths (W_i). This method was done using Equations 2.1 and 2.2 from Chapter II. The extent of sidewall overhang was 0.4572 m on each side of the building. The extend of end wall overhang was 0.3048 m on each end. A total of 0.9144 m was subtracted from the overall building roof width (W_i) and a total of 0.6096 m was subtracted from the overall

building roof length (L_i) dimensions. This allowed the measurement of building footprint dimensions in satellite imagery despite visual interference from rooftops.

The UAV imagery overpredicted the building dimensions by 0.69%, on average. The coefficient of determination was 0.9998, meaning that 99.98% of the sample variation in blueprint measurements was explained by the UAV measurements using the given least squares line.

The mean error for building width measurements was 0.0840 m with a standard deviation of 0.3035 and a 95% confidence interval of 0.111 m. The mean error for building length measurements was 1.6621 m with a standard deviation of 1.3021 and a 95% confidence interval of 0.478 m. The UAV measurement error for horizontal building dimensions was not significantly different from zero at the 95% level.

The poultry building lengths and widths were also measured using readily available satellite imagery provided by Google, Maxar Technologies, and US Geological Survey (Google, 2019). The building rooftop lengths (L_i) and widths (W_i) were measured using the Measure Distance tool (Google, 2019) on satellite imagery. The satellite imagery underpredicted building footprints by -0.36% on average, with an R^2 of 0.9991.

Adjusted building width (W) and length (L) measurements from satellite imagery were compared to building blueprints. The mean error between the blueprint width measurements and the adjusted satellite width measurements was -0.44 m with a standard deviation of 0.8151 m and a 95% confidence interval of 0.1372 m. The mean error between blueprint length measurements and the satellite length measurements was -0.46 m with a standard deviation of 2.8286 m and a 95% confidence interval of 0.4899 m.

Building Orientation and Rooftop Azimuth

Azimuth (aspect) is defined as a slope's downward facing direction. It is measured clockwise in degrees from 0 (due north) to 360 (also due north) in a complete circle. The azimuth class for each visited poultry building rooftop was determined for solar energy calculations. Every poultry building had an identical roof structure of open gable. This means the roof area of each building consisted of two planes of equal area that sloped symmetrically away from a central ridge. The rooftop ridgeline was oriented parallel to the length of the building. The roof azimuth of each plane was oriented perpendicular to the length of the building orientation. The relationship between rooftop azimuth direction and building orientation can be seen in Table 3.4.

Table 0.1. Building rooftop azimuth and orientation classes.

Range of Roof Azimuth (º)	Rooftop Azimuth Class	Building Orientation class
157.5 to 202.5	South	East-West (E/W)
112.5 to 157.5	Southeast	Northeast-Southwest (NE/SW)
202.5 to 247.5	Southwest	Northwest-Southeast (NW/SE)
247.5 to 292.5	West	North-South (N/S)
67.5 to 112.5	East	North-South (N/S)

Every cardinal direction class constitutes 45 degrees *e.g. a rooftop plane with an azimuth between 157.5° and 227.5° was classified as "South".* Azimuth was determined for farms visited using the GIS data produced from UAV images. This was done with the Aspect surface tool on each farm's DSM in ArcGIS Pro (ESRI, 2019). Each individual surface unit (0.15 meters) of the DSM was assigned an aspect class. Some roof area was excluded based on orientation. All roof planes with an aspect class of NW, N, or NE (292.5˚- 67.5˚) were considered unsuitable for PV and excluded (Margolis et al, 2016).

Building Rooftop Slope

Rooftop slope was calculated for visited farms using recorded building width and height information. Building peak heights and sidewall heights were recorded at farm visits. These building heights were measured with a tape measurer (accurate to 0.16 cm) from the concrete base to just under the building eave. It was determined that only three houses out of the 139 houses visited in the study area had a 4:12 slope, or 18.4º. All other houses had a 5:12 slope, or 22.6º. In light of this 98% majority, it was determined that the assumed slope for all houses in the study area would be 5:12.

The known roof slope was then used with the known building footprints to determine building rooftop area. This was done using the geometry equation for the hypotenuse of a triangle. Given a slope of 22.6º the amount of existing rooftop area (m^2) was determined to be 1.083 times that of building footprint area (m^2).

Global Solar Irradiance Availability by Slope

To determine the optimal slope for a PV rooftop array, a preliminary sensitivity analysis was done to compare irradiance in the study area on surfaces of different slopes. This would decide if brackets should be used to mount the PV panels at a specified slope other than the existing slope of the building rooftop. The existing rooftop slopes was 22.6°. In the literature review, some researchers made the case that the strongest relationship existed specifically between optimal PV panel slope and the latitude of the study area. A slope equal to site latitude was 34.5°. These two values were used to explore how slope affected irradiance. Measured global solar irradiance values were

taken from the National Solar Radiation Database (NSRDB) provided by the National Oceanic and Atmospheric Association (NOAA). Data consisted of recorded direct, indirect, and global irradiance throughout a year over eight decades. Irradiance for the study on slopes of both angles were compared at each azimuth class. The results are given in Table 3.5.

Table 0.2 Average annual solar irradiance (kWh/1000m2/day) by tilt for each azimuth class.

Azimuth class and orientation	34.5o Slope	22.6o Slope
East (90º)	4,370	4,580
Southeast (135º)	5,130	5,140
South (180º)	5,470	5,380
Southwest (225º)	5,170	5,170
West (270º)	4,410	4,610

The measured solar irradiance on slopes of 22.6 degrees were higher than irradiance values on slopes of 34.5 degrees for every azimuth class except south. The total annual average irradiance of all classes for existing building rooftop slopes received 1% more annual solar radiation than solar panels arrayed at a slope of 34.5°. In light of this, the PV panel slope for the peak reduction analysis was maintained at the existing building rooftop slope for the study.

Buildings oriented North and South (azimuth classes E/W) provided a unique opportunity compared to other building orientation classes. Although the annual average solar irradiance on slopes with azimuth classes East and West was less than slopes oriented south, these buildings had two planes sufficient for PV use. All other building

orientations only had one suitable rooftop plane per building, effectively half of its rooftop area. Therefore, these buildings could have PV installed on twice the available area relative to all other orientation classes in the study population.

Poultry Building Data Collection from Satellite Imagery

For the 55 poultry farms (267 houses, or 65% of population) in the study area that were not visited, satellite imagery was used to measure building length, width, number of houses per farm, and rooftop azimuth/building orientation. This imagery data was provided Google, Maxar Technologies, and US Geological Survey (Google, 2019).

Building Length and Width Dimensions

Building lengths and widths of farms not visited were examined similarly to the methods discussed previously and in Chapter II. The building rooftop lengths (L_i) and widths (W_i) were measured using the Measure Distance tool (Google, 2019). Equations 3.1 and 3.2 were used to adjust building width (W) and length (L) measurements for overhang.

Determining Building Rooftop Area Available for PV

Poultry building rooftops are exceptional relative to other facilities for PV installation. Therefore available roof area calculations were not limited by HVAC or other preexisting rooftop installations. The adjusted rooftop dimensions were used to estimate the available rooftop area, calculated as:

$$A = (S \times W \div 2) \text{ x } L. \quad (0.1)$$

Where,
A = available rooftop area for PV panel installation (m^2), and
S = Rooftop slope conversion factor (1.083).

The rooftop area was determined as a function of building footprint and roof slope. The area of available rooftop for PV installation was 1.083 multiplied by house width, then divided by two. This represents the width of a single rooftop plane, which is then multiplied by the length of the house. This method was applied to all houses in the study area. Buildings that were oriented North/South were not divided by 2, since they uniquely had two roof planes suitable for PV installation.

Spatial Distribution of Houses

The spatial distribution of the poultry houses was also analyzed. Farm centroid coordinates were compiled into ArcGIS Pro (ESRI, 2019) software for geospatial analysis. To consider distribution costs and line losses associated with energy generation, a proximity study consisted of a measure of distance between each poultry farm and the nearest transmission line. GIS data for the transmission lines was provided in the US Homeland Infrastructure Foundation Level Data library by the Department of Homeland Security (DoHS, 2019). The proximity study consisted of a measure of Euclidean distance between each poultry farm and the nearest transmission line using the Near tool in ArcGIS Pro (ESRI, 2019).

Building Orientation and Rooftop Azimuth

The building orientation for farms not visited were examined in the satellite imagery. The rooftop ridgeline orientation was determined in the images. The roof azimuth of each plane was calculated as a perpendicular orientation from the building ridgeline. Every rooftop was assigned a rooftop azimuth and orientation using Table 3.4

Shading

As demonstrated in Figure 3.2, the lack of existing neighboring structures vastly decreased the potential for impeded solar energy. Solar illumination issues were dealt with on basis of exception. For the instances where solar energy obstruction was in question a study of seasonal illumination duration on building rooftops was done using a hillshade analysis (ESRI, 2019) expounded on in Appendix A. A total of three houses were deemed to be significantly shaded as to justify their exclusion from the analysis.

Calculation of Electric Power Produced by Rooftop PV Arrays

Suitable roof area measurements were converted to PV capacity and electrical generation for all 398 houses (the 139 houses visited as well as the 267 houses not visited) to produce sum PV production estimates for the study area.

The amount of electricity an energy plant is capable of generating is referred to as its technical potential (Lopez et al, 2012). This common benchmark quantifies generation in light of fuel availability and quality, the performance of the technology harvesting the fuel, and the physical area suitable for installation. However, these methods operate

under a standardized operating assumption of solar energy measuring 1,000 W/m^2 for solar energy installations. This can be helpful for performance comparisons yet also highly misleading. Technical potential for a generation facility's technical potential essentially functions as a ceiling limit of a technology's present potential generation, not a realistic prediction of expected development. The main objective for this study was to calculate actual electrical production based on real irradiance for the study area. Therefore the formula used to calculate the hourly electric power produced by a PV array installed on one slope of a poultry house roof was (PVSoftware, 2009):

$$\mathbf{E = (f_C \times A) \times I \times r \times PR.} \qquad \mathbf{(0.2)}$$

Where,
E = Hourly electric power produced by a rooftop PV array (W/hr_{AC}),
f_C = Ratio of solar cell area to available roof area,
A = Available roof top area (m^2),
I = Hourly solar irradiance falling on PV array (W/m^2/hr, global),
r = panel efficiency, electrical power output (W_{DC}/m^2/hr) ÷ solar irradiance input (W/m^2/hr), and
PR = Performance ratio, coefficient that accounts for losses due to conversion from DC to AC power and other array performance losses.

Estimation of the Ratio of Solar Cell Area to Available Roof Area (f_C)

The dimensions of productive solar cell collector area were a fraction of the total PV installation footprint. An estimated ratio was calculated to accurately determine the total amount of SOLAR cell area per building and per farm, given in Table 3.6.

Table 0.3 Estimation of the ratio of solar cell area to available roof area (f_C) for a broiler building excluding roof overhangs.

Building Characteristics	
Floor plan length (L, m) =	152.4
Floor plan width (W, m) =	15.2
Rooftop slope =	5/12
Rooftop area (A) to mount PV panels (equation 3.3, m^2) =	1254
PV Panel Characteristics	
Panel length (m) =	1.0
Panel length (m) =	1.65
Area of a PV panel (m^2) =	1.65
Width of PV panel frame =	0.0254
Solar cell area per panel (m^2) = 1.599 x 0.949 =	1.52
Total area allowed to mount a PV panel (1.70 m x 1.051 m) =	1.787
Number of PV panels mounted on roof = (1254 m^2 / 1.787 m^2) =	702
Total PV panel area = 702 x 1.65 m^2 =	1158
Total solar cell area = 702 x 1.52 m^2 =	1067
Ratio of solar cell area to roof area = f_C = 1067 / 1254 =	**0.85**

Typical PV panel dimensions readily available at the time of the study for the chosen efficiency were 1 m x 1.65 m (Brightstar, 2019). These panels had a 2.54 cm aluminum frame border and a 2.54 cm gap allotted for airflow between panels to manage equipment temperature. The collector area for a single panel was equal to 1.52 m^2. The footprint for a single panel including gap space was 1.787 m^2. Thus, a ratio of 0.85 was calculated to accurately reflect the productive solar cell collector area relative to available rooftop area for PV installation. This value of 0.85 was used for f_C in equation 3.4 for all calculations. For a typical building size of 152.4 m (L) by 15.2 m (W) this equated to an area available for PV installation (A) of 1254 m^2 and 702 panels. The typical roof was determined to have 1,067 square meters of productive solar cell area. For a farm of four houses, this equated to 4,268 square meters of cell area.

Solar Irradiance Data (*I*)

The incoming solar energy was calculated using the Physical Solar Model (NOAA, 2017) which was the most recent version of the National Solar Radiation Database (NSRDB) at the time of the study. The United States National Centers for Environmental Information (NCEI) in collaboration with the Department of Energy's National Renewable Energy Lab (NREL), the National Aeronautics and Space Administration (NASA), the Northeast Regional Climate Center, and several universities and companies collaborated to create the NSRDB. This specific database used a physics-based modeling approach on historical solar and meteorological measurements taken from over 1,500 sites across North America at 0.5-hour intervals over 80 years to provide solar radiation data for the US at a 4 km^2 grid. The total amount of irradiance data for a particular location or area was expressed as global irradiance (W/m^2), which is the sum of direct and diffuse irradiance.

The incoming solar energy from NOAA databases was spatially modeled on the UAV-derived digital data for farms visited using the solar radiation analysis tools within ArcGIS Pro (ESRI, 2019). This software calculated insolation across a landscape based on methods from the hemispherical viewshed algorithm (Rich et al, 1994) and (Fu and Rich, 2002). These methods accounted for atmospheric effects, site latitude and elevation, slope and aspect, daily and seasonal shifts of the sun geometry, and effects of shadows cast by surrounding topography. Solar analysis software parameters included slope and azimuth, latitude, solar path vectors, time configuration, and atmospheric assumptions. These inputs are given in Table 3.7.

Table 0.4 Area solar radiation (ESRI, 2019) inputs.

Parameter	USED
General	
Input:	DSM raster
Lat:	Auto calculate
Sky size/resolution:	200 default
Time configuration:	Whole Year
Year:	2019
Hour interval:	1
Topographic	
Z:	1
Slope/aspect input:	input surface raster
Calculation directions:	32
Radiation (for entire year)	
Zenith divisions: 8	8
Azimuth divisions:8	8
Diffuse Model type:	uniform overcast sky
Diffuse proportion:	0.3
Transitivity:	0.5

GIS data of poultry houses in the study area (see Chapter II) were used as input for the analysis. For exact software data preprocessing used to convert aerial photo point cloud data into a digital surface model, see Appendix B. The existing building roof was used for surface aspect and slope in each analysis. The average study area latitude of 34.5° North was used for solar path calculations. The time period input was 2019 at hourly intervals, which was used to calculate the total number of days in the given year.

Solar radiation calculations were extremely sensitive to atmospheric model assumptions. The amount of solar radiation received by the surface of the earth was only a portion of what would be received outside the atmosphere. Transmittivity and diffuse proportions were two inversely related atmospheric parameters used as input values for this model. A diffuse proportion was used to represent the fraction of global normal radiation flux that is diffused. Transmittivity was the ratio of averaged overall irradiance

wavelengths reaching the earth's surface to that which was received at the upper limit of Earth's atmosphere.

These atmospheric conditions for the test area were independently determined with two other data sets. MODIS satellite imagery at 1-km resolution measured average cloud observations at the sample coordinates twice per day over the most recent 15-year period and totaling an excess of 10,950 observations. The mean climatological cloud frequency was 51% with an interannual variability expressed as a standard deviation of 5% (Wilson, Jetz, 2016). Furthermore, this was validated with average monthly rainfall data by zip code between 1952 and 1990 provided by South Carolina Department of Natural Resources (SC DNR, 2019). The data and observations were used to determine localized atmospheric conditions at the study area. In light of these findings, the diffuse proportion parameter was set to 0.3 and the transmittivity proportion used was 0.5, modeling generally clear conditions.

This resulted in a total 8,760 irradiance measurements ($W/m^2/hr$, *I* in Equation 3.4) for each $0.15m^2$ of the poultry farm DSM. *I* values were averaged across a roof plane using the Zonal Statistics tool (ESRI, 2019). This process was repeated on the UAV-derived GIS data for all farms visited and used to compare *I* across the rooftop azimuth classes.

Solar irradiance during the longest and shortest day of a year was contrasted. The longest day of the year was June 21^{st}, and had 13 hours of sunlight. The shortest day of the year was December 21^{st} and had 8 hours of sunlight. The *I* ($W/m^2/hr$) output for each of the 13 hours in June were compared to the 8 hours of *I* values in December. This

analysis of interannual variation was completed to determine the range of possible solar radiation within the study area.

Next, an analysis of greater temporal resolution was completed. The hourly *I* output was averaged for each month i.e. the irradiance *I* during 9:00 was averaged for all 31 days in January, representative of the 'typical' irradiance at 9:00 in January. This was done for all months within a year for daily irradiance for a month by hour. These calculations throughout a year demonstrated the effect of earth tilt and rotation on available solar irradiance at substantially finer detail. This method was also repeated for each suitable azimuth class.

The *I* ($W/m^2/hr$) on both solstice days was scaled to an entire building rooftop of typical size (1,067 m^2 of solar panel cell area) and converted to *E* electric power (kW_{ac}) supply using equation 3.4. This effectively demonstrated the range of hourly power output (kW/hr) for a building of typical size, the range in daily electric energy production (kWh/day) and the range of power produced. This analysis was performed in the context of time-of-use categories used by energy suppliers (Figure 3.1). These hourly categories included peak, shoulder, and base periods for summer and winter seasons.

Similarly, the monthly average *I* values by hour were scaled to a building and converted to power (*E*, expressed as kW/1000 m^2). These normalized solutions for each of the four orientation classes were used to calculate the hourly electric power contribution (kW/farm) of each of the 88 farms in the study area during baseload, shoulder, and peak periods. Lastly, these results were also summed to determine energy production over time (kWh) by month and year for a farm.

Panel Efficiency

Solar panel efficiency is determined by the electrical power (W_{DC}) output of one solar panel divided by the solar irradiance (W) input. Module performance is a function of the aggregate interconnected solar cells and measured under standardized testing conditions (STC) for comparison. The average panel cell material was silicon and performance values ranging from 0.16 – 0.19 (Svarc, 2019). According to the Institute of Electrical and Electronics Engineers (IEEE), the cell material with the maximum performance as research prototypes were those made of gallium phosphide, and performed at 45% efficiency (Gallucci, 2020). For this study the maximum performing panel was not chosen due to high cost and low availability. The panel efficiency of 0.19 was chosen as a conservative estimate of technology considered efficient and readily available at the time of the study.

Performance Ratio (*PR*)

Performance Ratio accounted for performance losses expected in real systems that are not explicitly calculated by other variables including inverters, temperature, wiring, age, nameplate rating, panel soiling, grid availability and other sources. The *PR* was critical to accurately evaluate the quality of a photovoltaic installation because it provided the performance of the installation independently of the orientation or inclination of the panel. These losses that defined performance were cumulative in nature. The inverter's nominal rated DC-to-AC conversion efficiency was defined as a ratio of the rated

nameplate DC power output capacity of the PV modules to the AC-rated power output capacity of the inverters. Operating solar cell temperature reflected variation in panel efficiency as a function of panel temperature, global solar irradiance, wind speed, and dry bulb temperature. Roof mounted arrays also had reduced airflow compared to ground-mounted arrays, resulting in a higher installed operating temperature and a lower voltage. Electrical resistive losses in the DC and AC wires connecting modules, inverters, and other parts of the system were due to slight differences caused by manufacturing imperfections between modules in the array that caused the modules to have slightly different current-voltage characteristics. Age losses reflected the effect of weathering and light-induced degradation of the photovoltaic modules on the array's performance over time. Soiling was the reduction in array power output caused by dirt and other foreign matter that prevented solar radiation harvest. The nameplate rating loss accounted for the accuracy of the manufacturer's nameplate rating. Availability referred to reduction of a system's output cause by scheduled and unscheduled system shutdown for maintenance, grid outages, and other operational factors.

The values used to estimate *PR* for the calculations in this study was based on information provided by Dobos (2014) and are shown in Table 3.8.

Table 0.5 Estimation of the performance ratio (*PR)* for a rooftop PV array (adapted from Dobos, 2014).

Loss	Range	Used in this Study
Inverter	0.02 to 0.10	0.05
Temperature	0.02 to 0.15	0.02
Wiring, mismatch, connection	0.01 to 0.03	0.01
Age, degradation	0.01 to 0.03	0.02
Nameplate rating	0.0 to 0.05	0.00
Availability	0.01 to 0.07	0.01
Soiling	0.01 to 0.05	0.01
	Sum losses =	0.12
	PR = (1 – sum losses) =	0.88

The total cumulative electric losses resulted in a 12% decrease. This meant that each unit of electrical system power output (W_{AC}) to the grid was only 88% of the panel array power input (W_{DC}). The value used with equation 3.4 was 0.88 and was believed to provide a conservative estimate of panel electric power production.

Collection of Data on Broiler Farm Electrical Energy Use and Connected Loads

The calculated results for *E*, rooftop PV supply, did not take into account the energy use and demand during critical broiler house loads. These were primarily a function of facility ventilation and lighting systems. If the process of net metering were to apply to facility electricity loads, then only electricity generated in excess of farm demand would be useful for peak-shaving contributions to the grid.

Farm Visits

An analysis of installed equipment at poultry farms was conducted as part of the Regional Conservation Partnership Program (RCPP) in SC. This project was carried out by Clemson University Extension with funding by the National Resource Conservation

Services (NRCS). Between 2015 and 2019 a team of 6 individuals visited 58 poultry farms (239 buildings) in SC including broiler farms, layer farms and pullet farms.

Data Collection

All installed electrical equipment data was recorded by quantity (count), demand (W or hp), and operational schedule (hr/day) for each building. Worksheets were created in advance for use in the data collection process by all individuals to ensure uniformity of records. Facility electric consumption data was also accumulated. Monthly energy bills (kWh/month) spanning a time period of two years were also collected for 52 farms (122 houses) in SC between 2015 and 2019. This data was acquired from growers in collaboration with their respective energy service providers.

Calculations for determining Farm Electrical Energy Use

The energy use data was used to calculate farm consumption over time (kWh/farm/month). The calculations included the average, range, standard deviation, and coefficient of variance for monthly energy use. These results were normalized by building footprint (kWh/100m^2/month) to determine average building energy consumption. The results were also categorized by bird type. The farm energy use data consisted of records from 41 broiler farms, 2 broiler breeder farms, and 8 pullet farms.

The monthly data was also used to determine the rate of electrical consumption for a farm as approximate average hourly connected load (kW/100m^2). This was done by dividing the actual monthly energy use by the number of hours in each month. Due to the

annual variation of days in a month, utility companies commonly define the duration of a billing cycle as 730.4 “month-hours” (DEP, 2019). This was the conversion number used to determine rate of consumption on farms.

These energy consumption results were then compared to the calculated results for *E*, rooftop PV supply. This provided an understanding of the unique relationship between supply and demand in the context of rural SC poultry facilities. This information was also categorized by the seasonal time of use categories that are essential to electricity supply management. These metrics included average power (kW/hr) contribution on the average day, average shoulder power (kW/hr) contribution, and average peak power contribution (kW/hr). These metrics were calculated for both summer and winter seasons. The sum annual energy production (MWh/yr) was also calculated. All of these were used to determine net-to-grid contributions for both power and energy on the typical farm.

Connected Load to estimate farm hourly peak demand in summer

The energy bill data was not indicative of accurate hourly farm loads during the most critical periods of peak demand for an energy supplier. These instances were also believed to be when the agricultural loads were the highest within a given year (Chastain, et al, 1990). The equipment inventory was used to estimate the total connected load of a farm, calculated as the total demand of all equipment operating during summer peak periods. This was chosen to represent average hourly peak demand (kW/hr) per farm.

The equipment consisted primarily of ventilation and lighting systems. The typical barn ventilation systems consisted of 6 to 10, 48” diameter fans operating during

summer peak (and an average total annual runtime of 2,500 hours). The typical lighting system consisted of 2 or 3 rows of ceiling lamps, spaced approximately 10 feet apart. During the majority of a bird's lifespan, the lights are dimmed down to 0.5 foot-candles to minimize bird activity.

An exact equipment inventory was not done for motors of feed augers. Instead, an approximate *E* value per feedline of 0.5kW was assumed based on typical installed equipment sizes. Building width (*W*) was used as a predictor of grain loads. It was observed that buildings with a width less than 15.2 m typically had two feedlines, while houses of 15.2 m or greater had three feedlines in each house. Using this assumption, the summation of total operating equipment was calculated for the connected load during peak periods in summer. The total connected load of an agricultural facility was a very close approximation of daily farm peak demand. Average demand results were normalized by building footprint (kW/hr/m_2) and projected onto the entire building population to estimate average total load during peak demand periods in summer months.

ANALYSIS AND RESULTS

The results of the data collection process for building characteristics and the application of equation 3.4 were summarized in this section. Further analysis on electricity production by time-of-use was done according to typical utility rate schedules. The location of the farms was analyzed, and a net contribution to grid was calculated in light of farm supply and demand.

Trends in Building Characteristics

Broiler houses were constructed using a select few standard building dimensions. Patterns in the results for the building characteristics of interest in the study area can be seen in the following sections.

Building Length (*L*) and Width (*W*)

The analysis of poultry house building dimensions in all farms within the study area included house width and length (*L*, *W*). These results are given in Table 3.9.

Table 0.1 Variation in poultry house length (*L*) as a function of house width (*W*) (n= 398).

House	House Width (m)						
Length (m)	11.0	12.2	12.8	13.7	15.2	15.8	16.5
106.7	1						
114.3		1					
121.9	7	9		1	1		
128.0		4					
129.2	3	3	1		1		
129.5	33	6					
137.2					2	4	
137.8		1					
143.2		1					
152.4	4	12	2		231		17
153.6			4				
153.9					14		
154.2					2		
155.4					8		
158.5		2					
160.0		2					
161.5		4					
182.9					17		
Total per W =	48	45	7	1	276	4	17

Building widths ranged from 11.0 m to 16.5 m. The most common building width was 15.2 m and included 69.3% of the buildings. Building length dimensions ranged

from 106.7 m to 182.9 m. Most of the poultry barns in the study area had building lengths in the range of 129.2 m and 152.4 m. By far the most common length (80%) was 152.4 m.

There were a total of 398 houses located at 88 farms, with an average 4.52 houses per farm. Farm building counts ranged from a minimum of 2 houses up to a maximum of 22 houses. The most prevalent building characteristics within the 398-house sample were 15.2 m wide (70%) and 152.4 m long (80%). These dimensions were used with the typical roof slope of 5:12 from the results of chapter II.

Building Orientation

The buildings were also organized by orientation (based on Table 3.4) to determine *I*, solar irradiance, on the rooftop. The results of the building orientation classification for all 398 houses is given in Table 3.10.

Table 0.2 Variation in poultry house orientation by house width (*W*).

House Width (m)	Building Orientation Class				
	SE/NW	SW/NE	E/W	N/S	Grand Total
11.0	4	20	23	1	48
12.2	12	10	23	0	45
12.8	0	4	1	2	7
13.7	0	0	1	0	1
15.2	75	74	87	40	276
15.8	0	0	4	0	4
16.5	6	7	0	4	17
Total =	97	115	139	47	398

These rooftop azimuth classes were taken from Table 3.4. The most common building orientation was East and West, 35% of the total. The next most common (29%)

were classified as Southwest and Northeast. The third most common (24%) were Southeast and Northwest. The least common orientation was barn oriented North and South (12%). Twenty-five percent of the roof planes fell within azimuth orientation classes that were unsuitable for PV installation due to northward facing slopes. The majority of the building rooftop planes (75%) were classified into classes that were suitable for PV installation.

Spatial Distribution of Farms Relative to Transmission Grid

It may not be practical to assume that a utility company would immediately recruit the entire group of farms as distributed PV plants to rural areas. An energy supplier would likely initiate this experiment with a subset of the entire population of the farms. In consideration of the distribution costs and line losses associated with energy supply, the most valuable farms to an energy supplier would be located furthest from the existing transmission grid. An analysis of poultry farm spatial distribution was done relative to the existing transmission grid within the study area. Measuring the distance between each farm and the T&D network was accomplished as a measure of Euclidean distance between each poultry farm and the nearest transmission line using the Near tool in ArcGIS Pro (ESRI, 2019). A map of the farms and transmission grid are given in Figure 3.4.

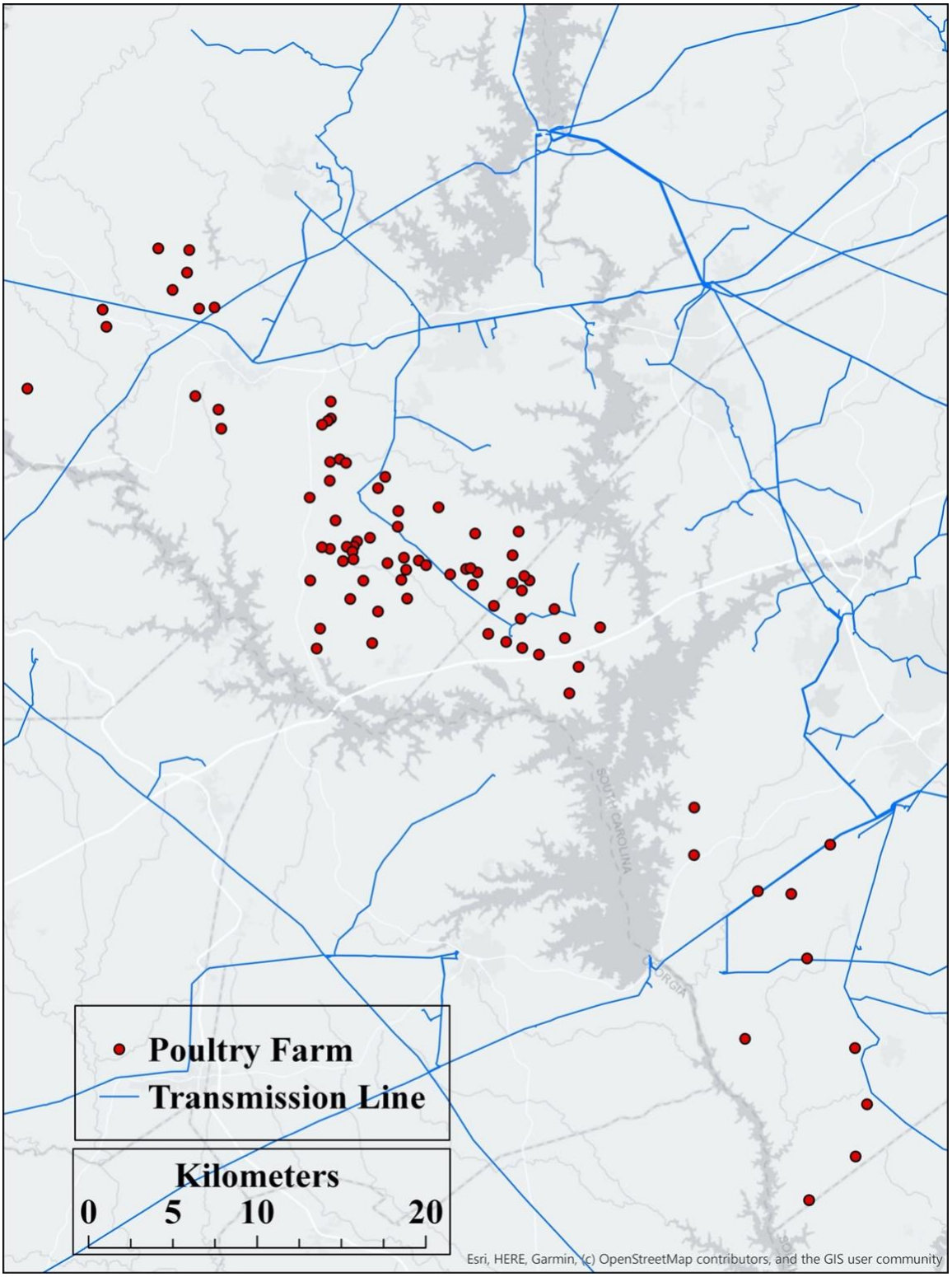

Figure 0.1 Spatial distribution of 88 poultry farms and transmission grid.

The map shows the study area of Oconee and Anderson Counties. The transmission lines were marked in blue. The 88 poultry farms were marked as red circles. A frequency distribution histogram for the results of proximity analysis is given in figure 3.5.

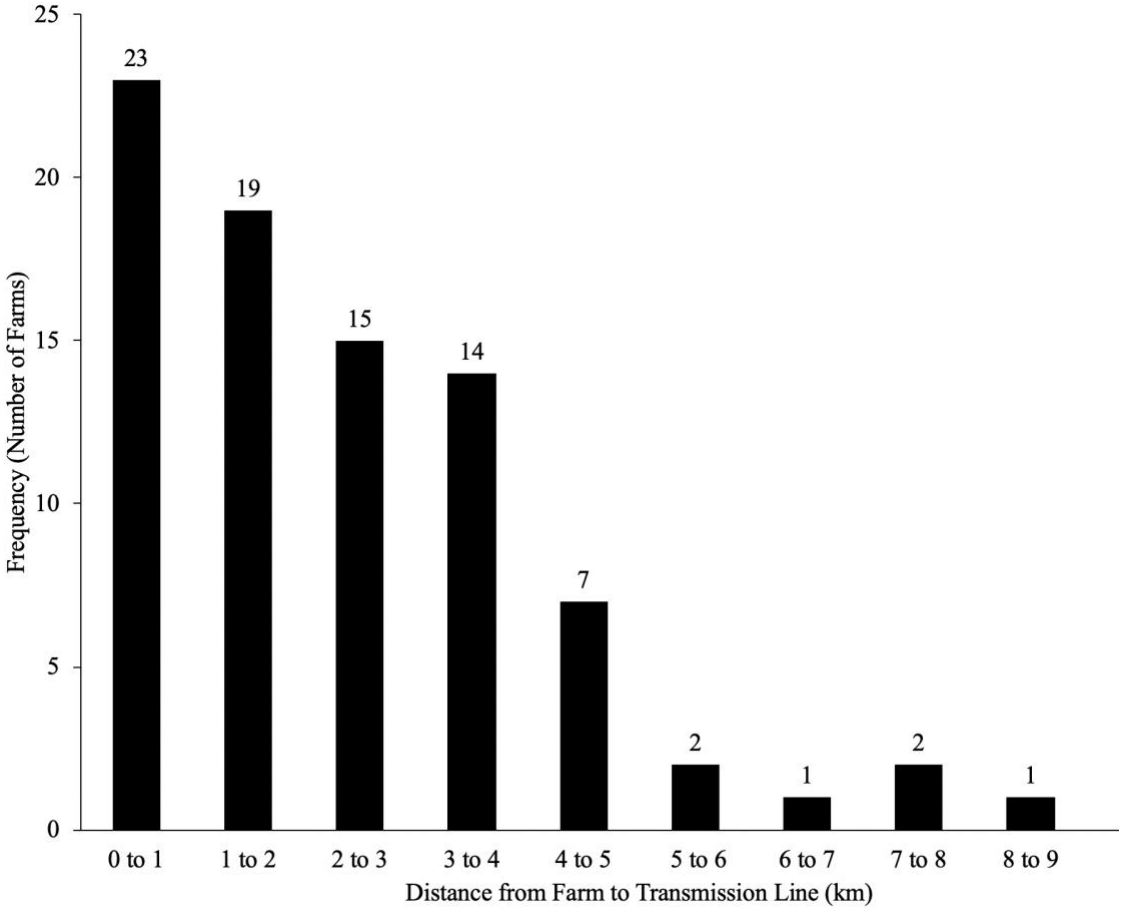

Figure 0.2 Frequency distribution of Euclidian distance between farm and nearest transmission line.

The vast majority of farms were within 5 km of an existing utility transmission line (92%). Exactly two-thirds of the farms in the population were within 3 km, and half

of the farms were within 2 km. The average distance between a farm and the transmission grid was 3.28 km. One-third of farms in the study area were located outside this region. The 3.28 km buffer around the transmission lines was chosen as a natural break in the population distribution by distance, and a practical division to assist an energy supplier in prioritizing feasible plant locations. Depending on existing local utility infrastructure, these farms were most likely to prove the most valuable in functioning as micro peak-shaving plants for an energy supplier due to their location in population scarce areas.

Calculation of Solar Electric Power Production from Roof Mounted PV Arrays for the Winter and Summer Solstice

The *I* data was used as inputs for determining electrical energy output, using Equation 3.4. These values and assumptions were used to determine hourly electrical production demonstrated for the typical broiler farm in the study area.

Solstice Solar Irradiance Data for Summer and Winter Solstice

The solar irradiance potential (*I*) for the region of interest was demonstrated across building characteristics including building size, roof slope, azimuth, time of day and seasonality. First, an analysis of interannual variation of solar irradiance within the study area was completed to determine the range of solar radiation. The average hourly solar irradiance ($W/m^2/hr$) during both the longest and the shortest day of a year was calculated and compared. Since irradiance harvest is sensitive to slope aspect, this solstice comparison was repeated for each azimuth class as defined in Table 3.4. The results are given in Table 3.11(a) and 3.11(b).

Table 0.3 (a) Global solar irradiance data (W/m2) on summer and winter solstice by rooftop azimuth (ESRI, 2019)1.

	South		Southwest		Southeast	
Time of Day	summer2	winter3	summer	winter	summer	winter
8:00	42		27		112	
9:00	195	67	128	38	334	73
10:00	384	203	293	140	542	192
11:00	564	318	471	247	692	267
12:00	703	376	631	319	775	279
13:00	782	364	746	334	783	234
14:00	793	286	803	282	726	151
15:00	734	159	789	169	613	52
16:00	611	33	705	38	462	11
17:00	442		555		294	
18:00	252		357		116	
19:00	84		146		41	
20:00	4		11		4	
Energy (Wh/m2/day)	5,590	1,807	5,662	1,567	5,496	1,260

1Daily solar energy values found with ESRI point solar tool, calibrated with NOAA meteorological and solar radiation datasets reflecting 80 years of data

2The summer solstice is Julien Date 172 (June 21st)

3The winter solstice is Julien Date 355 (December 21st)

Table 3.11 (b) Global solar irradiance data (W/m2) on summer and winter solstice by azimuth for buildings oriented North/South (ESRI, 2019)[1].

	summer[2]		winter[3]	
Time of Day	East	West	East	West
8:00	91	25		
9:00	276	99	33	73
10:00	454	281	98	204
11:00	595	458	147	299
12:00	686	617	164	331
13:00	723	733	145	299
14:00	706	790	99	214
15:00	639	778	42	105
16:00	561	694	10	17
17:00	391	546		
18:00	236	349		
19:00	92	142		
20:00	6	6		
Energy (Wh/m2/day)	5,457	5,518	738	1,543

[1]Daily solar energy values found with ESRI point solar tool, calibrated with NOAA meteorological and solar radiation datasets
[2]The summer solstice is Julien Date 172 (June 21st)
[3]The winter solstice is Julien Date 355 (December 21st)

The table shows the *I* data for the hours beginning at 8:00 through 20:00. This excluded hour classes with an output irradiance value less than 1 (W/m2) as below the threshold of useful radiation and to represent an effective generation day. For each azimuth class solar irradiance was significantly greater at the summer solstice in both intensity and duration. The total energy received for the entire day was greatest on the South and Southwest classes, while East and Southeast received the least. The azimuth classes with the highest irradiance were the most suitable for PV installation. The seasonal change in solar noon can also be seen by the maximum average irradiance in hour class 12:00 during winter and transitioning to hour class 14:00 in summer.

Similarly, the easterly azimuth slopes received higher irradiance values before the solar peak, while westerly slopes received higher irradiance after solar peak.

Solstice Photovoltaic Electric Power Production

The global solar irradiance (W/m^2) data on both solstice days was scaled to an entire building rooftop of typical size, with a building length (L) of 152.4 m and building width (W) of 15.2 m. The roof area of one roof plane available for installation was 1,254 m^2 (A) and had 1,067 m^2 of solar cell collector area (A x f_C). Using the results from Table 3.6 this equated to a solar array of 702 panels per building.

Electric power (kW_{ac}) output was calculated for an entire rooftop on the two solstice days from the hourly I data using equation 3.4. This involved the variables panel efficiency (r) of 0.19 and the electrical performance ratio (PR) of 0.88. These combined factors resulted in only 17% of solar irradiance (I) was converted to AC electric power (E).

The comparison of solstice PV supply from average sized buildings was repeated for each orientation, since I varied across roof slope azimuth class. The results of these calculations are given in Table 3.12 (a) and 3.12 (b).

Table 0.4 (a) Electric power output (kW/building) on summer and winter solstice by building orientation for a 15.2 m x 152.4 m broiler house.

	East/West		Northwest/Southeast		Northeast/Southwest	
Time of Day	Summer[1]	Winter[2]	Summer	Winter	summer	winter
8:00	7	0	5	0	20	0
9:00	35	12	23	7	60	13
10:00	68	36	52	25	97	34
11:00	101	57	84	44	123	48
12:00	125	67	112	57	138	50
13:00	139	65	133	60	140	42
14:00	141	51	143	50	129	27
15:00	131	28	141	30	109	9
16:00	109	6	126	7	82	2
17:00	79	0	99	0	52	0
18:00	45	0	64	0	21	0
19:00	15	0	26	0	7	0
20:00	1	0	2	0	1	0
Total (kWh/day)	996	322	1,009	279	979	225

[1]The summer solstice is Julien Date 172 (June 21st)
[2]The winter solstice is Julien Date 355 (December 21st

Table 3.12 (b) Electric power output (kW/building) on summer and winter solstice by rooftop azimuth for buildings oriented North/South and 15.2 m x 152.4 m.

	Summer[1]			Winter[2]		
Time of Day	East	West	Total	East	West	Total
8:00	16	4	21	0	0	0
9:00	49	18	67	6	13	19
10:00	81	50	131	17	36	54
11:00	106	82	188	26	53	79
12:00	122	110	232	29	59	88
13:00	129	131	259	26	53	79
14:00	126	141	267	18	38	56
15:00	114	139	253	7	19	26
16:00	100	124	224	2	3	5
17:00	70	97	167	0	0	0
18:00	42	62	104	0	0	0
19:00	16	25	42	0	0	0
20:00	1	1	2	0	0	0

Total (kWh/day)	973	983	1956	132	275	407

[1]The summer solstice is Julien Date 172 (June 21st)
[2]The winter solstice is Julien Date 355 (December 21st)

Electric power supply (kW_{AC}) was expressed per hour for each building orientation class. Since the E output was a function of *I* input, the same general quantitative trends were demonstrated here as with the irradiance tables. *E* values were still significantly greater at the summer solstice in both intensity and duration for each azimuth class.

Impact of Building Orientation on Peak Electric Power Production

During the winter months the peak demand period was defined as the hours from 6:00 to 8:00 (Figure 3.1a). The solar irradiance data, Tables 3.11a and 3.11b, indicated that solar energy was not available until the hour beginning at 9:00 on the winter solstice. Therefore, none of the roof mounted PV arrays provided any electric power output during the winter peaking period as indicated in Tables 3.12a and 3.12b. The PV arrays only provided power during the summer peak period which was defined as from 13:00 to the end of the hour beginning at 17:00 (Figure 3.1b).

The results provided previously (Table 3.10) indicated that 88% of the broiler houses in the study area had an East/West, Southwest/Northeast, or Southeast/Northwest orientation. In addition, the typical broiler house (15.2 m x 152.4 m) had one array of PV panels mounted on the south-facing roof slope with a useable roof area of 1254 m^2 and a total PV panel area of 1158 m^2. On the summer solstice day between 13:00 and 17:00 a building oriented East/West produced an average power output of 120 kW/hr, ranging

from 79 to 141 kW/hr over the peak period of the day. However, a building oriented Northwest/Southeast provided the highest power output with an average of 128 kW/hr during the peak period ranging from 99 to 143 kW/hr. An array mounted on a building with a Northwest/Southeast orientation produced 6.7% more power than for a building with an East/West orientation. This small increase in average power production during the peak period was due to the fact that the PV array was canted towards the Southwest allowing it to receive more solar irradiance during the period past solar noon (14:00 through 17:00, Table 3.11). A building oriented Northeast/Southwest provided the least electric power as compared to a building with an East/West orientation using the same number of panels. The average power output during the summer peak period was 103 kW/hr or 14.2% less than the PV array mounted on a building with an East/West orientation. In addition, the results in Table 3.12a show that such a PV array canted towards the Southeast provided the largest power output during the hours beginning from 11:00 to 13:00. Additional power production may be helpful on summer days when extremely hot temperatures begin in the late morning and cause the electrical system demand to be higher than typical due to increased demand for ventilation of farm buildings and air-conditioning in commercial and residential structures. The results provided in Table 3.12a clearly indicate that all three of these building orientations can provide electric power during the summer peak period. However, the least valuable of these three building orientations was Northeast/Southwest.

Only 12% of the broiler houses in the study area were constructed with a North/South orientation (Table 3.10). It was assumed that PV panels were mounted on

both roof slopes. As a result, one 1158 m^2 array of panels faced East and another 1158 m^2 array of panels faced West. The total area of panels mounted on a building with this orientation was 2316 m^2. The results provided in Table 3.12b show the hourly electric power production from both arrays and the total output power from the building. The results for the summer solstice (Table 3.12b) indicated that the maximum on-peak power production for the array facing East was 129 kW at 13:00 and the maximum on-peak power for the West facing array was 141 kW at 14:00. Near the middle and end of the peak period, 15:00 to 17:00, when afternoon air temperatures are near the daily maximum, the only array of panels that produced more power were those mounted on a building with a Northwest/Southeast orientation. During the peak period (13:00 – 17:00) the hourly power production ranged from 167 to 267 kW with an average of 234 kW. This average supply was 2.29 times greater than the average on-peak power production of a building with a Northeast/Southwest orientation, and 1.82 times greater than the average on-peak power production of a building with a Northwest/Southeast orientation.

Since buildings with a North/South orientation had twice as many PV panels installed as compared to the other three orientations, the summer-peaking efficacy of the four different building orientations was compared by normalizing the average summer peak power production per 100 m^2 of installed panel area. The most effective use of PV panels was for the Northwest/Southeast orientation with a summer peaking efficacy of 11.0 kW/100 m^2 of PV panel. The next most effective installation was for the East/West orientation with a summer peaking efficacy of 10.4 kW/100 m^2. Surprisingly, the third most effective installation was for the North/South orientation providing 10.1 kW/100 m^2

during the summer peak period. Finally, the least effective installation for summer peak electric power production was for the building with the Northeast/Southwest orientation at only 8.9 kW/100 m^2.

Impact of Building Orientation on Shoulder Electric Power Production

The next most important demand period after the daily peak period is called the shoulder period. During the summer season the shoulder period was defined as the hours from 11:00 to 12:00 in the morning and 18:00 to 19:00 in the evening (Figure 3.1b). During the winter season the shoulder period occurs from 9:00 to 11:00 in the morning and 17:00 to 19:00 in the evening (Figure 3.1a). Based on the solar irradiance data (Figures 3.12a and 3.12b) a roof-mounted array of PV panels would only be productive during the morning portion of the winter shoulder period. Therefore, only the hours from 9:00 to 11:00 were used to calculate average power production for the shoulder period for the winter solstice.

Average Electric Power Production During the Shoulder Period for the Winter Solstice

The average power production during the morning portion of the shoulder period (9:00 to 11:00) for buildings with one PV array of 1158 m^2 ranged from 25 kW for a building with a Northwest/Southeast orientation to 35 kW for a building with an East/West orientation. The average shoulder-period output for the building with a Northeast/Southwest orientation was at almost the average of the other two at 32 kW. The building with the North/South orientation provided 51 kW on the average during the morning portion of the shoulder period. Therefore, the North/South building again

provided the most electric power as compared to the other three orientations. However, a more precise comparison was made using the efficacy of the PV array calculated during the shoulder period. The most effective array was on a building with an East/West orientation with a winter shoulder period efficacy of 3.0 kW/100 m^2 of panel area. The next most effective was the Northeast/Southwest orientation with an efficacy of 2.8 kW/100 m^2. Both the North/South and Northwest/Southeast orientations had the same efficacy at 2.2 kW/100 m^2.

Average Electric Power Production During the Shoulder Period for the Summer Solstice

The electric power results in Tables 3.12a and 3.12b clearly show that the PV arrays for all four building orientations provided more power during the morning shoulder hours (11:00 to 12:00) on the summer solstice than in the evening (18:00 to 19:00). However, comparisons were made based on the average power production during all four hours of the shoulder period. Unexpectedly, the average power production during the summer shoulder period was 72 kW for all three orientations with PV panels mounted on the roof slopes facing South, Southeast, or Southwest (East/West, Northwest/Southeast, Northeast/Southwest). The summer shoulder production for the building with the North/South orientations with PV panels on both roof slopes was 142 kW. Therefore the efficacy for the buildings with 1158 m^2 of PV panels was 6.2 kW/100 m^2 and the efficacy for the North/South building was almost the same at 6.1 kW/100 m^2.

Impact of Building Orientation on Baseload Electric Power Production

Baseload has been defined as the average electric power required by the customers in a day or season. A solar power plant can only produce electricity during the day. After considering the variation in available solar irradiance (Tables 3.12a and 3.12b) and the day-time portion of the baseload defined by a generating utility (Figures 3.1a and 3.1b) it was determined that a reasonable estimate of a roof-mounted PV array's contribution to baseload would be the average electric power produced from the hour beginning at 9:00 till the end of the hour beginning at 17:00 for the longest and shortest day of the year.

Baseload for Winter Solstice

The average baseload contribution for the four building orientations on the winter solstice ranged from 25 kW for a building with a Northeast/Southwest orientation to 51 kW for the building with a North/South orientation. Again, the different orientations were compared based on the kW produced per 100 m^2 of PV area. The highest baseload efficacy was for a building with an East/West orientation and was 3.1 kW/100 m^2. The second most effective array had an efficacy of 2.7 kW/100 m^2 and was on the building with a Northwest/Southeast orientation. The arrays mounted on the buildings with a North/South and Northeast/Southwest orientation were the same at 2.2 kW/100 m^2.

Baseload for Summer Solstice

The average baseload contribution on the summer solstice for the three orientations with 1158 m^2 of PV panels were almost the same. Buildings with East/West and Northeast/Southwest orientations provided 103 kW/hr to baseload on the average. The efficacy for these two cases was 8.9 kW/100 m^2. The baseload contribution of the

building with a Northwest/Southeast orientation was 101 kW/hr with an efficacy of 8.7 kW/100 m2. The two arrays on the North/South building provided almost twice as much baseload power at 199 kW/hr with a slightly lower efficacy of 8.6 kW/ 100 m2.

Impact of Building Orientation on Daily Energy Production

Energy providers reflect the cost to supply electricity based on both the rate of power consumed (demand, kW) and the quantity of energy consumed (energy, kWh). For electricity production, energy is the sum quantity of power produced over time. Daily energy production was calculated as the total power produced during each hour, for all hours of daylight within each day. This was repeated for the longest and shortest day of the year.

Total Daily Electric Energy Production on Summer Solstice

Between the three orientations with 1158 m2 the sum energy production on the longest day was greatest on buildings oriented Northwest/Southeast at 1,009 kWh. The second highest summer energy output was on buildings oriented East/West at 996 kWh. Buildings within the Northeast/Southwest orientation produced the least energy of 979 kWh. The building oriented North/South had a substantially larger summer daily energy production at 1,956 kWh. The energy production efficiency of each building orientation was compared as the sum daily energy per 100 m2 of total array area. The total range of summer energy efficacy among all building orientations had a tight spread between 77.6 and 80.5 kWh/100m2. The most efficient performance was by the array on buildings oriented Northwest/Southeast with 80.5 kWh/100m2. The second most efficient was

buildings oriented East/West with 79.5 kWh/100m2. The third most efficient was the West azimuth of the North/South building at 78.4 kWh/100m2. The least two efficient orientation classes were the Northeast/Southwest with 78.1 kWh/100m2, followed by the East azimuth of the North/South building at 77.6 kWh/100m2.

Total Daily Electric Energy Production on Winter Solstice

The sum energy production on the shortest day of the year was analyzed for all orientations. Between those with a single roof plane suitable for PV, both daily energy production and efficacy in winter followed the same ranking trends among the three orientations. Buildings East/West had a daily energy production of 322 kWh/day and an efficacy of 25.68 kWh/100m2. The next orientation was buildings Northwest/Southeast of 279 kWh/day with efficacy of 22.28 kWh/100m2. Lastly, the Northeast/Southwest orientation had a total daily energy production in winter of 225 kWh/day and operated with an efficacy of 17.91 kWh/100m2. The two arrays on the North/South building produced the most energy at 407 kWh/day. The West facing array operated at an efficiency of 21.93 kWh/100m2, while the energy production on the East facing slope of the same buildings was only 10.49 kWh/100m2 (averaging 16.2 kWh/100m2 for the building).

These results illuminated a poultry barn's performance as a PV plant. A building of average size and orientation constituted a solar array of 702 solar panels which totaled 1,067 m2 of productive PV cell area. Despite the 83% energy losses associated with solar energy generation, the highly suitable building characteristics and vast extent of roof per

building both resulted in substantial power and energy contributions of potential electricity generated. The unique North/South buildings they were especially valuable in summer periods.

Prioritization of Building Orientation for Peaking Plant Value

Overall, the orientation of Northwest/Southeast had the greatest contribution to power and energy production metrics, and was therefore the most valuable. This orientation was the single most productive array (consisting of 1158m^2) for total daily energy of any orientation, and the second most productive by building. The Northwest/Southeast was also first in efficacy for summer peak periods, summer shoulder, and second in both summer base and winter base periods. Buildings oriented East/West were the second most productive overall to the electricity generation metrics with the highest daily energy output in winter, and the second highest daily energy output in summer. These buildings had the highest efficacy for summer and winter base periods, as well as summer shoulder and winter shoulder periods. East/West buildings also had the second highest efficacy at summer peak.

North/South orientated buildings were the third most useful overall. While they tended to have the lowest single-array production, the cumulative array area per building often offset this. These buildings only consisted of 12% of the population but contributed 40% of the combined total daily energy production by all orientations in summer, and 33% in winter. The panel efficacy was ranked third for peak summer periods, base

summer periods, winter shoulder periods, and last in summer shoulder and winter base periods.

Lastly, the buildings oriented Northeast/Southwest had the least contributions to power and energy metrics for a generation plant. They produced the least daily total energy in summer and winter days. They also had the lowest panel efficacy for each time-of-use metric except winter shoulder and base summer periods.

If an energy supplier were to pursue this investment, then the obvious consideration of cost comes into play. A detailed economic analysis of energy plant project cost or payback period was beyond the scope of this project. However, the current economics of renewable energy define the tipping point for solar technology adoption as a major energy supply contributor. Therefore a practical consideration of cost would be critical to decision making. This could further exploit the two performance variables of panel efficacy and average hourly building supply at critical demand curve metrics by a single building of each orientation on a single day. Since solar panel cost would be constant for any orientation, then the greatest electrical output per unit cost was the best investment for a supplier. This would support arrays on buildings of Northwest/Southeast and East/West orientations.

However, there was also the key investment of infrastructure needed for phase matching and distribution. This total infrastructure cost would be independent of individual panel output comparisons. This equipment would not be a function of building size or orientation, but rather quantity of buildings per farm. Farms with above average

(5+) building density would be the most valuable to an energy supplier, since many costs for distribution equipment would be fixed regardless of total plant output.

Calculation of Solar Electric Power Production for Each Month of the Year

Monthly Solar Irradiance

An analysis of greater temporal resolution was completed for solar irradiance at the region of interest. The method for determining hourly solar irradiance (W/m^2) for each solstice day was repeated for each day in a year using the area Solar radiation tool (ESRI, 2019). The solar irradiance for each hour was then averaged by month for each month throughout an entire year. This analysis demonstrated the effect of earth tilt and rotation on available solar irradiance at substantially finer detail. This method was repeated on each suitable azimuth class. The results are given for buildings orientated East and West in Table 3.13.

Table 0.5 Average global solar irradiance by month on buildings with East/West orientation.

Time of Day	Average hourly global solar irradiance (W/m2)											
	Jan	Feb	Mar	Apr	May	Jun	Jul	Aug	Sep	Oct	Nov	Dec
8:00				1	35	42	41	8				
9:00	78	68	87	106	179	195	192	121	92	69	77	67
10:00	237	210	269	328	372	384	379	339	286	213	235	202
11:00	371	350	453	552	559	564	556	558	481	359	372	316
12:00	439	450	593	722	702	703	693	726	630	470	446	374
13:00	425	495	666	812	783	781	771	815	709	529	441	362
14:00	334	479	664	809	791	792	782	816	708	528	362	285
15:00	186	406	587	715	727	734	724	727	627	467	224	158
16:00	39	291	445	542	596	611	603	561	476	355	81	33
17:00		167	260	317	418	442	436	343	280	209	28	
18:00		60	80	98	224	252	249	126	88	66	53	
19:00					69	84	83	14				
20:00					4	4	4	4				
Total (Wh/m2/ day)	2108	2977	4104	5002	5459	5586	5513	5159	4378	3264	2320	1797

The table shows modeled *I* results between 8:00 and 20:00 averaged by hour for each month over an entire year. The total energy produced per day was highest on the average day during the month of June, and lowest for the average day during December. This reinforces the results from the analysis of solar irradiance on solstice day. In addition to this, now it can be seen that the most predominant irradiance availability in the average year occurred between the months of April and August while the least availability was between November and February. Similarly, the trends in daylight duration were enhanced. Duration was greatest during the months of May through August, and shortest in December and January. The seasonal change in solar noon can also be seen as the maximum average irradiance in hour class 12:00 for months

November through January and transitioning to hour class 14:00 during May through August. The results for average hourly global solar irradiance for buildings orientated Northwest and Southeast are given in Table 3.14.

Table 0.6 Average global solar irradiance by month on buildings with Northwest/ Southeast orientation.

Time of Day	Average hourly global solar irradiance (W/m^2)											
	Jan	Feb	Mar	Apr	May	Jun	Jul	Aug	Sep	Oct	Nov	Dec
8:00		1	1	1	30	33	35	12	2	1	1	
9:00	54	63	79	104	157	154	164	130	97	63	79	53
10:00	164	195	243	321	327	305	322	344	296	197	242	162
11:00	257	325	410	541	490	450	473	556	497	331	386	254
12:00	304	418	536	708	616	562	590	718	650	433	469	301
13:00	294	460	603	796	687	625	656	806	731	488	474	293
14:00	231	445	601	794	694	634	665	808	730	487	403	232
15:00	129	377	531	701	638	586	616	724	647	431	271	133
16:00	27	270	402	531	523	486	513	564	492	327	126	33
17:00		155	235	311	367	350	371	355	292	193	57	4
18:00		55	73	84	196	197	211	108	77	61	42	
19:00		1	1	1	61	65	70	12	1	1		
20:00					3	3	3	3				
Total (Wh/m^2/ day)	1461	2766	3714	4894	4789	4449	4690	5141	4511	3012	2550	1464

The basic trends for daylight duration, ranges of irradiance, and solar noon in hourly *I* results per month applied to each rooftop azimuth. The main distinction for this orientation was that the total energy supplied on the average day was lower compared to that of the East/West orientation. The exception was in the months of September and November, where the total energy for the average day was marginally higher. This is likely due to the easterly orientation of the given azimuth, which coincides with sunrise.

The results for average hourly global solar irradiance for buildings orientated Northeast and Southwest are given in Table 3.15.

Table 0.7 Average global solar irradiance by month on building with Northeast/Southwest orientation.

Time of Day	Average hourly global solar irradiance (W/m2)											
	Jan	Feb	Mar	Apr	May	Jun	Jul	Aug	Sep	Oct	Nov	Dec
8:00		1	1	1	30	28	35	7	1	1	1	
9:00	54	63	79	94	157	132	164	107	83	63	71	43
10:00	164	195	243	291	327	260	322	301	257	197	217	132
11:00	257	325	410	490	490	382	473	495	432	331	343	206
12:00	304	418	536	641	616	477	590	643	566	433	411	244
13:00	294	460	603	721	687	530	656	722	637	488	407	236
14:00	231	445	601	719	694	538	665	723	636	487	334	185
15:00	129	377	531	635	638	498	616	644	563	431	207	103
16:00	27	270	402	481	523	414	513	497	428	327	75	21
17:00		155	235	281	367	300	371	304	252	193	26	
18:00		55	73	87	196	171	211	112	79	61	49	
19:00		1	1	1	61	57	70	13	1	1	1	
20:00					3	3	3	3				
Total (Wh/m2/ day)	1461	2766	3714	4442	4789	3789	4690	4569	3936	3012	2143	1171

Buildings in this orientation received lower irradiance totals for the average day each month than buildings oriented East/West. These results were nearly identical to irradiance values from buildings oriented Northwest/Southeast in January, February, March, May, July, and October months; and typically lower on the remaining months of the year.

Lastly, the average hourly global solar irradiance results for buildings orientated North and South are given in Table 3.16 (a) and 3.16 (b) by azimuth slope.

Table 0.8 (a) Average global solar irradiance by month on East azimuth of buildings with North/South orientation.

Time of Day	Average hourly global solar irradiance (W/m2)											
	Jan	Feb	Mar	Apr	May	Jun	Jul	Aug	Sep	Oct	Nov	Dec
8:00		1	1	1	33	36	39	13	2	1	1	
9:00	41	50	71	103	171	172	180	136	92	52	59	39
10:00	124	154	218	318	356	342	355	357	279	160	179	119
11:00	194	255	367	536	534	504	522	576	468	270	286	187
12:00	230	329	481	701	671	629	651	744	612	353	348	221
13:00	223	362	540	788	748	700	724	835	689	398	353	215
14:00	175	351	539	786	756	710	734	837	688	397	301	171
15:00	97	298	476	694	694	656	679	751	609	351	205	98
16:00	20	214	361	526	570	545	566	586	464	267	98	24
17:00		123	211	308	400	392	409	369	275	157	45	3
18:00		44	65	85	215	221	233	112	71	49	31	
19:00			1	1	67	73	78	13	1	1		
20:00					4	3	4	3				
Total (Wh/m2/ day)	1105	2182	3330	4846	5218	4983	5174	5333	4249	2456	1907	1078

Table 0.16 (b) Average global solar irradiance by month on West azimuth of buildings with North/South orientation.

Time of Day	Average hourly global solar irradiance (W/m2)											
	Jan	Feb	Mar	Apr	May	Jun	Jul	Aug	Sep	Oct	Nov	Dec
8:00	0	1	1	1	34	37	40	14	2	1	1	0
9:00	44	53	74	107	175	176	185	140	96	55	63	43
10:00	134	164	229	330	365	349	364	368	291	170	193	129
11:00	209	273	385	555	547	515	534	594	488	287	308	202
12:00	247	351	505	727	688	643	666	767	638	376	375	240
13:00	239	387	567	817	767	716	741	861	718	423	380	233
14:00	188	375	566	815	775	725	751	863	717	422	324	185
15:00	105	318	500	720	712	670	695	774	635	374	220	106
16:00	22	229	379	545	584	557	579	604	484	284	105	26
17:00	0	131	221	319	410	401	419	380	287	167	48	4
18:00		47	68	87	220	226	239	115	74	53	34	0
19:00		0	1	1	68	75	80	14	1	1	0	
20:00					4	3	4	3				
Total (Wh/m2/ day)	1189	2329	3496	5024	5349	5093	5296	5497	4432	2611	2051	1168

The West facing slope was higher than that of the east facing slope for every month. East and West slopes both had the lowest irradiance values of the group in the winter months, but exceptionally productive mid-summer irradiance values.

This unique building orientation had twice the effective rooftop area available to harvest solar energy. The combined monthly total energy was vastly more significant than the most productive roof plane. 195% in summer and 146% in winter. Ranging from 109% in January, to 210% in August.

Monthly Photovoltaic Electric Supply

The hourly *I* data (Tables 3.13 to 3.16) were converted to *E* electric power (kW_{AC}) supply using equation 3.4. To differentiate between solar energy and electrical energy *I* was expressed as W/m_2, while *E* was expressed in kW/1000 square meters of roof area. The comparison of monthly PV supply from average sized buildings was repeated for each orientation, since *I* varied across roof slope azimuth class. The results for buildings with an East/West orientation are given in Table 3.17.

Table 0.9 Hourly PV panel power output for an average day by month on buildings with East/West orientation (ESRI, 2019)[1].

Time of Day	Hourly AC Output Power (kW/1000m2)											
	Jan	Feb	Mar	Apr	May	Jun	Jul	Aug	Sep	Oct	Nov	Dec
8:00	0	0	0	0	5	7	6	2	0	0	0	0
9:00	11	10	12	17	25	31	27	21	15	10	12	11
10:00	34	30	38	51	53	61	54	55	47	30	37	33
11:00	53	50	64	86	79	90	79	90	79	51	59	52
12:00	62	64	84	113	100	113	99	116	103	67	72	61
13:00	60	70	95	127	111	126	110	130	116	75	73	60
14:00	47	68	94	127	112	127	111	130	116	75	62	47
15:00	26	58	83	112	103	118	103	117	103	66	42	27
16:00	5	41	63	85	85	98	86	91	78	50	19	6
17:00	0	24	37	50	59	70	62	57	46	30	9	1
18:00	0	8	11	13	32	40	35	17	12	9	6	0
19:00	0	0	0	0	10	13	12	2	0	0	0	0
20:00	0	0	0	0	1	1	1	0	0	0	0	0
Base[2]:	33	46	64	85	81	93	81	90	78	50	43	33
Peak[3]:	0	0	0	100	94	108	94	105	92	0	0	0
Shoulder[4]:	20	24	33	53	55	64	56	56	49	26	25	19
Energy (kWh/1000m2/day)[5]:	300	423	584	782	776	895	783	830	715	464	393	298

[1] Daily solar energy values found with ArcGIS Pro's Point Solar tool, calibrated with NOAA meteorological and solar radiation datasets

[2] The average hourly electric supply between 9:00 and 17:00 by month.

[3] The average hourly electric supply between April 1st and September 30th each day between 13:00 until 17:00.

[4] The average hourly electric supply between April 1st and September 30th each day between 11:00 through 12:00, and 18:00.
The average hourly electric supply between October 1st through March 30th each day between 9:00 through 11:00, and 17:00 through 19:00.

[5] The total electrical energy produced each day on average by month.

The table shows calculated *E* results between 8:00 and 20:00 averaged by hour for each month over an entire year. The seasonal divide between months was distinguished by the vertical dashed lines. Since the *E* output is a function of *I* input, the same general quantitative trends are demonstrated here as with the irradiance tables for the monthly analysis. The results of *E* average hourly supply for buildings with a Northwest/Southeast orientation are given in Table 3.18.

Table 0.10 Hourly electric power output for an average day by month on buildings with Northwest/Southeast orientation (ESRI, 2019)[1].

Time of Day	Hourly AC Output Power (kW/1000m^2)											
	Jan	Feb	Mar	Apr	May	Jun	Jul	Aug	Sep	Oct	Nov	Dec
8:00	0	0	0	0	5	5	5	2	0	0	0	0
9:00	8	10	12	16	24	23	25	20	15	10	12	8
10:00	25	30	37	49	50	46	49	52	45	30	37	25
11:00	39	49	62	82	75	68	72	85	76	50	59	39
12:00	46	64	81	108	94	85	90	109	99	66	71	46
13:00	45	70	92	121	104	95	100	123	111	74	72	44
14:00	35	68	91	121	106	96	101	123	111	74	61	35
15:00	20	57	81	107	97	89	94	110	98	66	41	20
16:00	4	41	61	81	79	74	78	86	75	50	19	5
17:00	0	24	36	47	56	53	56	54	44	29	9	1
18:00	0	8	11	13	30	30	32	16	12	9	6	0
19:00	0	0	0	0	9	10	11	2	0	0	0	0
20:00	0	0	0	0	1	0	1	0	0	0	0	0
Base[2]:	25	46	61	81	76	70	74	85	75	50	42	25
Peak[3]:	0	0	0	95	88	81	86	99	88	0	0	0
Shoulder[4]:	14	24	32	51	52	48	51	53	47	26	24	14
Energy (kWh/ 1000m^2/day)[5]:	222	420	564	744	728	676	713	782	686	458	388	223

[1] Daily solar energy values found with ArcGIS Pro's Point Solar tool, calibrated with NOAA meteorological and solar radiation datasets

[2] The average hourly electric supply between 9:00 and 17:00 by month.

[3] The average hourly electric supply between April 1st and September 30th each day between 13:00 until 17:00.

[4] The average hourly electric supply between April 1st and September 30th each day between 11:00 through 12:00, and 18:00.

The average hourly electric supply between October 1st through March 30th each day between 9:00 through 11:00, and 17:00 through 19:00.

[5] The total electrical energy produced each day on average by month.

The results of *E* average hourly supply for buildings with a Northeast/Southwest orientation are given in Table 3.19.

Table 0.11 Hourly electric power output for an average day by month on buildings with Northeast/Southwest orientation (ESRI, 2019)[1].

Time of Day	Hourly AC Output Power (kW/1000m2)											
	Jan	Feb	Mar	Apr	May	Jun	Jul	Aug	Sep	Oct	Nov	Dec
8:00	0	0	0	0	5	6	6	2	0	0	0	0
9:00	7	8	11	16	26	26	27	21	14	8	9	6
10:00	20	24	34	49	54	52	54	55	43	25	29	19
11:00	31	41	57	83	81	76	79	88	72	43	46	30
12:00	37	52	75	108	102	95	99	114	95	56	56	35
13:00	36	58	84	121	113	106	110	128	107	63	56	34
14:00	28	56	84	121	115	107	112	128	106	63	48	27
15:00	16	47	74	107	105	99	103	115	94	56	33	16
16:00	3	34	56	81	86	82	86	90	72	42	16	4
17:00	0	20	33	47	61	59	62	57	43	25	7	1
18:00	0	7	10	13	33	33	35	17	11	8	5	0
19:00	0	0	0	0	10	11	12	2	0	0	0	0
20:00	0	0	0	0	1	0	1	0	0	0	0	0
Base[2]:	20	38	56	82	83	78	81	88	72	42	33	19
Peak[3]:	0	0	0	96	96	91	95	104	84	0	0	0
Shoulder[4]:	12	20	29	51	56	54	56	55	45	22	19	11
Energy (kWh/1000m2/day)[5]:	177	348	519	747	792	753	787	818	658	389	304	172

[1] Daily solar energy values found with ArcGIS Pro's Point Solar tool, calibrated with NOAA meteorological and solar radiation datasets

[2] The average hourly electric supply between 9:00 and 17:00 by month.

[3] The average hourly electric supply between April 1st and September 30th each day between 13:00 until 17:00.

[4] The average hourly electric supply between April 1st and September 30th each day between 11:00 through 12:00, and 18:00.
The average hourly electric supply between October 1st through March 30th each day between 9:00 through 11:00, and 17:00 through 19:00.

[5] The total electrical energy produced each day on average by month.

The results of *E* average hourly supply for buildings with a North/South orientation are given in Table 3.20.

Table 0.12 Hourly electric power output for an average day by month on buildings with North/South orientation (ESRI, 2019)[1].

Time of Day	Hourly AC Output Power (kW/1000m2)											
	Jan	Feb	Mar	Apr	May	Jun	Jul	Aug	Sep	Oct	Nov	Dec
8:00	0	0	0	0	10	11	12	4	1	0	0	0
9:00	13	16	22	32	53	53	56	42	28	16	19	12
10:00	39	48	68	99	110	105	109	110	87	50	57	38
11:00	61	80	114	166	164	155	161	178	145	85	90	59
12:00	73	103	150	217	207	193	200	230	190	111	110	70
13:00	70	114	168	244	230	215	223	258	214	125	111	68
14:00	55	110	168	243	233	218	226	258	214	125	95	54
15:00	31	94	148	215	214	202	209	232	189	110	65	31
16:00	6	67	112	163	175	167	174	181	144	84	31	8
17:00	0	39	66	95	123	120	126	114	85	49	14	1
18:00	0	14	20	26	66	68	72	35	22	16	10	0
19:00	0	0	0	0	20	22	24	4	0	0	0	0
20:00	0	0	0	0	1	1	1	1	0	0	0	0
Base[2]:	39	75	113	164	168	159	165	178	144	84	66	38
Peak[3]:	0	0	0	192	195	185	191	209	169	0	0	0
Shoulder[4]:	23	39	58	102	114	110	114	112	89	43	38	22
Energy (kWh/1000m2/day)[5]:	349	686	1038	1500	1606	1532	1591	1646	1319	770	602	341

[1] Daily solar energy values found with ArcGIS Pro's Point Solar tool, calibrated with NOAA meteorological and solar radiation datasets

[2] The average hourly electric supply between 9:00 and 17:00 by month.

[3] The average hourly electric supply between April 1st and September 30th each day between 13:00 until 17:00.

[4] The average hourly electric supply between April 1st and September 30th each day between 11:00 through 12:00, and 18:00.
The average hourly electric supply between October 1st through March 30th each day between 9:00 through 11:00, and 17:00 through 19:00.

[5] The total electrical energy produced each day on average by month.

The table shows calculated *E* results between 8:00 and 20:00 averaged by hour for each month over an entire year. These hourly power output and summary time-of-use metrics are the sum of PV output on both rooftop slopes for this orientation.

Estimation of Farm Performance as a Power Plant by Demand Curve Metrics

The hourly electric power results by hour for each month in Tables 3.17 to 3.20 were organized according to the utility time-of-day hour classes (Figure 3.1) into the rows labeled as base, peak, shoulder, and Energy. These further demonstrate a farm's potential contributions in supply-side energy management. These categories were established using the equations given in Table 3.21.

Table 0.13 Calculations for determining key summary power output metrics by season[1].

	Calculations by Hour Class	
	Summer	Winter
Base[2]:	(9:00 + 10:00 + 11:00 + 12:00 + 13:00 + 14:00 + 15:00 + 16:00 + 17:00) ÷ 9	
Peak[3]:	(13:00+14:00+15:00+16:00+17:00)÷5	(6:00 +7:00 +8:00) ÷ 3
Shoulder[4]:	(11:00 +12:00 +18:00 +19:00) ÷ 4	(9:00 +10:00 +11:00 +17:00 +18:00) ÷ 5
Energy (kWh/ 1000m2/day)[5]:	Σ all hour classes within a day	

1 Summer months are April through September. Winter months are October through March.
2 The average hourly electric supply between 9:00 and 17:00 by month.
3 The average hourly electric supply during seasonal peak periods by month. Peak summer hours are 13:00 through 17:00. Peak winter hours are 6:00 through 8:00.
4 The average hourly electric supply during seasonal shoulder periods by month. Shoulder summer hours are 11:00 through 12:00, and 18:00. Shoulder winter hours are 9:00 through 11:00, and 17:00 through 18:00.
5 The total electrical energy produced each day on average by month.

Time of use classes included base, peak, and shoulder and varied by season. Base load was defined by the local utility in the study area as the average expected demand. Therefore, the installed PV's contribution to base load was represented as the average hourly output between 9:00 and 18:00 for any given day throughout the entire year. An important distinction in defining time periods was between a specific time (such as 18:00 o'clock, with a 60-second duration) and an hour class (18, with a 60-minute duration). For the contribution to base load on the average day, the time period between 9:00

o'clock and 18:00 o'clock does not include production during the 60-minute hour period between 18:00:00 and 18:00:59. Rather it constitutes production *within* the 9-hour time span between 9:00:00 and 17:59:59. This distinction applies to all temporal references for time-of-use analysis.

Peak load was defined as the periods of maximum load in a given day. The local utility in the study area defined peak demand hours as between 13:00 and 17:00 in the summer, and 6:00 until 8:00 in the winter. A farm's contribution to peak load was calculated as the average hourly output for all hour classes within those periods. Shoulder loads were defined as the transitional demand between average (base) load and maximum (peak) loads. The local utility classified shoulder hours as 11:00 through 12:00 and 18:00 through 19:00 in summer, and 9:00 through 11:00, and 17:00 until 18:00 in winter. (The utility DEP included the hour of 19:00 in winter shoulder periods, however these were not included in calculations due to a lack of production). A farm's contribution to shoulder load was calculated as the average hourly power output during each hour class within those periods. Lastly, a farm's total PV energy production was considered. This was calculated as the sum of all power produced throughout a day.

Estimation of Farm Performance with Peak Electric Power Production

On a summer day between 13:00 and 17:00 a building oriented East/West provided a power output from 92 to 108 kW/hr in the summer season. This orientation, nor any other orientation, had a contribution to peak during winter months. A building oriented Northeast/Southwest peak load contribution ranged from 84 to 104 kW/hr in

summer. A building oriented Northwest/Southeast provided the least electric power as compared to a building with an East/West orientation using the same number of panels with a peak load contribution between 81 and 99 kW/hr in summer. Lastly, the 12% of buildings within the North/South orientation had a peak load contribution ranging from 185 to 209 kW/hr in the summer season. The total panel area per building was 2316 m_2 instead of 1158 m_2, resulting in the highest peak supply per building of any orientation.

Estimation of Farm Performance with Shoulder Electric Power Production

The shoulder period was defined as the hours from 11:00 to 12:00 and 18:00 to 19:00 in summer, and from 9:00 to 11:00 and 17:00 to 18:00 in winter. The buildings oriented East/West had shoulder contributions ranging from 20 kW/hr for the average day in January to 64 kW/hr for the average day in June. Buildings oriented Northeast/Southwest had shoulder contributions ranging from 11 kW/hr for the average day in December to 56 kW/hr for the average day in July. The buildings oriented Northwest/Southeast had shoulder supply that ranged from 14 kW/hr for the average day in January to 53 kW/hr for the average day in August. North/South oriented buildings had contributions to shoulder periods that ranged from 22 kW/hr for the average day in December to 114 kW/hr in May. This supply was 10% larger than the shoulder supply of East/West buildings in winter months, and 78% larger in summer months.

Estimation of Farm Performance with Baseload Electric Power Production

Baseload was defined as the average electric power required by the customers in a day or season, and a roof-mounted PV array's contribution to baseload was calculated as the average electric power produced from the hour beginning at 9:00 till the end of the hour beginning at 17:00. The East/West oriented buildings had an average daily baseload contribution ranging from its lowest output of 33 kW/hr in January to its highest output of 93 kW/hr in August. In comparison, the average daily baseload contribution for buildings that were oriented Northeast/Southwest ranged from 20 kW/hr in January to 88 kW/hr in August. Buildings that were oriented Northwest/Southeast had an average daily baseload contribution ranged from 25 kW/hr in January to 85 kW/hr in August. Lastly, the buildings within the North/South orientation had 19-89 per 1000m_2, or 39 to 178 for both arrays.

Estimation of Farm Performance with Daily Electric Energy Production

A building's total energy supply per day was calculated as the sum of all power produced throughout a day. For the building oriented East/West, the total energy produced on an average day ranged from the lowest amount of 298 kWh in December to the highest amount of 895 kWh in June. This was the highest of any single-array building. The second highest daily average energy production was from buildings oriented northwest/Southeast. The total energy produced on an average day ranged from 222 kWh in January to 782 kWh in August. The lowest energy production was on buildings oriented Northeast/Southwest, where total energy produced on an average day ranged from 172 kWh in December to 818 kWh in August. The buildings oriented

North/South had the highest output per building, with total energy produced on an average day ranging from 341 kWh in December to 1646 kWh in June. This summer energy output was over 80% higher than the next largest summer daily energy output by buildings oriented East/West.

Solar Electric Power Production from Roof Mounted PV Arrays on Poultry Farms in a Region

If the fuel source for this energy production were the typical fossil fuel, or even hydroelectric, then the facility output would only be a function of installed equipment. These calculated *E* results were based on modeled *I* data, which was heavily sensitive to atmospheric assumptions. In reality, a seasonal rain shower or afternoon thunderstorm was common in the Southeastern United States, making the fuel availability in the context of solar highly variable. Therefore, the range of estimated hourly supply as farm performance were averaged to determine realistic estimates representative of hourly and monthly production across a season. The key summary power supply metrics of seasonal base, peak, and shoulder contributions were averaged for each orientation. These summary values were then normalized by area to accurately scale power supply independent of variation in building size or orientation. The seasonal averages are given in Table 3.22.

Table 0.14 Average hourly electric supply for each building orientation by seasonal time of use category.

	Average Hourly PV Supply (kW/1000m2)			
	E/W	NW/SE	NE/SW	N/S
Average summer peak power1:	99	90	94	95
average shoulder summer2:	56	50	53	53
average shoulder winter3:	24	22	19	19
average summer power4:	85	77	81	81
average winter power5:	45	41	35	34
sum annual energy (kWh/1000m2/yr)6:	220,279	200,845	196,576	197,406

1 The average hourly electric supply between April 1st and September 30th each day between 13:00 until 17:00.
2 The average hourly electric supply between April 1st and September 30th each day between 11:00 through 12:00, and 18:00.
3 The average hourly electric supply between October 1st through March 30th each day between 9:00 through 11:00, and 17:00 through 19:00.
4 The average hourly electric supply between April 1st and September 30th each day between 9:00 and 17:00.
5 The average hourly electric supply between October 1st through March 30th each day between 9:00 and 17:00.
6 The total electrical energy produced in a year

The key summary power supply metrics are given for each season and orientation, expressed as kW/hr/1000m2 and sum annual energy expressed as kWh/1000m2/yr.

Estimation of Farm Performance with Peak Electric Power Production

On a summer day between 13:00 and 17:00 a building oriented East/West provided an average power output of 99 kW/hr in summer. The 12% of buildings that were oriented North/South had the second highest power supply per unit area of any array at 95 kW/hr. With twice the panel area per building, the average peak load contribution for two arrays would be 190 kW/hr in the summer season. A building oriented Northeast/Southwest peak load contribution averaging 94 kW/hr in summer. A building oriented Northwest/Southeast provided the least electric power as compared to a building with an East/West orientation using the same number of panels with an average peak contribution of 90 kW/hr in summer.

Estimation of Farm Performance with Shoulder Electric Power Production

The shoulder period was defined as the hours from 11:00 to 12:00 and 18:00 to 19:00 in summer, and from 9:00 to 11:00 and 17:00 to 18:00 in winter. The buildings oriented East/West had shoulder contributions of 24 kW/hr in winter and 56 kW/hr for in summer. Buildings oriented Northeast/Southwest had slightly less shoulder contributions of 22 kW/hr in winter and 50 kW/hr in summer. The buildings oriented Northwest/Southeast and North/South had a lower winter shoulder average of 19 kW/hr but a higher summer average supply of 53 kW/hr.

Estimation of Farm Performance with Baseload Electric Power Production

Baseload was defined as the average electric power required by the customers in a day or season, and a roof-mounted PV array's contribution to baseload was calculated as the average electric power produced from 9:00 till 17:00. The East/West oriented buildings had an average daily baseload contribution of 45 kW/hr in winter and 93 kW/hr in summer. In comparison, the average daily baseload contribution for buildings that were oriented Northeast/Southwest were 41 kW/hr in Winter to 77 kW/hr in Summer. Buildings that were oriented Northwest/Southeast had an average daily baseload contribution ranged from 35 kW/hr in January to 81 kW/hr in August. Lastly, the buildings within the North/South orientation had only slightly less production at 34 kW/hr in Winter and 81 kW/hr in Summer.

Estimation of Farm Performance with Daily Electric Energy Production

A building's total energy supply per day was calculated as the sum of all power produced annually. For the building oriented East/West, the total energy produced per year ranged from the lowest amount of 220,279 kWh/1000m2/yr . This was the highest of any single-array building. The second highest daily average energy production was from buildings oriented northwest/Southeast. The total energy produced on an average year was 200,845 kWh/1000m2. The lowest energy production was on buildings oriented Northeast/Southwest, where total energy produced on an average year was 196,576 kWh/1000m2. Buildings in the North/South orientation produced an average 197,406 kWh/1000m2 of array per year. Combining both productive array areas, the buildings oriented North/South had the highest output per building, with total energy produced on an average year of 398,811 kWh/1000m2. These averaged seasonal results help to scale power supply independent of variation in building size, orientation, or atmospheric conditions.

Monthly Photovoltaic Supply for an Entire Farm

An analysis of *E*, rooftop supply, was first scaled up onto an entire farm. This was done by multiplying *E* (kW/1000m2) power supply for buildings oriented East/West by 1254 m2 of roof area for a building (*A*), and by 4 buildings per farm. Equations from Table 3.21 were used to average the hourly time-of-use metrics for the average day of each month. Then Equations from Table 3.23 were used to further summarize the average monthly supply for each month in a season. This was done to determine single-

season metrics of power supply of an entire farm similar to the process done for a single building. These results, given in Table 3.23, concisely communicate plant performance from hourly PV panel output on an average day of each month to the average hourly output per 6 months for a typical farm.

Table 0.15 Hourly electric power output for an average day by month for an average farm[1] with East/West orientation (ESRI, 2019)[2]**.**

Time of Day	Hourly AC Output Power (kW/farm)											
	Jan	Feb	Mar	Apr	May	Jun	Jul	Aug	Sep	Oct	Nov	Dec
8:00					25	33	30	10				
9:00	56	49	62	83	127	155	137	106	77	49	61	55
10:00	169	150	192	257	265	308	270	278	235	152	187	166
11:00	265	249	323	433	398	454	396	450	395	256	298	260
12:00	313	321	422	567	501	566	494	581	517	335	362	308
13:00	303	353	475	638	558	630	550	652	581	377	366	300
14:00	238	342	474	636	564	639	557	654	580	376	311	237
15:00	132	290	419	562	518	591	516	586	514	333	209	134
16:00	27	208	317	426	425	491	430	457	392	253	97	32
17:00		119	185	249	298	353	311	288	232	149	44	3
18:00		42	57	68	160	200	177	87	61	47	32	
19:00					49	66	59	10				
20:00					3	3	3					
Base[3]:	188	231	319	428	406	465	407	450	392	253	215	166
Peak[4]:	0	0	0	502	473	541	473	527	460	0	0	0
Shoulder[5]:	98	122	164	267	277	322	282	282	243	130	124	97
Energy (MWh /farm/day)[6]:	1.50	2.12	2.93	3.92	3.89	4.49	3.93	4.16	3.58	2.33	1.97	1.50

1 Typical farm is 4 houses oriented East/West with interior area of 2316 m^2 and rooftop solar cell area of 1,067 m^2.

2 Daily solar energy values found with ArcGIS Pro's Point Solar tool, calibrated with NOAA meteorological and solar radiation datasets

3 The average hourly electric supply between 9:00 and 17:00 by month.

4 The average hourly electric supply between April 1st and September 30th each day between 13:00 until 17:00.

5 The average hourly electric supply between April 1st and September 30th each day between 11:00 through 12:00, and 18:00.
The average hourly electric supply between October 1st through March 30th each day between 9:00 through 11:00, and 17:00 through 19:00.

6 The total electrical energy produced each day on average by month.

Using equations (Table 3.21) to average the time-of-use metrics for each season, the average baseload contribution ranged from 166 kW/hr in December to 465 kW/hr in June. Peak load contribution was 0 during winter seasons, and ranged from 460 to 541 kW/hr in the summer season. Shoulder contributions ranged from 97 kW/hr in December to 322 kW/hr in May. The total energy produced on an average day ranged from 1.50 MWh in December to 4.49 MWh in June. These ranges of average supply by time-of-use summary categories help to demonstrate the potential feasibility of an entire farm of poultry buildings functioning as distributed PV plants.

Further averaging monthly supply from an entire farm (as with Table 3.23 for a single building) within a seasonal range was done to determine single-season metrics of power supply to concisely communicate plant performance. This equated to an average supply from an entire farm of 496 kW per hour during peak periods. This farm supplied an average 279 kW per hour during summer shoulder periods and 123 kW in winter shoulder periods. A typical farm also had a seasonal contribution to base load of 229 kW per hour each day in winter months and 425 kW per hour during summer months. Lastly, the average energy output on the typical farm was calculated to be 1,104 MWh over an entire year.

The industry standard description of energy system size is known as nameplate capacity, which is representative of its maximum sustainable output performance. This standard measurement has the potential to be grossly misleading for renewable energy plants due to the significant disparity between the energy output potential of the equipment installed and the availability of fuel. A plant's Capacity Factor (CF) is the

ratio of actual energy generated compared to the installed nameplate capacity. This takes into account resource availability factors such as cloudiness and sunlight duration. Average CF for solar plants range from 10-20% depending on region. In contrast, nuclear energy has an average CF of 90% (US EIA, 2019).

Instead of determining a farm's nameplate capacity and then a CF for the region of interest, a single descriptor was chosen based on the study's intended purpose. Since the most critical need in this scenario of energy supply was SSM peak shaving, farms were categorized according to their corresponding peak supply. For the above example of an average farm, the single quantitative descriptor of size and performance was therefore a 496 kW/hr peaking plant.

To further put this performance into perspective: a 4-house farm supplies 496 kW for each of the five hours within a day's peak periods, for each 30.4 days of every month, for the 6 months in the summer season. That would result in an annual cumulative 452,501 kWh of peak-shaving electricity from a single, typical farm in the study area. These results are indicative of the value a typical farm in the study area had when functioning as a PV plant.

Solar Electric Power Production from Roof Mounted PV Arrays on Poultry Farms in a Region

The normalized power and energy metrics (Table 3.22) were scaled to each building on each farm. The study population totaled 499,486 m^2 of productive solar cell area (A x f_C). One hundred and thirty-nine buildings were oriented East/West and had a total collector area of 149,026 m^2 (30% of total). Ninety-seven buildings were categorized as Northwest/Southeast, and had a total collector area of 111,518 m^2 (22%). One hundred and fifteen buildings were categorized as Northeast/Southwest and had a total collector area of 124,850 m^2 (25%). Forty-seven buildings oriented North/South had a total collector area of 114,092 m^2 (23% of total).

The farms in the study area were all described according to hourly average summer peak power supply. A map of all farms by peak performance is given in Figure 3.6.

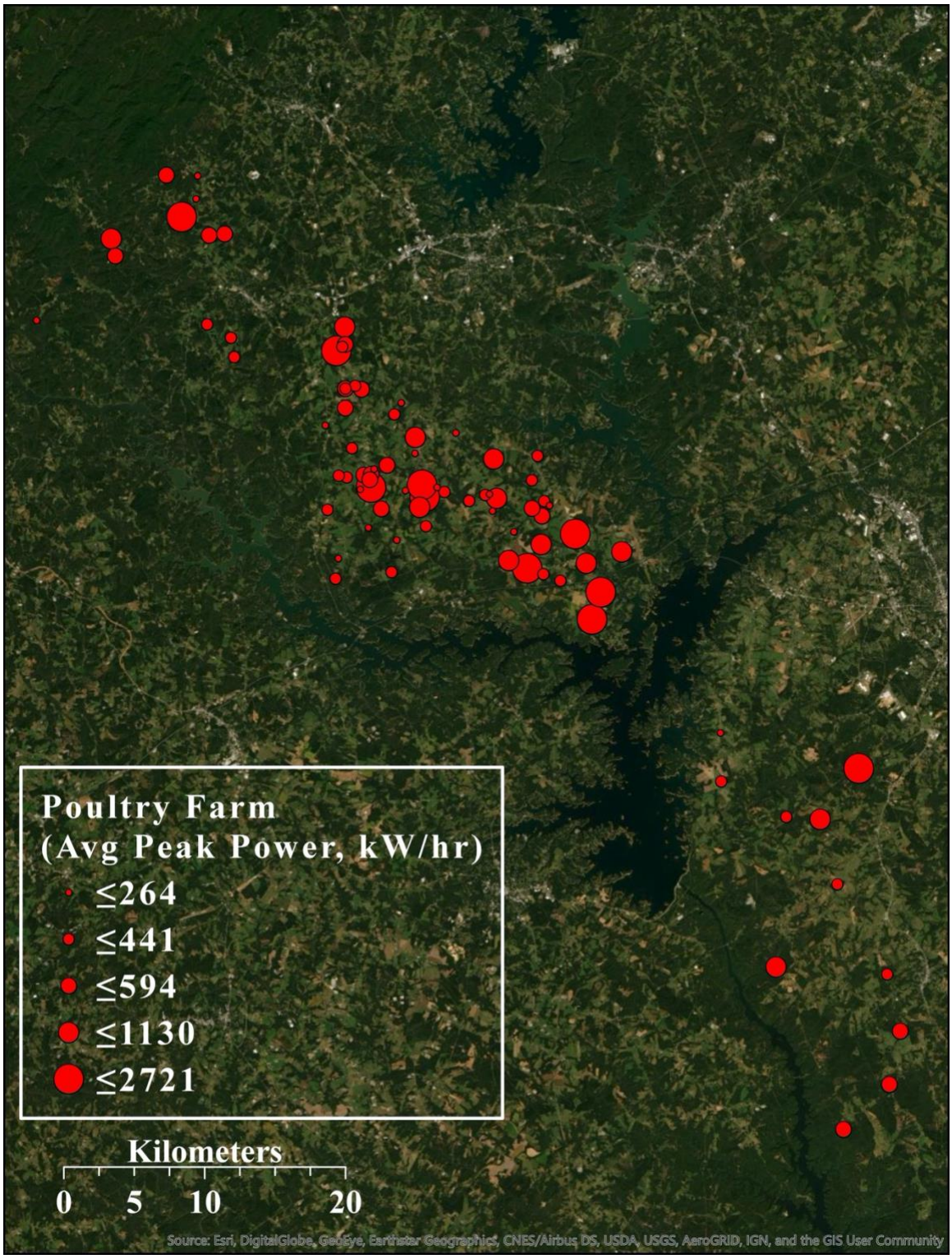

Figure 0.3 Spatial distribution of 88 aggregated PV plants.

The study area as delineated with opaque shading. The location of each farm was marked in red. The graduated size was representative of average total PV rooftop power supply during summer peak hours.

The proximity study results (Figure 3.5) were reintroduced to combine farm location with the established summary power output during the annual average summary time-of-use categories. The distance of a farm from the transmission grid (km) was plotted relative to each power output metric (summer peak, winter and summer shoulder, and winter and summer base) separately. This covariate analysis of space and performance further organized the population of farms for better comparisons and prioritization of value to an energy supplier.

First, farm distance (km) was plotted relative to its average hourly summer peak power output. The results are given in Figure 3.7.

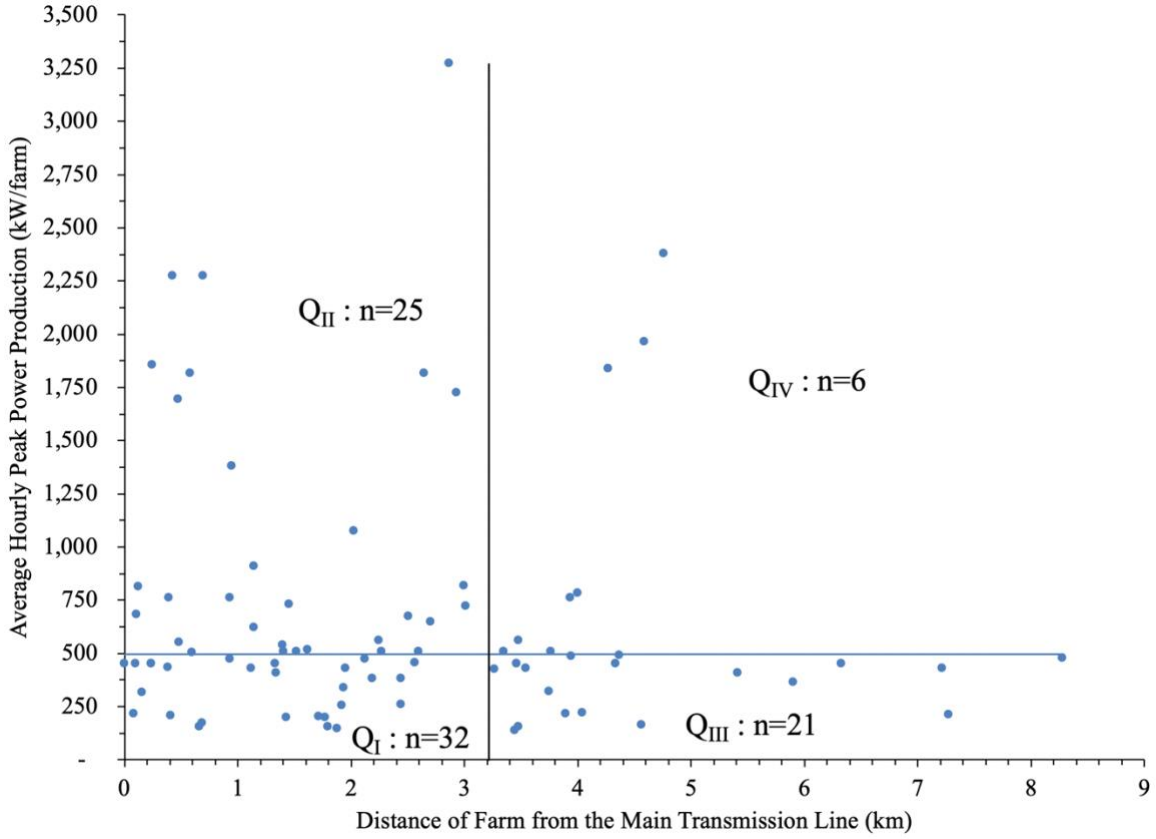

Figure 0.4 Plot of farm distance and average peak power produced on summer days between 13:00 and 17:00.

Each farm is plotted according to its average peak power in summer. For reference, the qualities of the average farm were included in each graph. The spatial boundary of 3.28 km that represents the average farm distance is on the plot as a vertical black line. The average summer peak power for the typical farm was 496 kW/hr/farm, denoted by a horizontal blue line. This illustrated how each farm performed relative to average farm individually, and organized the entire group into four groups, or quadrants. The Quadrant I had 32 farms and represented the farms that had less than average output and less than average distance. Quadrant II had 25 farms and represented farms that had above average

output, and below average distance. Quadrant III had 21 farms and represented farms that had above average distance and below average output. Quadrant IV had 6 farms and represented farms that had above average distance and above average output. The farms in Quadrand IV are likely the most valuable to an energy supplier.

The results of the spatial distribution of each farm plotted relative to the average shoulder power output in summer and winter are given in Figure 3.8.

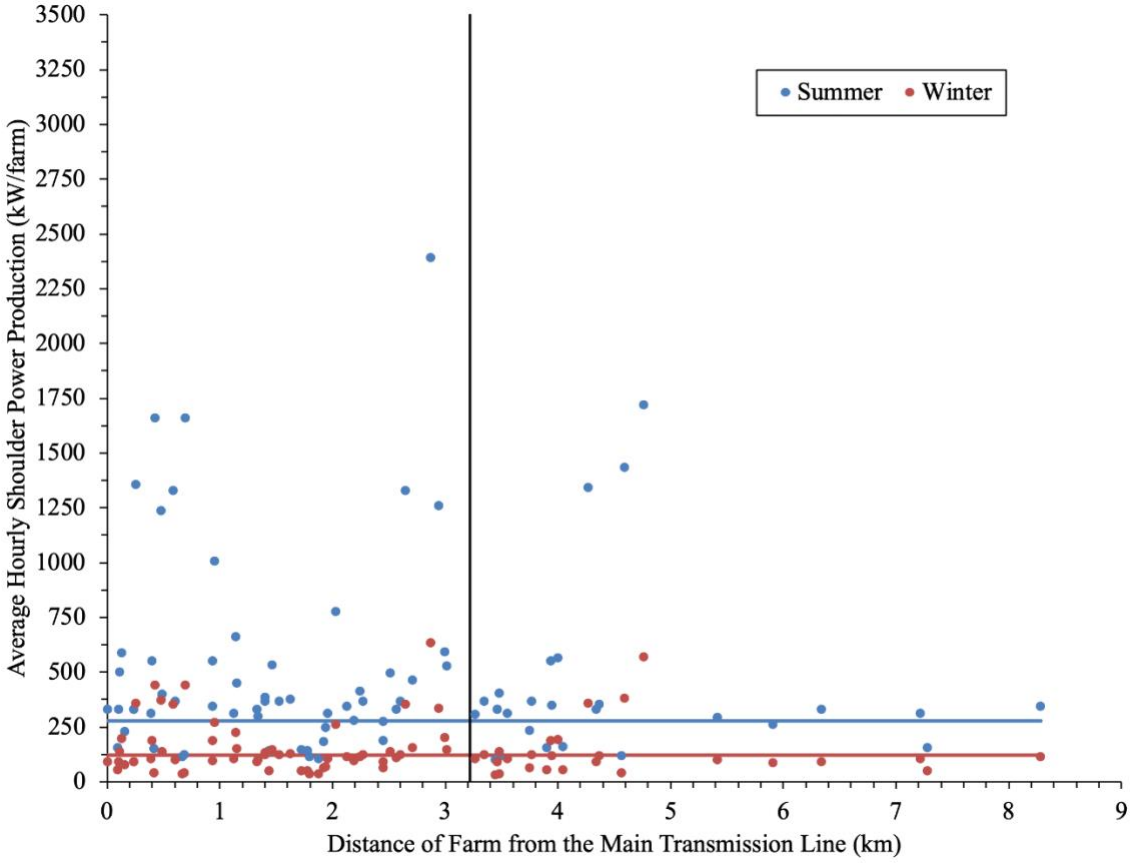

Figure 0.5. Plot of farm distance and average shoulder power produced in summer between 11:00 and 13:00, and 18:00; and in winter from 9:00 to 11:00, then 17:00 through 19:00.

This graph illustrated the average hourly contribution to shoulder load by farm (kW/farm) for the average day in each season. Each farm was plotted twice on the y-axis. Once by the calculated average shoulder summer production and again by average winter shoulder production. The typical farm average shoulder power supply was also given for reference. The typical farm was located 3.28 km from a transmission line, supplied an average 123 kW/hr/farm during winter shoulder periods (red), and 279 kW/hr/farm in summer shoulder periods (blue). As was to be expected, the shoulder contributions were less than what each farm could supply to peak loads. The axis scale in each graph were held constant for comparison between each key summary metric. The spatial distribution of farms plotted relative to average power output in summer and winter are given in Figure 3.9.

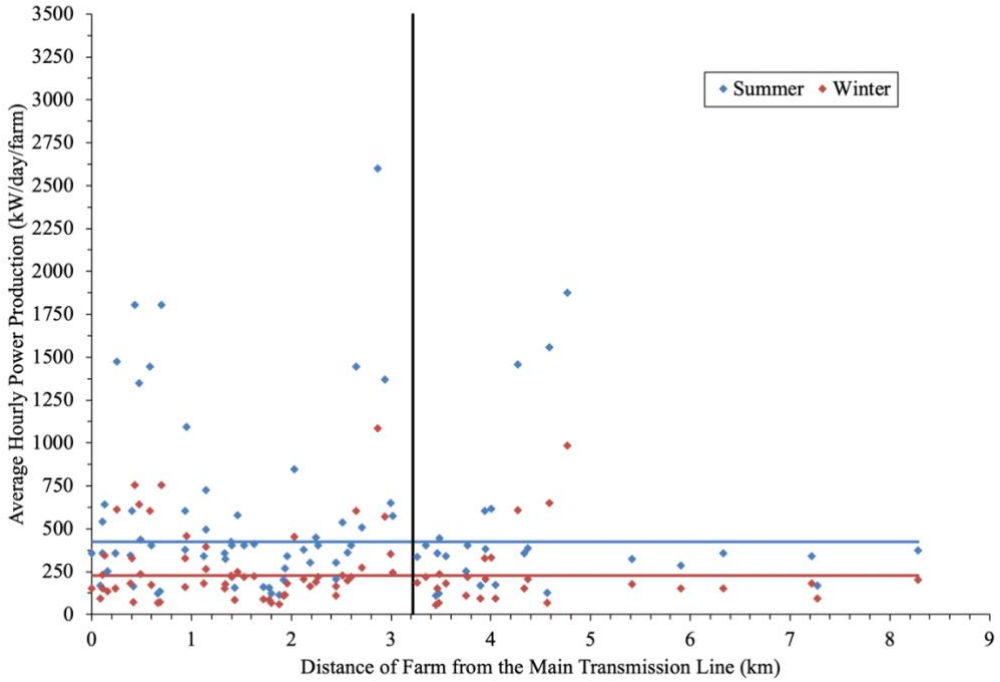

Figure 0.6 Plot of farm distance and average baseload power produced per hour each day between 9:00 and 17:00.

This graph illustrated the average hourly contribution to base load for the average day (kW/farm) by season. Each farm was plotted twice, once by calculated average summer production and again by average winter production. The typical farm average power supply was also given for reference. The typical farm was located 3.28 km from a transmission line, supplied an average 229 kW/hr/farm in winter (red), and 425 kW/hr/farm in summer (blue).

The population of farms within in the study area were organized by performance and location relative to the average farm (Figure 3.7). The four quadrants represent the four combinations of relationship to the typical farm. The contributions of each farm in a quadrant category were totaled according to each of the key summary time-of-use metrics that were used to estimate a farm's performance as a PV plant. The total contribution for each collective quadrant category to the five time-of-use summary farm output values are summarized in Table 3.24.

Table 0.16 Summary output metrics for all farms by seasonal time-of-use and by quadrant.

	Q_I	Q_{II}	Q_{III}	Q_{IV}
Number of farms:	32	25	21	6
Available roof area (m_2):	115,399	217,262	80,310	68,382
average summer peak power (kW/hr)[1]:	11,445	29,463	7,735	8,275
average shoulder summer (kW/hr)[2]:	8,347	21,514	5,628	6,019
average shoulder winter (kW/hr)[3]:	2,654	6,216	1,809	1,827
average summer power (kW/hr)[4]:	9,105	23,414	6,141	6,558
average winter power (kW/hr)[5]:	4,589	10,658	3,123	3,140
sum annual energy (MWh/yr)[6]:	25.03	62.64	16.98	17.85
Nominal capacity (kW/hr):	22,229	40,371	15,259	12,993
Total distance (km):	42.3	36.2	97.1	25.0

[1] The average hourly electric supply between April 1st and September 30th each day between 13:00 until 17:00.
[2] The average hourly electric supply between April 1st and September 30th each day between 11:00 through 12:00, and 18:00.

[3] The average hourly electric supply between October 1st through March 30th each day between 9:00 through 11:00, and 17:00 through 19:00.
[4] The average hourly electric supply between April 1st and September 30th each day between 9:00 and 17:00.
[5] The average hourly electric supply between October 1st through March 30th each day between 9:00 and 17:00.
[6] The total electrical energy produced in a year.

Each quadrant group of farms had a total count, total available roof area (m^2), average peak power (kW/hr), average shoulder summer (kW/hr), average shoulder contribution in winter (kW/hr), average contribution to base in summer (kW/hr), average contribution to base in winter (kW/hr), total annual energy produced (MWh/yr), the nominal capacity according to industry standards (kW/hr) and total distance (km) between all farms and the transmission grid.

Quadrant I had the highest number of farms. However, Quadrant II had the greatest total solar cell area, and therefore the highest contribution to any single supply metric by over 50%. The 27 houses located furthest from the transmission grid (QIII and QIV) had a sum rooftop collector area of 142,383 square meters and 37.1 GWh of annual generation. The total amount of energy generated during summer and winter peak hours for these houses was 15.3 GWh. The on-peak demand during summer for houses outside the 3.28 km boundary was 1.4 MW, while the potential on-peak supply to grid (on-peak reduction) was 27.1 MW.

Another insightful variable was the analysis of total distance (km) between all farms and the transmission grid. As previously mentioned, the distance analysis was limited in its usefulness because it was not representative of the existing distribution network in place between the transmission grid and each farm. However, the measurement was still indicative of the spatial relationship between the two subjects

which provided an approximation of potential savings from line losses and infrastructure costs needed to supply energy over that distance. The 32 farms in Quadrant I had a total 42.3 km of distance between farm and grid. The 25 farms in Quadrant II had a total distance of 36.2 km. The 21 farms in Quadrant III had a total distance of 97.1 km. The 6 farms in Quadrant IV had a total distance of 25.0 km. Normalizing these two variables of distance (km) by farm (count) for each group, Quadrant I had a ratio of 1.3 km/farm, Quadrant II had a ratio of 1.4 km/farm, Quadrant III had a ratio of 4.6 km/farm, and Quadrant IV had a ratio of 4.2 km/farm. This demonstrated further value to all farms in Quadrant III, in which there are over three times the number of farms as Quadrant IV.

Additionally, the category of nominal capacity (kW/hr) was calculated for each farm and totaled by quadrant. This industry standard measurement was included for comparison to the chosen metrics of plant performance by time-of-use categories. These impractical results reinforced the lack of clarity provided when defining a photovoltaic energy generation facility by the potential production output of the equipment installed.

Estimation of Electrical Energy Use and Demand on Broiler Farms

The calculated rooftop supply for the study area did not include energy use and demand during critical broiler house loads. These were primarily a function of facility ventilation and lighting systems. If the process of net metering were to apply to facility electricity loads, then only electricity generated in excess of farm demand would be useful for peak-shaving contributions to the grid.

Facility Energy Consumption

The energy bills for 51 farms (122 houses) in SC were analyzed. These results were also normalized by respective building footprint and categorized by bird type (provided in Appendix C). The results of the broiler facility electricity consumption are summarized in Table 3.25.

Table 0.17 Average broiler farm electricity consumption (kWh/100m2) (n = 41).

Month	Mean	Max.	Min.	St.dev.	C.V. (%)
January	119	238	22	56	47
February	107	265	21	46	43
March	129	259	30	52	40
April	135	367	18	75	56
May	160	269	26	55	35
June	218	582	5	135	62
July	211	657	35	123	58
August	244	475	58	111	46
September	220	620	28	126	57
October	165	353	26	85	52
November	140	462	23	83	59
December	110	276	33	53	48
kWh/100m2/year	1946	3409	395	693	36

Energy consumption increased on average during the first seven months to peak in August, and then decreased during the remaining 5 months. The average monthly consumption ranged from 107 kWh/100m2 in February to 244 kWh/100m2 in August. The range of average annual energy use was from 395 to 3,409 kWh per 100 square meters. The annual grand mean consumption for broiler facilities was 1,946 kWh per 100 square meters. The results of the broiler breeder facility electricity consumption are summarized in Table 3.26.

Table 0.18 Average broiler breeder farm electricity consumption (kWh/100m2) (n = 2).

Month	Mean	Max	Min	St. Dev.	C.V. (%)
January	187	324	50	194	104
February	181	320	43	196	108
March	123	194	53	99	81
April	194	209	180	21	11
May	364	435	293	101	28
June	456	512	400	79	17
July	556	635	478	111	20
August	583	669	497	122	21
September	543	625	461	116	21
October	395	446	345	71	18
November	316	377	255	86	27
December	220	292	149	101	46
Annual	4120	4867	3372	1057	26

Energy consumption increased on average during the first seven months to peak in August, and then decreased during the remaining 5 months. The range of average annual energy use was from 3,372 to 4,876 kWh per 100 square meters. The annual mean consumption was 4,120 kWh per 100 square meters. The average broiler breeder house consumed over twice as much electricity as the average broiler house. This is because breeder houses contain adult chickens which require more energy to climate control, as well as refrigerated storage for eggs. The results of the pullet facility electricity consumption are summarized in Table 3.27.

Table 0.19 Average pullet farm electricity consumption (kWh/100m2) (n =8).

Month	Mean	Max	Min	std	C.V. (%)
January	86	169	20	45	52
February	100	251	28	70	70
March	111	285	38	75	68
April	77	143	24	43	56
May	101	181	58	41	40
June	119	212	20	65	54
July	197	354	40	106	54
August	217	333	87	97	45
September	199	385	76	103	52
October	142	328	68	82	58
November	105	173	35	44	42
December	83	131	49	32	38
Total	1535	2015	867	409	27

Energy consumption increased on average during the first seven months to peak in August, and then decreased during the remaining 5 months. The range of average annual energy use was from 867 to 2015 kWh per 100 square meters. The annual mean consumption was 1,535 kWh per 100 square meters. The average pullet house consumed less electricity than the average broiler house because pullet barns are stocked at a lower bird density and use a lower flock exchange rate.

Facility Connected Load

The energy consumption (kWh/mo) was used to determine the average collected load (kW/hr) for each farm. This was done by dividing the monthly consumption data by 730.4 month-hours, which is the typical conversion number used by utility to define a monthly billing cycle. The results are given in Table 3.28.

Table 0.20 Average hourly poultry farm connected load (kW/100m2).

Month	Broiler (n = 41)	Pullet (n=8)	Broiler Breeder (n=2)
January	0.163	0.093	0.256
February	0.149	0.100	0.248
March	0.171	0.110	0.169
April	0.186	0.089	0.266
May	0.219	0.141	0.499
June	0.306	0.171	0.624
July	0.292	0.263	0.762
August	0.344	0.307	0.799
September	0.308	0.282	0.744
October	0.224	0.209	0.541
November	0.195	0.154	0.433
December	0.148	0.115	0.302
Total	2.704	2.031	5.643

The average hourly connected load for the 41 broiler facilities ranged from 0.149 kW/100m2 in February to 0.308 kW/100m2 in August. The average hourly connected load for the 8 pullet facilities ranged from 0.089 kW/100m2 in April to 0.307 kW/100m2 in August. The average hourly connected load for the 2 broiler breeder farms ranged from 0.169 kW/100m2 in March to 0.799 kW/100m2 in August. The annual total of the monthly average connected load was 2.7 kW/100m2for the broiler farms, 3.0 for pullet farms, and 5.6 kW/100m2 for the broiler breeder facilities. These numbers were limited in their accuracy but were still useful in providing an approximate scope of average connected load for comparison to rooftop hourly supply.

Connected Load to Estimate Farm Hourly Peak Demand in Summer

The on-farm equipment inventory analysis was used to compare the rooftop power supply during peak periods more accurately to farm demand during peak periods.

Hourly farm loads during the most critical periods of peak demand were likely estimated to be the highest agricultural loads throughout a year. This was accomplished by collecting technical specifications for ventilation, lighting, and feeding systems at fifty-eight poultry farms (239 houses) in SC. Building dimensions were also recorded. Average demand results were then normalized by building footprint (kW/hr/m^2) and projected onto the entire building population to estimate average total load during peak demand periods in summer months. The results are expressed in Table 3.29 as average demand for each electrical system and normalized by area.

Table 0.21 Estimated average summer peak demand for poultry houses in SC based on installed equipment and energy consumption records.

	demand (kW/1000m^2)				
	average	max	min	std	n
Electrical System:					
Tunnel Ventilation:	6.3	12.2	1.2	2.4	46
Lighting:	1.2	3.5	0.1	0.9	33
Feed/other:	0.6	1.4	0.2	0.2	58
estimated summer peak demand for typical house[1] (kW):	19.0	39.7	3.4		
estimated summer peak demand for typical farm (kW):	75.9	159.0	13.6		

[1]Typical farm is 4 houses with interior footprint of 2316 m^2

Out of 58 farms visited, 46 growers provided information on existing ventilation equipment installed (192 houses). The average estimated tunnel ventilation demand during summer peak was 6.3 kW/1000m^2, ranging from 1.2 to 12.2 kW/1000m^2. Thirty-three growers provided information on existing lighting equipment installed (130 houses). The average estimated lighting demand during summer peak was 1.2 kW/1000m^2, ranging from 0.1 to 3.5 kW/1000m^2. All farms visited had feeding

equipment installed. The average estimated feeding load during summer peak was 0.6 kW/1000m2, ranging from 0.2 to 1.4 kW/1000m2.

Based on these results, the estimated average hourly demand during summer peak was calculated for a house of typical size. The average estimated total hourly connected load during summer peak was 19.0 kW per building, ranging from 3.4 to 39.7 kW. This was scaled up and repeated for an entire farm. The average estimated total hourly connected load during summer peak was 75.9 kW for an entire farm, ranging from 13.6 to 159 kW. These solutions were used across the entire study area to estimate the average total load during peak demand periods in summer months for all farms as a function of square footage.

Net Supply to Grid

The calculated results for *E*, rooftop supply, were compared to the results of both facility connected load (kW) and energy consumption (kWh) within the context of the seasonal time-of-use categories. This provided a net-to-grid contributions for both power and energy on the typical farm. The summary output metrics and net to grid can be seen in Table 3.30.

Table 0.22 Net contribution to utility transmission grid for a typical farm[1].

	PV Supply	Farm Demand[2]	Net to Grid	
average peak power (kW/hr)[3]:	496	82	414	84%
average summer power (kW/hr)[5]:	425	21	404	95%
average winter power (kW/hr)[6]:	229	21	208	91%
sum annual energy (MWh/yr)[7]:	1,104	193	911	83%

1 Typical farm is 4 houses oriented East/West with interior area of 2316 m2 and rooftop solar cell area of 1,067 m2.
2 Demand takes into account T&D losses as 7%
3 The average hourly electric supply for the average day between 13 and 18, averaged for each day April through September.
4 The average hourly electric supply for the average day between 9 and 12, and 17 through 18; averaged for each day October through March.
5 The average hourly electric supply for the average day between 9 and 18, averaged for each day April through September.
6 The average hourly electric supply for the average day between 9 and 18, averaged for each day October through March.
7 Total energy produced for an average year.

The average power generated on the typical farm at peak hours was 496 kW/hr. The on-peak demand was estimated to be 82 kW/hr. This value was inflated by 7% to include the typical T&D losses and represent realistic facility demand. The potential contribution to peak demand reduction for a typical farm that uses net-metering would be 414 kW/hr, or 84% of rooftop supply. The average net contribution to grid during summer months was 404 kW/hr (95%), and 208 kW/hr in winter months (91%). The total annual energy generation for an average farm was 1,104 MWh, with facility consumption only 193 MWh. The annual net to grid contribution for the typical farm as a peaking plant was 911 MWh, or 83%.

These calculations were repeated for all 88 farms to determine the net contribution of all farms functioning as peaking plants to the distribution grid. The results are given in Table 3.31.

Table 0.23 Net contribution to utility grid for entire study area.

	PV Supply	Farm Demand[1]	Net to Grid	
average peak power (mW/hr)[2]:	59.2	7.6	51.6	87%
average summer power (mW/hr)[4]:	47.0	2.1	44.9	96%
average winter power (mW/hr)[5]:	22.3	2.1	20.2	91%
sum annual energy (GWh/yr)[6]:	127.3	17.9	109.4	86%

1 Demand calculations take into account 7% T&D losses
2 The average hourly electric supply for the average day between 13 and 18, averaged for each day April through September.
3 The average hourly electric supply for the average day between 9 and 12, and 17 through 18; averaged for each day October through March.
4 The average hourly electric supply for the average day between 9 and 18, averaged for each day April through September.
5 The average hourly electric supply for the average day between 9 and 18, averaged for each day October through March.
6 Total energy produced for an average year.

The average hourly summer peak supply was 59.2 MW/hr each day between 13:00 and 18:00 for every day between April 1st and September 30th. The estimated hourly farm loads during the hours of facility peak load were 7.6 MW, which was only 13% of the rooftop supply. This meant that a collective 51.6 MW/hr (87%) produced from all farms could be used to contribute to critical periods of peak demand for each hour between 13:00 and 18:00 for every day between April 1st and September 30th. Additionally, the sum of this total peak demand generated on all poultry house rooftops contributed was 45.4 GWh.

The average hourly summer power contribution of all farms was 47 MW/hr for each hour between 9:00 and 18:00 for every day between April 1st and September 30th. The estimated hourly farm loads during the average day were 2.1 MW, which was only 4% of the rooftop supply. This meant that a collective 44.9 MW/hr (96%) produced from all farms could be used to contribute to baseload for each hour between 13:00 and 18:00 each day between April 1st and September 30th.

The average hourly winter power contribution of all farms was 22.3 MW/hr for each hour between 9:00 and 18:00 for every day between October 1st and March 31th. The estimated hourly farm loads during the average day were 2.1 MW, which was only 9% of the rooftop supply. This meant that a collective 20.2 MW/hr (91%) produced from all farms could be used to contribute to baseload for each hour between 13:00 and 18:00 each day between October 1st and March 31th.

Lastly, the sum annual energy generation from all farms in the study area was 127.3 GWh. The estimated facility consumption was only 17.9 GWh, or 14% or supply. The annual net to grid was 109.4 GWh.

These results demonstrate the significant benefits of meeting high, rural agricultural loads without distribution losses or infrastructure. These high net-to-grid percentages between 86 and 96% also demonstrate the substantial contributions that can be made to meeting demand of the surrounding rural community.

DISCUSSION

The solar irradiance values in this study are exceptionally conservative, possibly by as much as 40%. Many credible sources, including other NOAA and NREL models, give credence to potentially +1.5 kWh/m^2/day for each azimuth orientation class. The results modeled by ESRI were chosen to prevent an optimistic bias that over-represented the potential success of a burgeoning technology. Additionally, it should be noted that the average rainfall for the study area was over twice that of the national average (O.

A regression analysis was done for the average power output in each season on each farm against its nominal capacity according to industry definitions. The results are given in Figure 3.10.

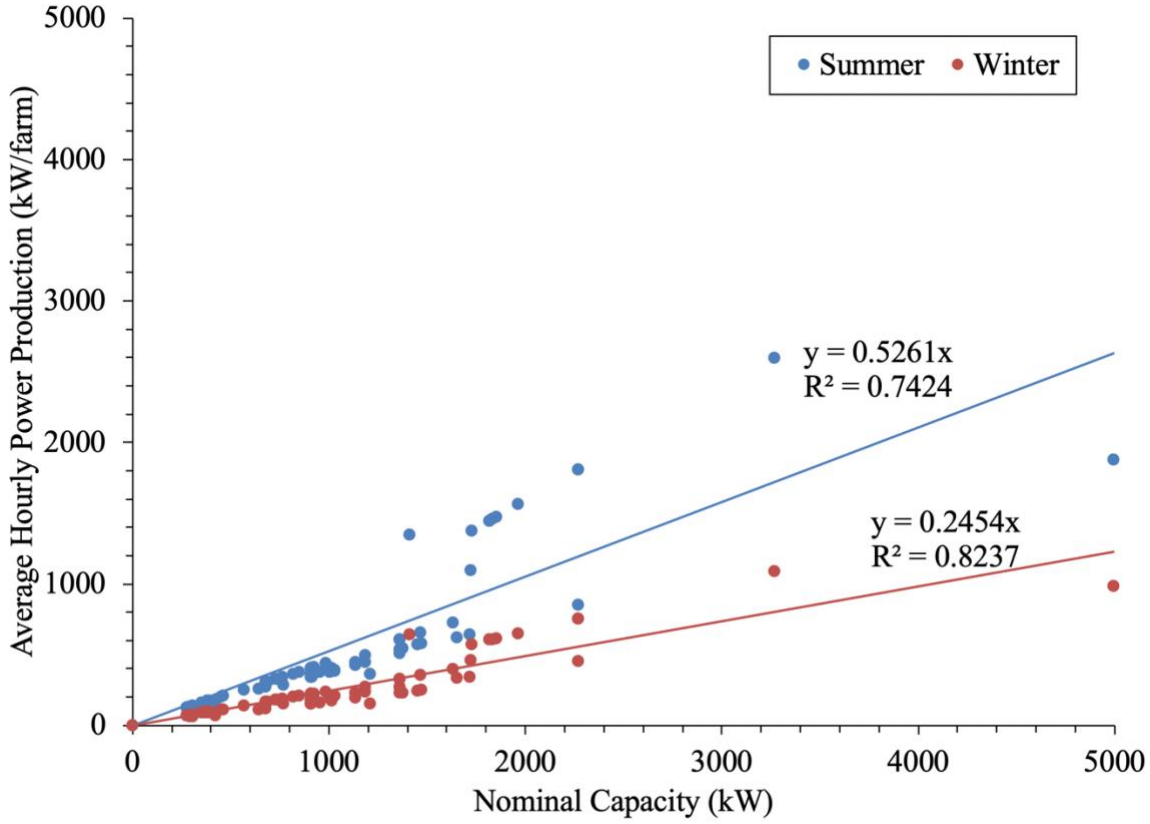

Figure 0.1 Correlation between Farm PV peaking plant nominal capacity and average farm power supply during summer peak and winter shoulder periods.

The slope of the line is the percentage of actual output relative to the technical potential of the electrical system. The average summer output is 53% of the nameplate capacity, and the average winter output is 25% of the nameplate capacity.

Duke energy reported 53,240 South Carolina customers enrolled in annual and peak demand energy saving programs in 2017 (US EIA, 2018). The average residential

energy consumption in SC is 13,751 kWh/y. Gross annual farm energy supply is sufficient for 9,097 SC residents- or 7,793 net. Duke reported an estimated potential peak demand savings of 265 MW of electricity in 2017 and spent $9,336,000 for DSM incentives (US EIA, 2018). Actual measured peak-demand savings was only 0.5 MW (0.18%). Similarly, BREC reported 1.9 MW of installed nominal capacity between a collective 238 customers, yet only recorded a net 19.9 MWh back to the grid 2017. BREC's recorded annual maximum peak demand, defined as the 60-minute interval which contains the highest sum of energy needed to satisfy a service area including losses, was 259 MW (the average peak demand is likely much lower). In addition to meeting the cost to supply high poultry farm loads, the average summer peak supply of all poultry farm rooftop PV is a total 37% peak-demand reduction for the local utility. Customer incentives for DSM can be substantially lower or provide a superior return on energy savings. The peak plant distribution will likely decrease T&D losses. The typical cost of land associated with solar will be replaced with a leasing agreement between the utility and farmer at the cost of a reduced electric rate or net metering. Other regular costs associated with PV DSM installation, such as permitting and certified technicians, can be internally supplied by a utility company. These economic benefits will be shared by both the utility company and the grower, allowing the poultry farmer a feasible method for PV applications (Dennis et al, 2016). Poultry houses consume minimal electricity for approximately ten weeks per year, allowing for unfiltered energy supply to the grid. The lifetime generating costs of solar electricity may decrease relative to conventional sources

of fuel and change the tipping point of solar technology adoption as a major energy supply contributor.

CONCLUSION

A cumulative 398 poultry houses in Oconee and Anderson Counties were analyzed for building dimensions, orientation, rooftop area, and rooftop slope to determine rooftop PV power and energy supply in light of facility consumption. (1) The typical farm consisted of four poultry houses, each 15.2 meters by 152.4 meters oriented East/West with a rooftop slope of 22.6º and a suitable rooftop area of 1,254 m^2. (2) These farms were grouped into 88 peaking plants with 499,485 m^2 of productive solar cell collector area. The total annual solar irradiance striking that area was estimated to be 677 GWh/yr, equal to 127.3 GWh (AC) of electricity. Seventy percent of this energy was generated during hours classified by a utility as above baseload (shoulder or peak). Total consumption for all poultry farms was only 17.9 GWh/yr, resulting in a net surplus of 109.4 GWh (ac). More specifically, a single farm could produce an average of 496 kW/hr during critical peak periods, with 414 kW/hr being contributed as net-to-grid (83%). The average hourly summer peak power supply of all poultry farms was 59.2 mW/hr, while the coincidental farm summer peak demand was 7.6 mW/hr, resulting in a peak demand reduction potential of 51.6 mW/hr. Twenty-seven farms were located further than 3.28 km from existing transmission lines, which would be the most impactful in peak demand reduction, the mitigation of T&D costs, and distributed energy supply to rural areas.

CONCLUSION I

(1) A UAV captured 8,043 images at 139 poultry houses in Anderson and Oconee Counties to produce GIS data for solar energy applications, and (2) photogrammetric processing produced dense point clouds of each flight location for a total of 1,626,284,298 points. Orthophotos of the study areas were generated from the acquired 3D image sequences using Structure from Motion (SfM) techniques. (3) The actual building widths and lengths ranged from 10.8 to 184.0 m and the measurement error within the UAV-derived orthophotos was 0.69% on average. Building width measured error was 0.047 ± 0.13 m, or 0.32% mean error. Building lengths had a mean error of 1.66 ± 0.48 m and 1.1% mean error. The actual building sidewall, side entrance, and peak heights ranged from 1.9 to 5.6 m and the measured error within the orthophotos was 1.69% on average. Building heights had a mean error of 0.06 ±.04 m or 1.2% mean error. The higher vertical error was expected with the given flight parameters (non-oblique imagery), which was more suited for horizontal accuracy. (4) In contrast, satellite-derived orthomosaic images of the same building widths and lengths had a measurement error of -0.36%. Building lengths had a mean error of -0.46 ± 0.49 m or -0.30% mean error. Building widths had a mean error of -0.44 ± 0.14 m and -2.83% mean error.

The results proved that using consumer-grade UAV's and photogrammetric SfM could create accurate DSM and orthomosaics of a study area at efficient use of economic and temporal resources without the use of survey grade equipment or GCPs. When compared to the horizontal accuracy of readily available satellite imagery, the results

were mixed. The satellite-derived orthomosaic was more accurate on average for length predictions with a smaller average error. However, the UAV-derived orthomosaic images were more accurate for average width predictions.

The the disparity in horizontal measurement accuracy between the compared remote sensing techniques was likely due to flight altitude and building shape. The rectangular building dimensions had an average length-to-width ratio of 10:1. The lower flight altitude of the UAV required 10 to 15 pictures to capture building lengths, and only 1 to 3 photos for building widths. In contrast, the satellite field of view likely captured an entire building, if not an entire farm, in a single image frame. This would result in less stitching error in remodeling building length and may also explain the higher uniformity of error between building length and width measurements from satellite images.

The satellite imagery had low cost and ease of access that allowed a convenient determination of structural orientation and planimetric dimensions. However, the UAV provided dependably current data, whereas the temporal accuracy of satellite imagery data was highly variable (sometimes ±12 months). The UAV-derived data was also useful for determining vertical dimensions, and therefore variables such as surface slope and aspect. Lastly, the UAV-derived data was more useful for absolute accuracy to establish true object positions in a geodetic coordinate system. This would be critical for analysis of spatial distribution or combining data with GIS data layers from other sources. With an average flight time of 13.5 minutes per farm area (2.5 ha), and an average GSD of 4.84 cm/pi, the results obtained from a relatively inexpensive UAV mounted camera

and image analysis demonstrated sufficient accuracy for planning and monitoring purposes in agricultural applications.

CONCLUSION II

A cumulative 398 poultry houses in Oconee and Anderson Counties were analyzed for building dimensions, orientation, rooftop area, and rooftop slope to determine rooftop PV power and energy supply in light of facility consumption. (1) The typical farm consisted of four poultry houses, each 15.2 meters by 152.4 meters oriented East/West with a rooftop slope of 22.6º and a suitable rooftop area of 1,254 m^2. (2) These farms were grouped into 88 peaking plants with 499,485 m^2 of productive solar cell collector area. The total annual solar irradiance striking that area was estimated to be 677 GWh/yr, equal to 127.3 GWh (AC) of electricity. Seventy percent of this energy was generated during hours classified by a utility as above baseload (shoulder or peak). Total consumption for all poultry farms was only 17.9 GWh/yr, resulting in a net surplus of 109.4 GWh (ac). More specifically, a single farm could produce an average of 496 kW/hr during critical peak periods, with 414 kW/hr being contributed as net-to-grid (83%). The average hourly summer peak power supply of all poultry farms was 59.2 mW/hr, while the coincidental farm summer peak demand was 7.6 mW/hr, resulting in a peak demand reduction potential of 51.6 mW/hr. Twenty-seven farms were located further than 3.28 km from existing transmission lines, which would be the most impactful in peak demand reduction, the mitigation of T&D costs, and distributed energy supply to rural areas.

APPENDICES

Appendix A: Building Measurements

Table A.1 Landing pad diameter measurement data (non-paired).

Trial #	Hand (cm)	Agisoft (cm)
1	74.45	74.5
2	74.61	74.3
3	74.45	74.3
4	74.45	74.9
5	74.61	73.8
6	74.45	75.5
7	74.61	75.1
8	74.3	74.8
9	74.61	75.2
10	-	75.5
11	-	75.7
12	-	74
13	-	74.7
14	-	74.7
15	-	76.1
16	-	75
17	-	74.5
18	-	75.1
19	-	78
20	-	72
21	-	73.8
22	-	74.5
23	-	75.3
24	-	74.9
25	-	73.4
26	-	73.6
27	-	73.7
28	-	75.4
29	-	73.5
30	-	75.1
31	-	72.3

Table A.2 Building width measurement data from blueprints and UAV-derived orthomosaic.

Trial #	blueprint (m)[1]	UAV (m)[2]
1	16.46	16.1856
2	12.19	11.4766
3	15.24	15.3716
4	15.24	16.3716
5	16.46	16.5356
6	15.24	15.3416
7	12.19	12.1856
8	12.80	12.2746
9	15.24	15.3906
10	15.24	15.3866
11	15.24	15.2476
12	15.24	15.2526
13	15.24	15.3566
14	10.97	10.9166
15	15.24	15.2106
16	15.24	15.1626
17	15.24	15.1476
18	16.46	16.3246
19	15.85	15.1296
20	12.19	11.8406
21	15.24	15.0306
22	15.24	15.1046
23	15.24	14.9746
24	15.24	16.2026
25	12.19	12.1576
26	15.24	15.1516
27	15.24	15.0776
28	15.24	14.9386
29	15.24	15.0786
30	15.24	15.2906
31	15.24	15.2436

[1] Converted from imperial (blueprint ft x 0.3048 m)

[2] Corrected for roof overhang (W_i - 0.9144 m)

Table A.3 Building length measurement data from blueprint and UAV-derived orthomoasic.

Trial #	blueprint (m)[1]	UAV (m)[2]
1	152.40	151.3931
2	114.30	113.1521
3	152.40	151.0331
4	152.40	151.4011
5	152.40	151.2161
6	152.40	151.1731
7	160.02	159.6251
8	153.62	153.6801
9	152.40	152.1931
10	152.40	151.9161
11	152.40	150.5581
12	152.40	150.6891
13	154.23	153.8241
14	129.54	129.0331
15	152.40	151.2721
16	182.88	183.3881
17	152.40	150.8931
18	152.40	149.2181
19	137.16	134.8751
20	161.54	156.8641
21	152.40	148.6431
22	152.40	151.7481
23	152.40	149.3871
24	152.40	149.1921
25	152.40	150.7671
26	152.40	148.9271
27	152.40	148.9661
28	152.40	149.3481
29	152.40	149.3911
30	152.40	151.8181
31	152.40	151.3811

[1] Converted from imperial (blueprint ft x 0.3048 m)

[2] Corrected for roof overhang (L_i - 0.6096 m)

Table A.4 Building height measurement data.

Trial #	Hand (m)	Agisoft (m)
1	3.23	2.93
2	2.44	2.44
3	2.21	2.29
4	1.92	1.86
5	2.23	2.32
6	2.13	2.07
7	2.36	2.16
8	2.44	2.35
9	2.44	2.32
10	2.69	2.64
11	2.72	2.60
12	2.21	2.10
13	2.13	2.11
14	2.26	2.22
15	2.25	2.26
16	5.74	5.55
17	5.66	5.61
18	4.40	4.45
19	5.15	5.27
20	5.15	5.46
21	5.49	5.33
22	5.41	5.24
23	5.16	5.02
24	5.13	5.02
25	5.38	5.14
26	5.38	5.16
27	4.75	4.49
28	4.70	4.75
29	2.77	2.90
30	2.77	2.55
31	2.18	2.09
32	2.21	2.24
33	2.24	2.09
34	2.29	2.38
35	2.90	2.68
36	2.92	2.80
37	2.26	2.40
38	3.34	3.40
39	2.21	2.24

Table A.5 Building width measurements from blueprint and Satellite-derived orthomosaic.

Trial #	Blueprint (m)[1]	Satellite(m)[2]	Trial #	Blueprint (m)	Satellite (m)
1	17.37	16.41	36	16.1544	16.1
2	17.3736	15.96	37	16.1544	16.32
3	17.3736	16.65	38	16.1544	16.47
4	17.3736	16.23	39	16.1544	17.15
5	17.3736	15.48	40	16.1544	13.9
6	17.3736	16.29	41	16.1544	17.19
7	13.1064	12.84	42	16.1544	16.09
8	11.8872	11.86	43	16.1544	15.01
9	13.1064	13.38	44	16.1544	13.98
10	16.1544	16.74	45	16.1544	17.68
11	16.1544	16.05	46	16.1544	18.01
12	16.1544	17.59	47	16.1544	18.08
13	16.1544	17.89	48	16.1544	18.15
14	16.1544	16.54	49	11.8872	11.94
15	16.1544	16.12	50	11.8872	13.83
16	16.1544	16.41	51	11.8872	11.93
17	16.1544	16.57	52	16.1544	16.56
18	16.1544	17.53	53	16.1544	16.45
19	17.3736	18.41	54	16.1544	16.53
20	17.3736	18.17	55	16.1544	16.81
21	17.3736	18.05	56	16.1544	16.82
22	17.3736	18.25	57	16.1544	18.53
23	11.8872	12.24	58	11.8872	12.49
24	11.8872	12.54	59	11.8872	12.79
25	13.1064	13.41	60	16.1544	16.15
26	13.1064	13.84	61	16.1544	16.93
27	16.1544	16.49	62	16.1544	17.45
28	16.1544	16.51	63	16.1544	16.88
29	13.1064	13.76	64	16.1544	16.74
30	13.1064	13.22	65	16.1544	17.01
31	13.716	12.96	66	16.1544	18.06
32	13.716	13.78	67	16.1544	18.21
33	13.716	14.35	68	16.1544	18.4
34	13.716	13.11	69	16.1544	16.98
35	16.1544	17.52	70	16.1544	16.74

Trial #	Blueprint (m)	Satellite(m)	Trial #	Blueprint (m)	Satellite (m)
71	16.1544	17.44	106	16.1544	16.54
72	13.1064	12.97	107	16.1544	16.94
73	14.6304	14.75	108	13.1064	13.45
74	16.1544	16.94	109	13.1064	13.55
75	16.1544	16.42	110	13.1064	13.43
76	16.1544	17.01	111	13.1064	13.07
77	16.1544	16.54	112	13.1064	13.2
78	16.1544	16.52	113	13.1064	13.04
79	17.3736	19.36	114	16.1544	16.07
80	17.3736	17.88	115	16.1544	16.17
81	17.3736	19.11	116	16.1544	16.89
82	17.3736	16.24	117	16.1544	16.44
83	17.3736	17.25	118	16.1544	15.98
84	17.3736	16.98	119	16.1544	15.87
85	17.3736	17.56	120	16.1544	16.77
86	16.764	16.69	121	16.1544	15.98
87	16.764	16.54	122	16.1544	16.45
88	16.764	16.99	123	16.1544	17.1
89	16.764	17.21	124	16.1544	16.33
90	13.1064	13.34	125	16.1544	16.38
91	13.1064	13.55	126	16.1544	16.29
92	16.1544	16.45	127	16.1544	16.87
93	16.1544	16.79	128	16.1544	16.155
94	16.1544	17.46	129	16.1544	16.34
95	16.1544	17.21	130	16.1544	18.01
96	16.1544	16.99	131	16.1544	18.08
97	16.1544	17.03	132	13.1064	13.25
98	16.1544	18.01	133	13.1064	13.01
99	16.1544	16.55	134	16.1544	16.99
100	16.1544	16.31	135	16.1544	17.24
101	16.1544	16.82	136	16.1544	15.89
102	16.1544	16.96	137	16.1544	16.18
103	16.1544	16.73	138	16.1544	16.57
104	16.1544	17.03	139	16.1544	16.39
105	16.1544	16.87			

1 Converted from emperial (blueprint ft x 0.3048 m)

2 Corrected for roof overhang (W_i - 0.9144 m)

Table A.6 Building length measurements from blueprint and Satellite-derived orthomosaic.

Trial #	Blueprint (m)[1]	Satellite(m)[2]	Trial #	Blueprint (m)	Satellite (m)
1	153.01	153.76	36	153.01	153.46
2	153.01	152.91	37	153.01	153.65
3	153.01	153.34	38	153.01	152.96
4	153.01	153.39	39	153.01	152.73
5	153.01	152.76	40	153.01	153.55
6	153.01	152.06	41	153.01	153.19
7	114.91	114.88	42	153.01	152.88
8	130.15	129.64	43	153.01	152.43
9	122.53	122.46	44	153.01	153.37
10	153.01	153.53	45	153.01	152.47
11	153.01	153.32	46	153.01	153.09
12	153.01	155.67	47	153.01	153.59
13	153.01	155.25	48	153.01	152.04
14	153.01	153.53	49	122.53	123.24
15	153.01	153.03	50	122.53	123.33
16	153.01	153.82	51	122.53	123.23
17	153.01	152.72	52	122.53	124.1
18	153.01	153.16	53	153.01	153.68
19	153.01	153.56	54	153.01	153.81
20	153.01	152.94	55	153.01	159.06
21	153.01	153.09	56	154.84	156.03
22	153.01	152.41	57	154.84	153.02
23	122.53	125.71	58	130.15	130.21
24	122.53	123.94	59	130.15	130.56
25	122.53	123.41	60	153.01	152.8
26	122.53	122.53	61	153.01	150.9
27	153.01	153.25	62	153.01	152.3
28	153.01	153.41	63	153.01	153.42
29	160.63	163.95	64	153.01	150.99
30	160.63	162.99	65	153.01	151.97
31	154.23	156.18	66	183.49	185.96
32	154.23	155.74	67	183.49	188.01
33	154.23	155.6	68	183.49	179.99
34	154.23	156.44	69	183.49	184.5
35	153.01	153.2	70	183.49	183.07

Trial #	Blueprint (m)	Satellite(m)	Trial #	Blueprint (m)	Satellite (m)
71	153.01	153.46	106	153.01	155.01
72	153.01	153.65	107	153.01	153.02
73	153.01	152.96	108	153.01	154.54
74	153.01	152.73	109	153.01	153.39
75	153.01	153.55	110	153.01	155.87
76	153.01	153.19	111	153.01	153.69
77	153.01	152.88	112	122.53	122.56
78	153.01	152.43	113	122.53	122.38
79	153.01	153.37	114	153.01	152.72
80	153.01	152.47	115	153.01	152.25
81	153.01	153.09	116	153.01	152.07
82	153.01	153.59	117	153.01	152.49
83	153.01	152.04	118	153.01	152.88
84	122.53	123.24	119	153.01	153.3
85	122.53	123.33	120	153.01	152.6
86	122.53	123.23	121	153.01	153.01
87	122.53	124.1	122	137.77	153
88	153.01	153.68	123	137.77	152.19
89	153.01	153.81	124	153.01	137.29
90	153.01	159.06	125	153.01	138.12
91	154.84	156.03	126	153.01	152.69
92	154.84	153.02	127	153.01	152.97
93	130.15	130.21	128	153.01	153.4
94	130.15	130.56	129	153.01	153.67
95	153.01	152.8	130	153.01	153.22
96	153.01	150.9	131	153.01	153.4
97	153.01	152.3	132	130.15	129.66
98	153.01	153.42	133	130.15	129.72
99	153.01	150.99	134	153.01	152.92
100	153.01	151.97	135	153.01	152.84
101	183.49	185.96	136	153.01	152.95
102	183.49	188.01	137	153.01	153
103	183.49	179.99	138	153.01	153.48
104	183.49	184.5	139	153.01	152.66
105	183.49	183.07			

1 Converted from emperial (blueprint ft x 0.3048 m)

2 Corrected for roof overhang (L_i - 0.6096 m)

Appendix B: Hillshade Analysis for Building Shading

To determine the effect of solar shading on the area of interest an illumination analysis was done in ArcGIS Pro (ESRI, 2019) using the HillShade tool on each farm DSM. Illumination duration and intensity were modeled by establishing a position for a light source and neighboring topography to quantify illumination values of each cell. The location of the sun can be established using the solar azimuth and the solar altitude. The solar azimuth is the angular direction of the sun, measured from north in clockwise degrees from 0 to 360. The solar altitude is the slope or angle of the illumination source above the horizon. The units are in degrees, from 0 (on the horizon) to 90 (overhead). The exact solar path for the study area on the days of interest was ascertained with values recorded by the Astronomical Applications Department of the US Naval Observatory, as seen in Table B.1.

Table B.1 Solar altitude and azimuth for Westminster, SC on 3/21/19 (US NO, 2019).

Time (h:m)	Altitude (o)	Azimuth (o, E of N)
7:00	-7.7	84.2
8:00	4.8	92.8
9:00	16.9	101.7
10:00	28.7	111.7
11:00	39.6	124.2
12:00	48.7	140.9
13:00	54.6	163.3
14:00	55.4	189.6
15:00	50.8	213.5
16:00	42.4	231.7
17:00	31.9	245.2
18:00	20.3	255.8
19:00	8.3	264.9
20:00	-4.2	273.5

The solar azimuth and altitude were recorded each hour for Westminster SC on March 21st, 2019. As can be seen in the Altitude column of the table, the transition from negative to positive represent the sun breaching the horizon between 7:00 and 8:00, and again between 19:00 and 20:00.

Figure B.1 provides example simulation output, demonstrating the variation of solar location and intensity throughout the day as a function of Earth rotation.

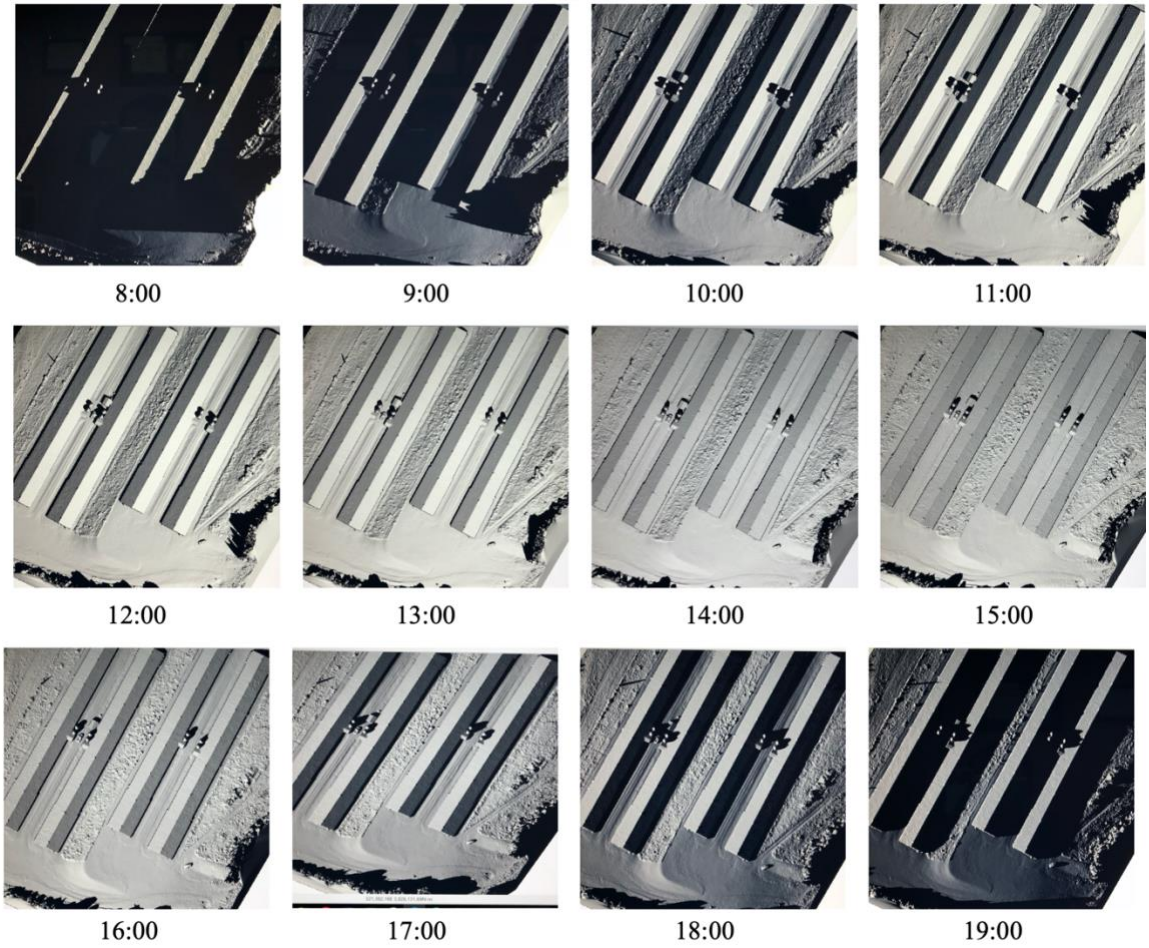

Figure B.1 Hillshade Analysis hourly output on a poultry farm on March 21st, 2019.

Seasonal variation within the year was modeled by running the hourly simulation on four key calendar days: March 21st, June 21st, September 21st, and December 21st. These four days represent the extremes of seasonal variation in daylight duration, solar intensity, and solar angle for all 365 Julien days. The hourly hillshade value for each 0.15 meters on each of the four seasonal days was then averaged to produce a representation of annual illumination.

The hillshade illumination values were reclassified into a binary output raster. In typical hillshade analysis applications, any hillshade value between 1 and 255 would be determined as "being illuminated" and reclassified as a value of 1. However, for the purpose of photovoltaics, a certain illumination intensity has to be met in order for the use of the technology to be justified. Seasonal illumination thresholds established by a function of daylight duration was used to classify a cell as being in sunlight, as seen in Table B.2.

Table B.2 Reclassified hillshade values with seasonal solar illumination threshold (Melius et al, 2013).

Day	Illumination Threshold (%)	Hillshade values Reclassified as 0	Hillshade values reclassified as 1
March	60	0 - 152	153 - 254
June	70	0 - 178.5	178.5 - 254
September	60	0 - 152	153 - 254
December	50	0 - 127.5	127.5 - 254

The hillshade value for each hour was classified into "in sun" or "in shade" based on the percentage of illumination. March requires 60% illumination (values > 152), June requires 70% illumination (values > 178), September requires 60% illumination (values > 152), and December requires 50% illumination (values > 127). The reclassified binary

values for each cell of each hourly raster layer for were then averaged for each of the respective four seasonal days, illustrating the interannual variability of solar illumination, and can be seen in Figure 3.7. All four seasonal averages were again averaged together to represent an annual average, which can be seen in Figure B.2.

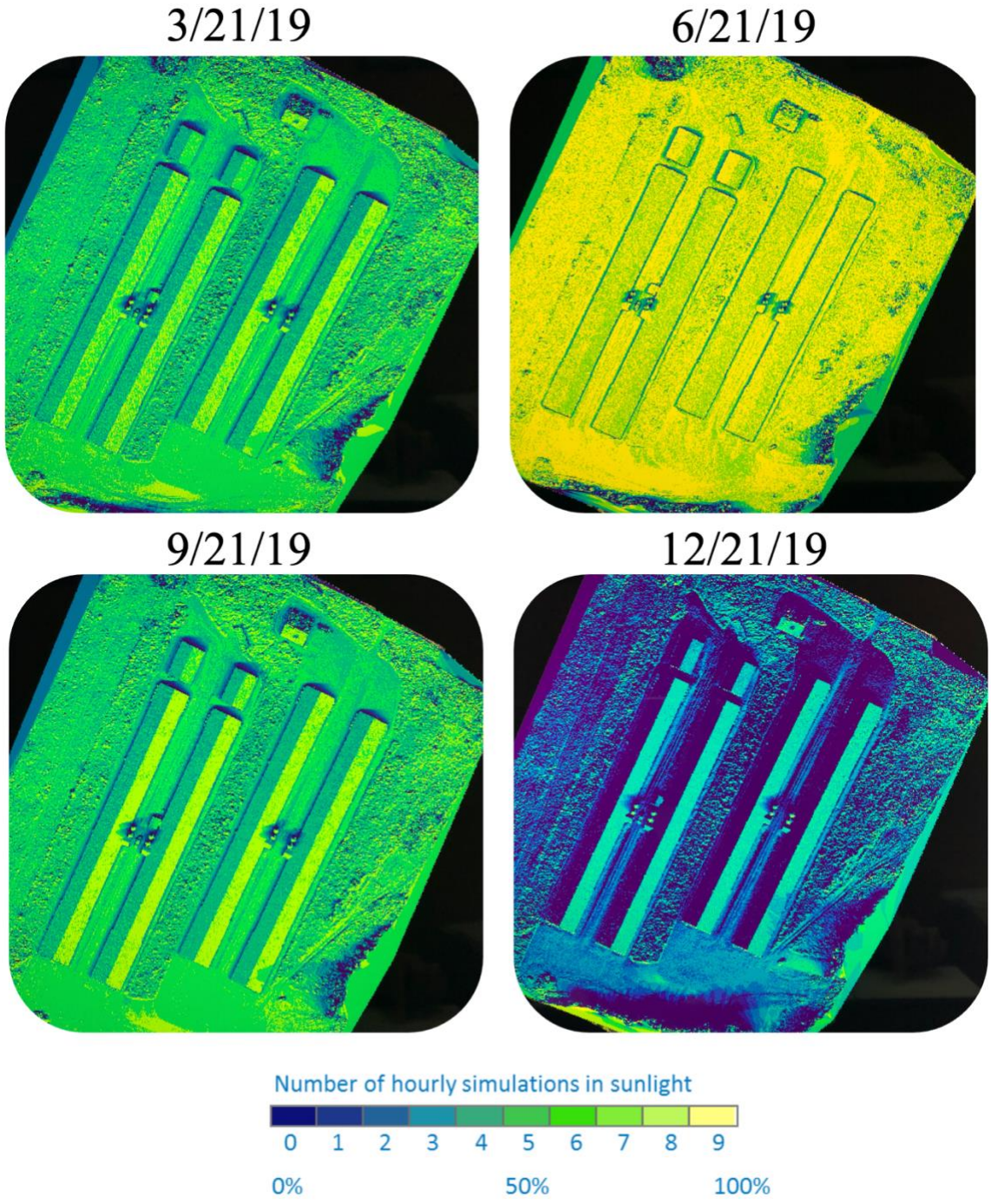

Figure B.2. Seasonal average illumination duration (hr).

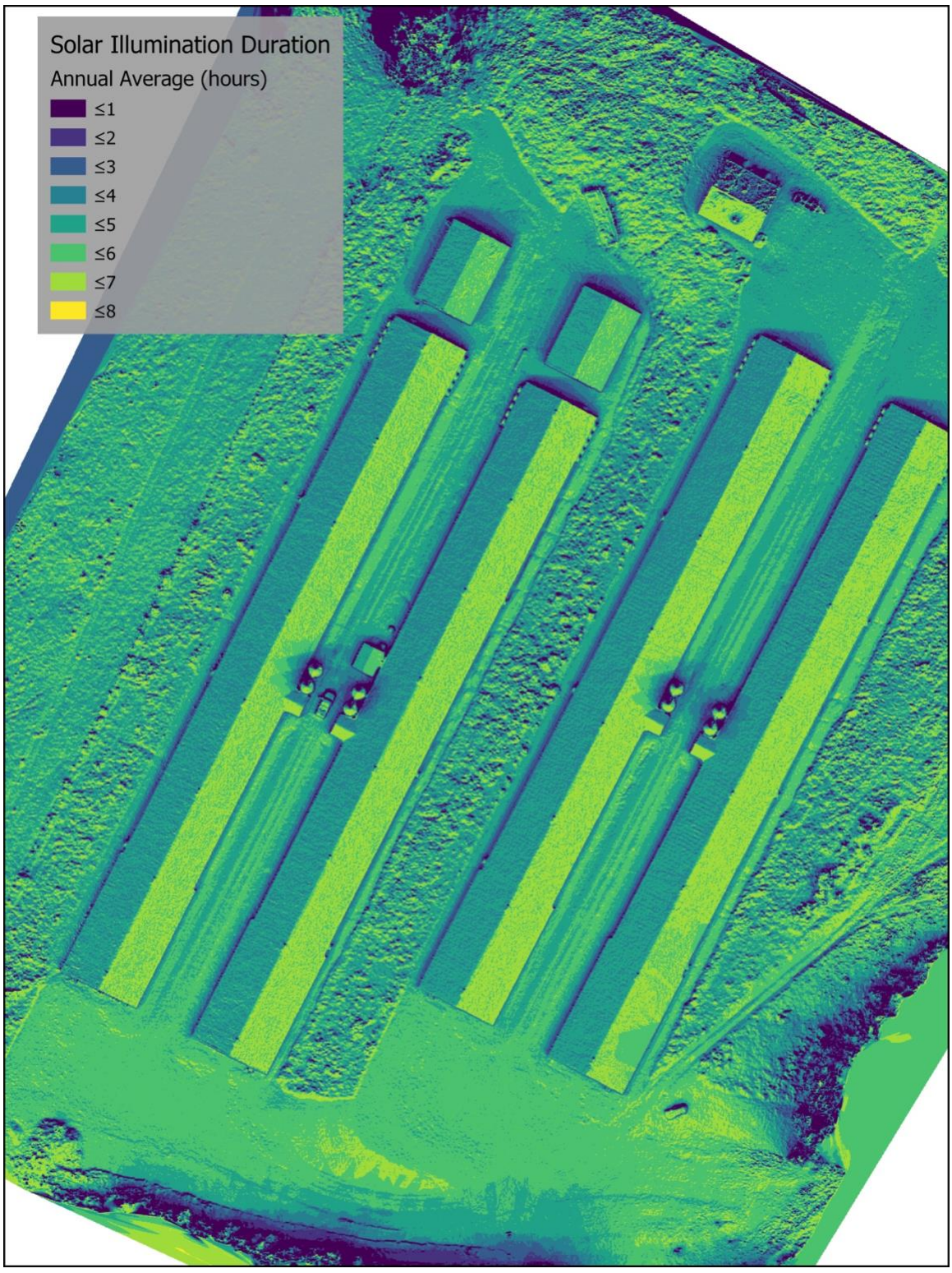

Figure B.3 annual average solar illumination duration (hr).

Appendix C: Geospatial Data Processing Workflow

The input data was converted to a DSM file with 0.15-meter horizontal resolution in ArcGIS Pro (ESRI, 2019). Martin Isenburg's proprietary LAStools were used for the improved data conversion quality (Isenburg, 2018). The data conversion process can be seen in figure C.1.

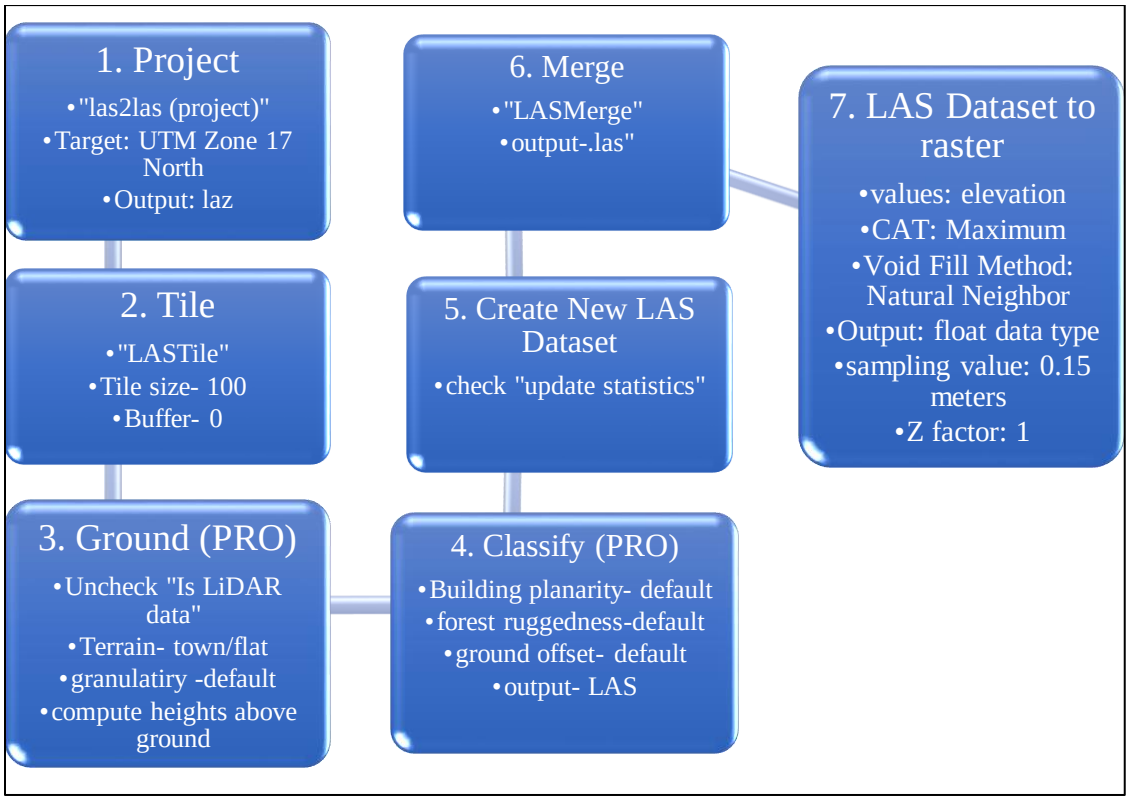

Figure C.1 Input data preprocessing GIS workflow with tool parameters.

Project

The input data has a spatial reference associated with the 3-D WGS 84 geographic projection. The data is converted to a 2-D projected coordinate system for the study area called UTM Zone 17 North.

Tile

Due to the large nature of the point cloud files, the tiling tool splits the points into multiple files of non-overlapping squares of a specified size and format. The optimal tile size for this study was found to be 100 units, and no buffer was applied.

Ground

The ground tool is used for bare-earth extraction, which classifies points into ground and non-ground classes. Both the ground, height, and classify tools classify each point based on the specifications defined in the American Society of Photogrammetry and Remote Sensing (ASPRS). The distinction between these two classes is determined by a terrain function, which instructs the tool to expect the environment's typical vertical object heights off the ground. For our study, the most accurate results were accomplished with the "town/flat" class, which uses a default step size of 10 meters. According to the developer's instructions, it is important to specify the horizontal and vertical units to the tool. Lastly, computing the height above ground for each point allows you to skip the LASheight step.

Classify

This tool classifies buildings and high vegetation, requiring the bare-earth points and point heights above ground to be previously established. This step also converts the file type from compressed points (.laz) to uncompressed points (.las).

Create New LAS Dataset

This tool creates a triangulated surface type that allows for rapid read/display processes of point cloud data. Calculating statistics allows for quality assurance and control through a summary report, which is generated as an auxiliary text file (.lasx). Statistics include average point spacing, range, elevation, and intensity values, quantity of data points per class code, existence of RGB values, as well as point format ID, Project ID, and file source ID.

Merge

An orthomosaic image was constructed from the dense cloud in the WGS 84 geographic projection. Mosaic blending was applied, and hole filling was enabled.

LAS Dataset to Raster

This last step is the conversion of the data file types from point cloud (.las) to raster (tif). A binning interpolation technique was used to determine a cell's elevation values of the output raster which includes a maximum value Cell Assignment Method and natural neighbor interpolation for Void Filling Methods. The sampling cell size value was specified at 0.15 meters output resolution. The data output type was 32 bit floating point.

Appendix D: Poultry Facility Energy Consumption Data

Table D.1 Average pullet farm electricity consumption (kWh/100m2).

	Farm							
	1	2	3	4	5	6	7	8
January	124	20	169	83	55	87	71	82
February	129	40	251	93	64	28	105	86
March	64	38	285	108	92	76	110	112
April	128	48	143	80	84	31	75	24
May	181	86	69	58	91	74	134	111
June	204	132	85	115	114	71	212	20
July	263	40	79	254	234	123	354	227
August	219	145	87	294	333	106	328	221
September	114	163	107	267	385	76	224	254
October	130	165	77	155	328	112	101	68
November	125	127	70	83	173	35	137	92
December	131	104	102	59	63	49	111	49
Total	1812	1107	1523	1651	2015	867	1962	1344

Table D.2 Average broiler farm electricity consumption (kWh/100m^2).

	Farm									
	1	2	3	4	5	6	7	8	9	10
January	82	22	44	137	85	32	70	165	167	198
February	83	21	59	78	90	64	167	103	118	130
March	88	30	62	139	193	130	43	113	117	133
April	110	18	55	115	93	221	134	157	150	170
May	149	26	130	165	165	145	141	80	84	100
June	149	43	58	324	307	511	5	260	252	272
July	228	35	155	200	81	657	143	83	49	62
August	162	58	103	434	373	394	217	112	105	224
September	182	30	95	336	447	239	28	128	144	130
October	113	58	77	164	163	288	50	114	105	122
November	88	23	26	199	462	215	191	184	178	209
December	83	33	73	135	81	155	69	53	58	53
Total	1518	395	938	2427	2541	3053	1258	1553	1526	1803

Table D.3 Average broiler farm electricity consumption (kWh/100m2).

	Farm									
	11	12	13	14	15	16	17	18	19	20
January	163	104	52	238	99	194	148	69	185	138
February	76	86	120	265	93	186	130	72	88	68
March	114	103	98	239	188	183	147	78	259	129
April	122	106	109	286	77	146	150	103	77	155
May	106	126	232	266	129	216	196	111	269	127
June	201	198	64	311	78	157	165	93	227	366
July	61	177	137	261	125	309	261	102	202	156
August	108	211	223	340	149	241	195	145	272	317
September	48	154	177	292	162	283	220	96	146	146
October	119	138	26	271	142	186	138	88	288	167
November	156	112	84	148	85	216	170	69	86	146
December	75	98	103	276	139	139	114	64	126	78
Total	1348	1612	1427	3193	1464	2457	2034	1090	2224	1993

Table D.4 Average broiler farm electricity consumption (kWh/100m2).

	Farm									
	21	22	23	24	25	26	27	28	29	30
January	235	203	56	102	93	130	44	82	88	187
February	151	161	134	91	136	149	63	86	63	79
March	194	198	52	114	172	150	80	112	100	206
April	367	317	113	156	143	158	67	24	56	126
May	164	151	163	238	232	216	108	111	145	209
June	464	389	119	309	233	233	109	20	133	328
July	260	353	322	285	246	328	115	227	142	209
August	413	377	187	406	295	366	137	221	220	422
September	367	620	316	249	325	211	152	254	190	144
October	262	190	117	175	159	353	74	68	145	239
November	343	220	146	87	165	129	77	92	134	145
December	189	175	133	110	116	161	54	49	76	86
Total	3409	3353	1858	2321	2316	2585	1080	1344	1492	2381

Table D.5 Average broiler farm electricity consumption (kWh/100m2).

	Farm									
	31	32	33	34	35	36	37	38	39	40
January	92	154	159	147	133	67	129	108	81	89
February	114	163	149	178	88	142	90	89	93	53
March	106	142	149	104	32	68	102	109	139	130
April	103	167	110	242	128	121	108	257	118	69
May	125	104	156	167	254	226	143	141	226	177
June	159	199	204	268	217	60	165	582	116	137
July	147	162	322	509	367	275	200	143	228	204
August	228	123	206	184	340	330	174	475	108	141
September	177	264	334	507	227	120	172	270	137	107
October	116	85	341	172	313	340	173	150	77	104
November	120	202	147	177	86	60	98	110	102	40
December	111	105	212	196	122	63	123	59	76	73
Total	1599	1872	2488	2850	2307	1872	1678	2495	1499	1322

Table D.6 Average broiler breeder farm electricity consumption (kWh/100m2).

	Farm 1	Farm 2
January	50	324
February	43	320
March	194	53
April	209	180
May	293	435
June	400	512
July	478	635
August	497	669
September	461	625
October	345	446
November	255	377
December	149	292
Total	3372	4867

The comparison of energy consumption by facility type is demonstrated in Figure D.1.

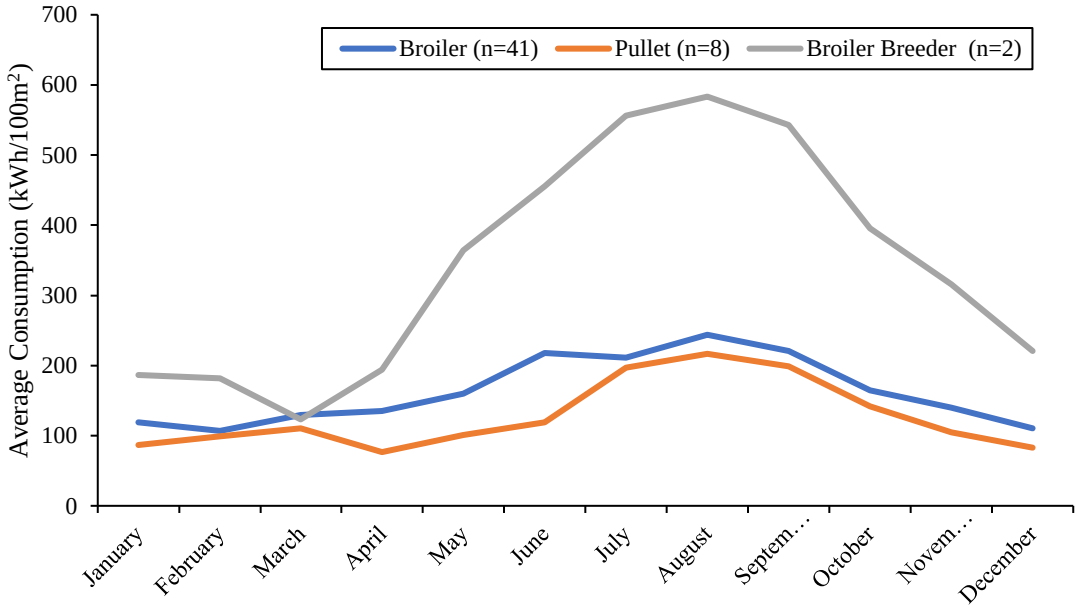

Figure D.1 Comparison of poultry facility energy efficiency by bird type.

References I

Agisoft. (2018). Agisoft Photoscan User Manual, Professional Edition, Version 1.4.1, Moscow, Russia. Available from http://www.agisoft.ru [accessed 2/20/2018].

Akturk, E., Altunel, A. (2019). Accuracy assessment of a low-cost UAV derived digital elevation model (DEM) in a highly broken and vegetated terrain. Measurement: Journal of the International Measurement Confederation, Vol. 136, pp 382-386.

B. Le Mauff, M. Juigner, B. Antoine, R. Marc, P.Launeau, P. Fattal. (2018). Coastal monitoring solutions of the geomorphological response of beach-dune systems using multi-temporal LiDAR datasets. Vendée coast, France. *Geomorphology*, Vol. 304, pp. 121-140.

Barry, P., Coakley, R. (2013). Accuracy of UAV Photogrammetry Compared with Network RTK GPS. Ireland, *International Archives of the Photogrammetry, Remote Sensing and Spatial Information Sciences*, Volume XL-1/W2, UAV-g2013.

Haala, N., Rothermel, M. (2012). Dense multi-stereo matching for high quality digital elevation models. *PFG Photogrammetry*. Fernerkund. Geoinf. pp. 331-343.

Hill, A.C. 2019. Economical Drone Mapping for Archeology, Comparisons of Efficiency and Accuracy. *Journal of Archeological Science: Reports*, Vol. 24, pp. 80-91.

I. Colomina, P. Molina. (2014). Unmanned aerial systems for photogrammetry and remote sensing: a review *ISPRS Journal of Photogrammetry and Remote Sensing*, Vol. 92, pp. 79-97.

Mansurav, N. (2020). *EXIF Data Explained*. Retrieved from Photographylife. https://photographylife.com/what-is-exif-data [accessed 2/20/2020].

Remondino, F., Barazzetti, L., Nex, F., Scaioni, M., Sarazzi, D. (2011). UAV Photogrammetry for mapping and 3D modeling- current status and future perspectives- *International Archives of the Photogrammetry, Remote Sensing, and Spatial Information Sciences*, Vol 38, In: Proceedings of the ISPRS ICWG I/V UAV-g Conference, Zurich, Switzerland.

Sammartano, G., Spanò, A. (2016). DEM generation based on UAV photogrammetry data in critical areas. In: Proceedings of the 2nd International Conference on Geographical Information Systems Theory, Applications and Management (GISTAM 2016), pp. 92–98.

Ulman S. and Brenner Sydnrey. (1979). The Interpretation of structure from motion. *Proceedings of the Royal Society*. London, Britain. Vol 203, 405-426. https://doi.org/10.1098/rspb.1979.0006.

Uysal, M., Toprak, A., Polat, N. (2015). DEM generation with UAV photogrammetry and accuracy analysis in Sahitler hill. *Measurement*, Vol. 73, pp. 539-543.

Westoby, M.J., Brasington, J., Glasser, N.F., Hambrey, M.J., Reynolds, J.M. (2012). 'Structure-from-Motion' photogrammetry: A low-cost, effective tool for geoscience applications. *Geomorphology*, Vol. 179, pp 300-314.

References II

AEC. (2019). *Retail Rate Schedule*. Retrieved from Aiken Electric Cooperative, INC: http://www.aikenco-op.org/retail-rate-schedule/ [accessed 9/10/2019].

Anderson, J. (2016). *Municipal Utilities had Lowest frequency, duration of outages in 2015.* Retrieved from American Public Power Association: https://www.publicpower.org/periodical/article/municipal-utilities-had-lowest-frequency-duration-outages-2015 [accessed 11/15/2019].

ASCE. (2019). *Conditions and Capacity.* ASCE Foundation. Infrastructure Report Card [accessed 11/15/2019].

BEC. (2019). *Commercial Rate Summary*. Retrieved from Berkeley Electric Cooperative: https://www.berkeleyelectric.coop/content/commercial-rate-summary [accessed 9/9/2019].

Branker, K., Pathak, M., Pearce, J. (2011). A review of solar photovoltaic levalized cost of electricity. Kingston, Canada: *Renewable and Sustainable Energy Reviews*. Vol 15, pp. 4470-4482.

Brightstar. (2019). *Common Solar Panel Dimensions*. Retrieved from Brightstar Solar: https://brightstarsolar.net/common-sizes-of-solar-panels/ [accessed 3/12/2018].

Chastain, J. (2016). Opportunities and Challenges Related to Improving Energy Efficiency for Broiler Facilities. *SEEA & AESP Southeast Conference.* Atlanta: Momentum.

Chastain, J. (1990). Electric demand and energy usage for grain centers on Kentucky farms. *Applied Engineering in Agriculture*, 6(4):515-522.

Chastain, J., Anderson, P., & Vassalos, M. (2017). Analysis of Available Efficiency and Performance Data for Axial Flow Agricultural Ventilation Fans. Clemson, SC, U.S.: *ASABE*.

DEC. (2017). *SC 2017 Integrated Resource Plan Annual Report.* Columbia: Duke Energy Carolinas, LLC [accessed 10/10/2017].

Dennis, C., Davis, J., Simpson, G., Donald, J. (2016). Exploration of Solar Power for the Modern Poultry Farm. Auburn University Cooperative Extension System. *National poultry technology center* (pp. 1-6).

DEP. (2019). *Paying my Bill: Rates*. Retrieved from Duke Energy : https://www.duke-energy.com/business/billing/rates [accessed 9/10/2019].

DEP. (2019). *Residential Time of Use Rate Program*. Retrieved from Duke Energy: https://www.duke-energy.com/business/billing/rates/residential-time-of-use-rate/how-it-works?jur=NC02 [accessed 1/18/2019].

DoHS. (2019). *Electric Power Transmission Lines*. Retrieved from Homeland Infrastructure Foundation-Level Data: https://hifld-geoplatform.opendata.arcgis.com/datasets/electric-power-transmission-lines?geometry=-84.034%2C34.511%2C-81.727%2C34.906 [accessed 9/25/2019].

EPA. (2015). NSPS for GHG Emissions from New, Modified, and Reconstructed Electric Utility Generating Units. Traingle Park, NC, USA [accessed 10/23/2019].

ESRI. (2019). *ArcGIS Pro.* Redlands, CA: Version 3.4.

FAA. (2016). *FAA News*. Summary of small unmanned aerial systems (part 107). Washington, DC. [accessed 10/05/2017]

Fu, P., Rich, P. (2002). A Gemoteric Solar Radiation Model with Applications in Agriculture and Forestry. *Computers and Electronics in Agriculture*, 25-35.

Gallucci, M. (2020). *Prototype Offers High Hopes for High-Efficiency Solar Cells.* Retrieved from IEEE Spectrum: https://spectrum.ieee.org/energywise/energy/renewables/prototype-high-efficiency-solar-cells-news [accessed 2/20/2019]

GANC. (2017). *House Bill 589.* Session Law 192 [accessed 10/25/2017].

Gilman, P. (2019, 2 12). Re: PV System Design. (P. Anderson, Interviewer)

Google. (2019). *Google*. Retrieved from Google Maps: https://www.google.com/maps

Isenburg, M. (2018). *LAStools*. Retrieved from Rapidlasso: https://rapidlasso.com/lastools/

Jothibasu, S., Santoso, S. (2017). *Will Rooftop Solar Really Add to Utility costs?*IEEE Spectrum: https://spectrum.ieee.org/energywise/energy/policy/calculating-the-full-cost-of-electricity-rooftop-solar-pv [accessed 1/24/2017].

Klaić, Z., Fekete, K., Šljivac, D. (2015). Demand side load management in the distribution system with photovoltaic generation. Kneza Trpimira, Osijek, Croatia: *Technical Gazette*.

Kostková, K., Omelina, Ł., Kyčina, P., Jamrich, P. (2012). An introduction to load management. *Electrical Power Systems Research*. Vol 95, pp. 184-191.

Lockeheart Power. (2019). *Lockeheart Power*. Retrieved from Rate Information: http://www.lockhartpower.com/rate-information.php [accessed 9/10/2019].

Lopez, A., Roberts, B., Heimiller, B., Porro, G. (2012). U.S. Renewable Energy Technical Potentials: A GIS-Based Analysis. Golden: *National Renewable Energy Laboratory*.

Margolis, R., Gagnon, P., Phillips, J., Melius, J., Elmore, R. (2016). Rooftop Solar Photovoltaic Technical Potential in the United States: A Detailed Assessment. Golden: *National Renewable Energy Laboratory*.

NOAA. (2017). *Solar Radiation*. Retrieved from NSRDB: https://www.ncdc.noaa.gov/data-access/land-based-station-data/land-based-datasets/solar-radiatio [accessed 1/25/2018].

Raymond, W. (2009). *Vocab Lesson: On-Peak, Off-Peak*. Retrieved from plotwatt: https://www.plotwatt.com/2009/02/24/vocab-lesson-peak-off-peak/ [accessed 11/20/2017].

Rich, P., Dubayah, R., Hetrick, W., Saving, S. (1994). Using view ship models to calculate intercepted solar radiation: applications in ecology. *American Society of Photogrammetry and Remote Sensing*, pp. 524-529.

SC DA. (2020). *About*. Retrieved from South Carolina Department of Agriculture: https://agriculture.sc.gov/about/ [accessed 2/16/2020].

SC DNR. (2019). *Period of Record Monthly Climate Summary for Oakway, SC*. Retrieved from SC State Climate Office : http://www.dnr.sc.gov/cgi-bin/sco/hsums/cliMAINnew.pl?sc6423 [accessed 7/28/2018].

SC PF. (2019). *Economic Impact*. Retrieved from SC Poultry Federation: https://scpoultry.org/ecoimpact/ [accessed 11/12/2019].

SCEG. (2019). *Rates*. Retrieved from Dominion Energy: https://www.sceg.com/paying-my-bill/rates [accessed 9/10/2019].

Smith, B. (2017). CAMM Certified Poultry Grower List. (P. Anderson, Interviewer)

Stacy, T., Taylor, G. (2018). *The Levelized Cost of Electricity from Existing Generation Resources*. Retrieved from Institute for Energy Research: https://www.instituteforenergyresearch.org/wp-content/uploads/2019/06/IER_LCOE2019Final-.pdf [accessed 6/8/2019].

Svarc, J. (2019). *Most Efficient Solar Panels.* Retrieved from Clean Energy Reviews: https://www.cleanenergyreviews.info/blog/most-efficient-solar-panels [accessed 3/10/2018].

US DOE. (2015). *Expedited Permit Process Report*. Retrieved from Solar America Board for Codes and Standards: http://www.solarabcs.org/about/publications/reports/expedited-permit/ [accessed 11/18/2018].

US EIA. (2018). *US Electric System Operating Data.* Retrieved from Independant Statistics and Analysis: https://www.eia.gov/realtime_grid/#/data/table?end=20190622T00&start=20190615T00&dataTypes=k&bas=0000002&regions=4 [accessed 10/15/2019].

US EIA. (2019). *Annual Electric Power Industry Report, Form EIA-861 detailed data files.* Washington, DC: Independant Statistics and Analysis [accessed 10/12/2019].

US EIA. (2019). *Electric Power Monthly Table 6.07.B Capacity Factors for Utility Scale Generators.* Independant Statistics and Analysis [accessed 10/12/2019].

US EIA. (2019). *Lynches River Electric Cooperative*. Retrieved from U.S. Utility Rate Database: https://openei.org/apps/USURDB/?utilRateFinder=Lynches%20River%20Elec%20Coop%2C%20Inc [accessed 9/19/2019].

USDA. (2019). *Census of Agriculture - 2017 SC State Profile.* National Agricultural Statistics Service [accessed 2/16/2020].

Warwick, W., Hardy, T., Hoffman, M., Homer, J. (2016). *Electricity Distribution System Baseline Report.* Department of Energy [accessed 2/16/2018].